NAVAL POSTGRADUATE SCHOOL
MONTEREY, CALIFORNIA

THESIS

LASER DOPPLER VELOCIMETRY AND VISCOUS COMPUTATION OF THE FLOW THROUGH A COMPRESSOR CASCADE NEAR STALL

by

Andrew John Harold Williams

June 1995

Thesis Advisor: Garth V. Hobson

Approved for public release; distribution is unlimited.

DISCLAIMER NOTICE

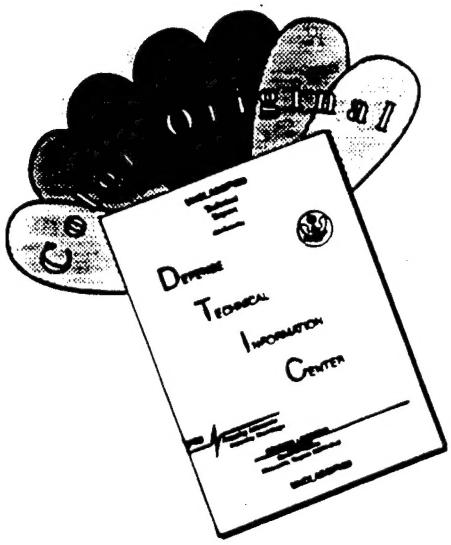

THIS DOCUMENT IS BEST QUALITY AVAILABLE. THE COPY FURNISHED TO DTIC CONTAINED A SIGNIFICANT NUMBER OF COLOR PAGES WHICH DO NOT REPRODUCE LEGIBLY ON BLACK AND WHITE MICROFICHE.

REPORT DOCUMENTATION PAGE

Form Approved OMB No. 0704-0188

1. AGENCY USE ONLY *(Leave blank)*	2. REPORT DATE	3. REPORT TYPE
	June 1995	Master's Thesis

4. TITLE AND SUBTITLE
LASER-DOPPLER VELOCIMETRY AND VISCOUS COMPUTATION OF THE FLOW THROUGH A COMPRESSOR CASCADE NEAR STALL

5. FUNDING NUMBERS

6. AUTHOR(S)
Williams, Andrew J. H.

7. PERFORMING ORGANIZATION NAME(S) AND ADDRESS(ES)
Naval Postgraduate School
Monterey CA 93943-5000

8. PERFORMING ORGANIZATION

9. SPONSORING/MONITORING AGENCY NAME(S) AND ADDRESS(ES)

10. SPONSORING/MONITORING AGENCY REPORT NUMBER

11. SUPPLEMENTARY NOTES **The views expressed in this thesis are those of the author and do not reflect the official policy or position of the Department of Defense or the U.S. Government.**

12a. DISTRIBUTION/AVAILABILITY STATEMENT
Approved for public release; distribution is unlimited.

12b. DISTRIBUTION CODE

13. ABSTRACT ***(maximum 200 words)***

Laser-Doppler velocimeter measurements were made in the flow field of a stalled cascade of controlled-diffusion stator blades. Tests were conducted at 10 degrees of incidence above the design inlet-flow angle in order to verify previous measurements. A unique method of data presentation was offered to characterize the unsteady positive and negative velocities about their mean. Laser-sheet flow visualization was performed and showed the unsteadiness of the stalling phenomena within the blade row passages. Additionally, a leading-edge separation bubble was observed and reversed flow was measured within the bubble using the laser-Doppler anemometer. Power-spectral density and auto-correlation analysis results are presented. In parallel with the experimental measurements, a computational fluid-dynamics study was initiated in an attempt ultimately to predict stall. Viscous flow computations were completed at on-design and near-stall conditions. Pressure distributions, separation bubble re-attachment locations, and loss predictions were compared to previous experimental studies. Generally good agreement was obtained for on-design conditions with degradation in prediction nearing stall.

14. SUBJECT TERMS	15. NUMBER OF PAGES
Laser-Doppler Velocimetry, Viscous Flow Computations, Stall, Unsteady Flow, Controlled-Diffusion Stator Blades, Flow Visualization	118
	16. PRICE CODE

17. SECURITY CLASSIFICATION OF REPORT	18. SECURITY CLASSIFICATION OF THIS PAGE	19. SECURITY CLASSIFICATION OF ABSTRACT	20. LIMITATION OF ABSTRACT
Unclassified	Unclassified	Unclassified	UL

NSN 7540-01-280-5500

Standard Form 298 (Rev. 2-89)
Prescribed by ANSI Std. 239-18 298-102

Approved for public release; distribution is unlimited.

LASER-DOPPLER VELOCIMETRY AND VISCOUS COMPUTATION OF THE FLOW THROUGH A COMPRESSOR CASCADE NEAR STALL

Andrew J. H. Williams
Lieutenant, United States Naval Reserve
B.S., Purdue University, 1987

Submitted in partial fulfillment
of the requirements for the degree of

MASTER OF SCIENCE IN AERONAUTICAL ENGINEERING

from the

NAVAL POSTGRADUATE SCHOOL
June 1995

Author: 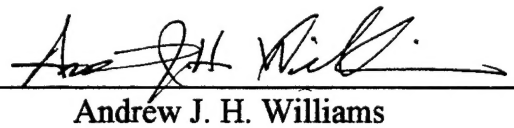
Andrew J. H. Williams

Approved by: 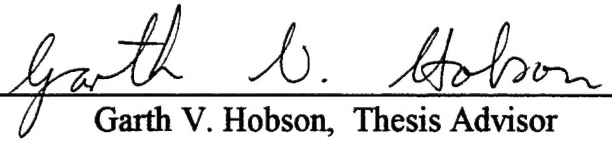
Garth V. Hobson, Thesis Advisor

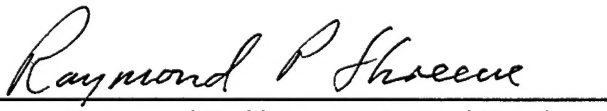
Raymond P. Shreeve, Second Reader

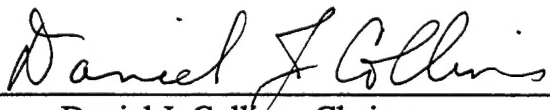
Daniel J. Collins, Chairman
Department of Aeronautical and Astronautical Engineering

ABSTRACT

Laser-Doppler velocimeter measurements were made in the flow field of a stalled cascade of controlled-diffusion stator blades. Tests were conducted at 10 degrees of incidence above the design inlet-flow angle in order to verify previous measurements. A unique method of data presentation was offered to characterize the unsteady positive and negative velocities about their mean. Laser-sheet flow visualization was performed and showed the unsteadiness of the stalling phenomena within the blade row passages. Additionally, a leading-edge separation bubble was observed and reversed flow was measured within the bubble using the laser-Doppler anemometer. Power-spectral density and auto-correlation analysis results are presented. In parallel with the experimental measurements, a computational fluid-dynamics study was initiated in an attempt ultimately to predict stall. Viscous flow computations were completed at on-design and near-stall conditions. Pressure distributions, separation bubble re-attachment locations, and loss predictions were compared to previous experimental studies. Generally good agreement was obtained for on-design conditions with degradation in prediction nearing stall.

TABLE OF CONTENTS

LIST OF FIGURES

LIST OF TABLES

ACKNOWLEDGMENTS

I would like to thank Dr. Garth Hobson for his tireless enthusiasm towards my work. It kept me motivated throughout. Thanks to Dr. Raymond Shreeve for first putting the curiosity there. And to Rick Still and Ted Best for their technical expertise and support. Finally, to Dawn, my wife and best friend, who supported what I believed to be important work while tending to far greater work at home ... our girls, Jessica and Sydney.

I. INTRODUCTION

Compressor stall and off-design behavior impose performance constraints on gas turbine engines. The open literature currently lacks adequate documentation of quantitative measurements of turbomachinery flow fields at and beyond stall. This knowledge is essential for predicting the onset of stall with computational methods and optimizing blade geometries for off-design range with minimal degradation in design-point performance. Towards optimum design-point performance, controlled-diffusion (CD) blading was developed. The purpose of these blades was to avoid boundary layer separation and, in the case of supercritical (SC) blading, to be shock-free in the transonic range.

Extensive laser-Doppler velocimeter (LDV) investigations [Refs. 1 - 3] of flow through a controlled-diffusion compressor cascade have been conducted in the region below stall at the Naval Postgraduate School (NPS). Recently, the reported cascade was stalled with an inlet-flow angle of 50 degrees and an extensive mapping of the flow field was performed using a two-component LDV system by Ganaim [Ref. 4]. The motivation for the present study was to partially map the flow field near stall and to establish the repeatability of the results reported in Reference 4. Between Ganaim's work and the present, the tunnel was reconfigured twice to pre-stall flow angles. This was done to confirm the repeatability of the flow field and to expand the available database for unsteady separated flows. Also, since the previous data were presented on a mean-flow basis, it was desired to more properly characterize the mean flow into its positive and negative components. This required a special method of post-processing the velocity-histogram data, as described within this report.

It was also desired to characterize the unsteady flow using power-spectrum and auto-correlation analyses. It was hypothesized that there could exist a fundamental frequency for the stalled cascade, that it could be determined from the measurements made in the present study and should match that of the previous data [Ref. 4].

In parallel with the LDV study, a computational fluid dynamics (CFD) study was initiated in an attempt ultimately to predict stall. Previous CFD studies on the present

cascade include those of Elazar [Ref. 1], Stow, et al [Ref. 5], Hobson [Ref. 6], and Kang, et al [Ref. 7].

Before attempting to calculate the unsteady, stalled, flow through a cascade (as was measured in the present study), it was necessary first to evaluate the code's predictive ability at incidence angles off-design and near the stall point. A quasi-three-dimensional computer code [Refs. 8-9] for the solution of the thin-layer Navier-Stokes equations was used to predict the cascade performance from design (40 degrees inlet-flow angle) to near stall (48 degrees inlet-flow angle). The code was used to successfully compute the blade surface pressure distribution, the leading edge separation bubble and total pressure loss coefficient, for inlet flow angles from 40 to 48 degrees.

II. EXPERIMENTAL SETUP

A. LOW-SPEED CASCADE WIND TUNNEL

The subsonic cascade wind tunnel contained 20 controlled-diffusion blades. Each blade was 10 inches in span, 5.01 inches in chord and separated by 3 inches in the pitchwise direction. The cascade solidity (blade chord-to-pitch ratio) was 1.67 and Reynolds number based on chord was approximately 700,000. A detailed description of the test facility, test section and CD blading was fully documented in Reference 1. Figure 1 shows a schematic of the cascade. The tunnel was configured for an inlet-flow angle (β_1) of 50 degrees, and an exit-flow angle (β_2) such that the downstream end-wall static pressure distribution was uniform.

B. INSTRUMENTATION

Blade surface pressure measurements were recorded using a 48-channel Scanivalve system controlled by an HP-9000 computer. Figure 1 shows the "fully-instrumented blade" location within the test section. Reference 1 gives the location of the blade surface pressure points. A full description of the data acquisition system is given in Reference 10.

A two-component, four-beam TSI Model 9100-7 LDV system was used for all flow field measurements. The LDV setup, including laser type, optics, atomizer, seeding, traverse mechanism and data acquisition were thoroughly documented in Reference 4.

The flow was visualized by injecting fog particles of 2 μm in size through a wand inserted through the end wall upstream of the blading. A 300 mW air-cooled argon-ion laser was used as the light source for laser-sheet flow visualization. The laser beam was transmitted to a lens system via a fiber-optic cable. The lens system ended with a cylindrical-plano lens, which produced the laser sheet. The laser sheet was introduced into the cascade tunnel, ahead of the blades, through the sidewall. A schematic of the system, showing the location of the introduction of the fog and the position of the video camera (located outside the window), are shown in Figure 2.

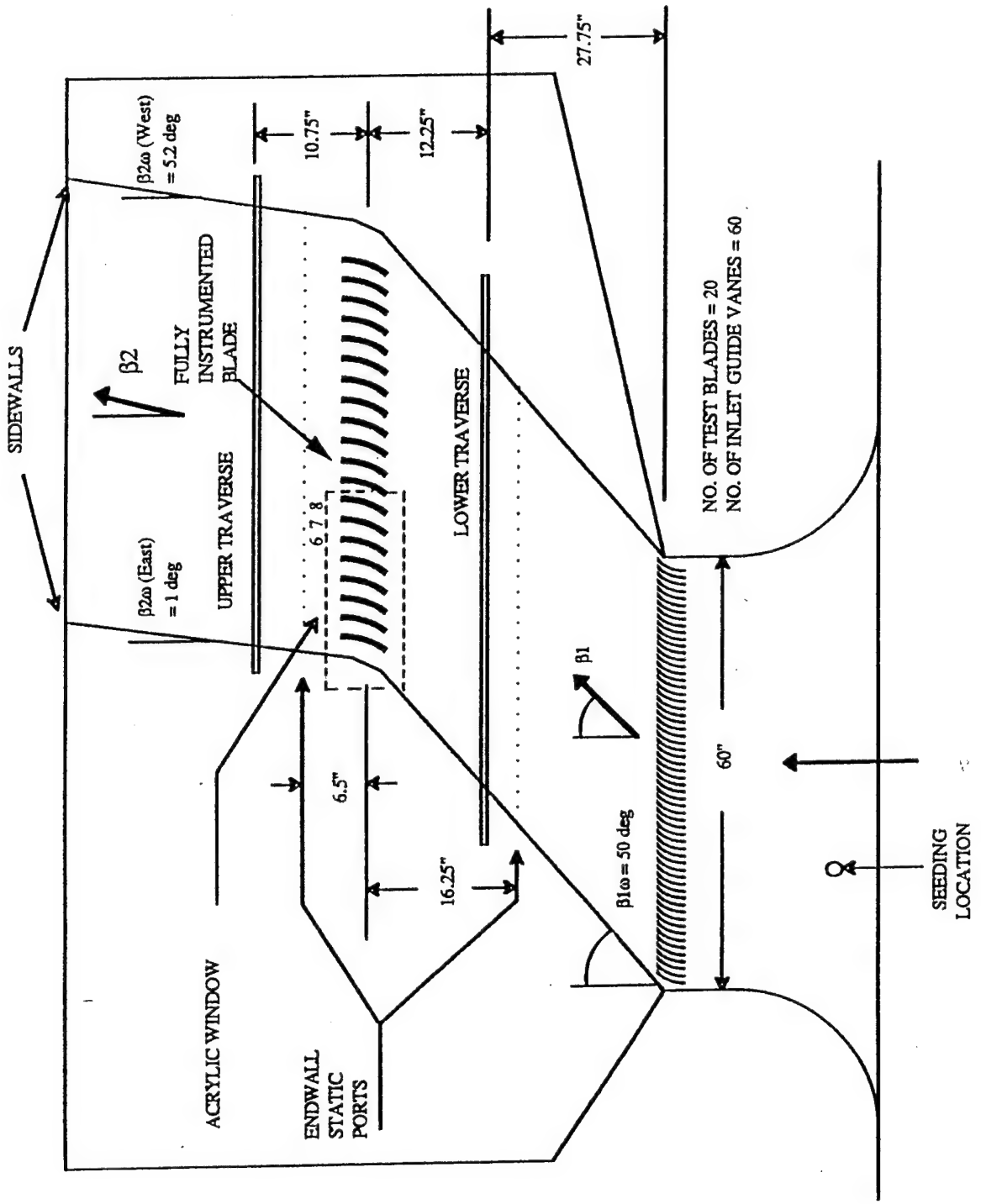

Figure 1. Schematic of the Cascade Wind Tunnel

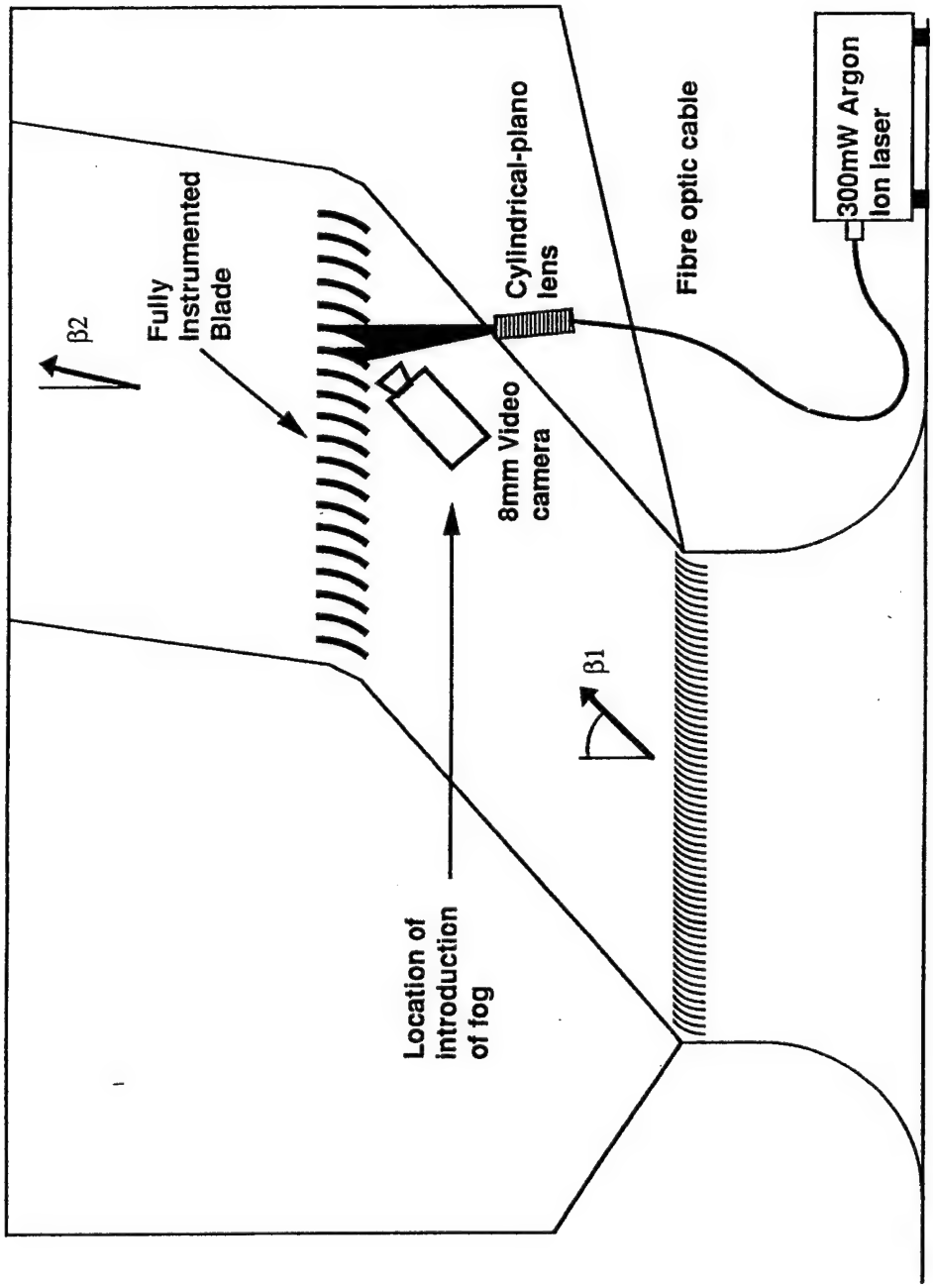

Figure 2. Laser-Sheet Flow-Visualization System

C. EXPERIMENTAL PROCEDURE

1. Surface Pressure Measurement

The tunnel plenum chamber pressure was set at 12 inches of water (gauge) and the blade surface pressure measurements were taken as described in Appendix B of Reference 10. Inlet total and static pressures were recorded 2 1/3 chord lengths ahead of the blades. These pressures were used to non-dimensionalize the blade-surface pressure measurements as a coefficient of pressure; i.e., $C_p = (p_{local} - p_\infty) / (p_{t\infty} - p_\infty)$.

2. LDV Measurements

A full listing of the experimental runs is contained in Appendix A. Blade-to-blade surveys were conducted at eleven stations ahead of, between, and downstream of the blade row. All surveys were taken by collecting 3,000 data points at each location in the survey. All LDV data were collected in the "coincidence mode" with a 2.0×10^5 μsec window used for validation. Table 1 summarizes the survey stations and locations. Figure 3 illustrates the same information graphically. The numbers in parentheses on the figure indicate the horizontal distance between measurement points. The present study gave an average inlet-flow angle of 50.05 degrees. Reference 4 results were for an average β_1 of 50.21 degrees.

Station	Region	Location (% Axial Chord)
1	Inlet	30.9 % forward of LE (1.5 inches forward of LE)
1b	"	4.28 % "
1d	"	1.00 % "
2a	Passage (Suction Side)	0 % @ LE
3	"	5.15 % aft of LE
7	"	30.9 % " (1.5 inches aft of LE)
14	"	93.6 % "
15	"	98.7 % "
17	Wake	6.18 % aft of TE
18	"	12.7 % "
19	"	20.6 % " (1.0 inches aft of TE)

Table 1. LDV Survey Stations and Locations

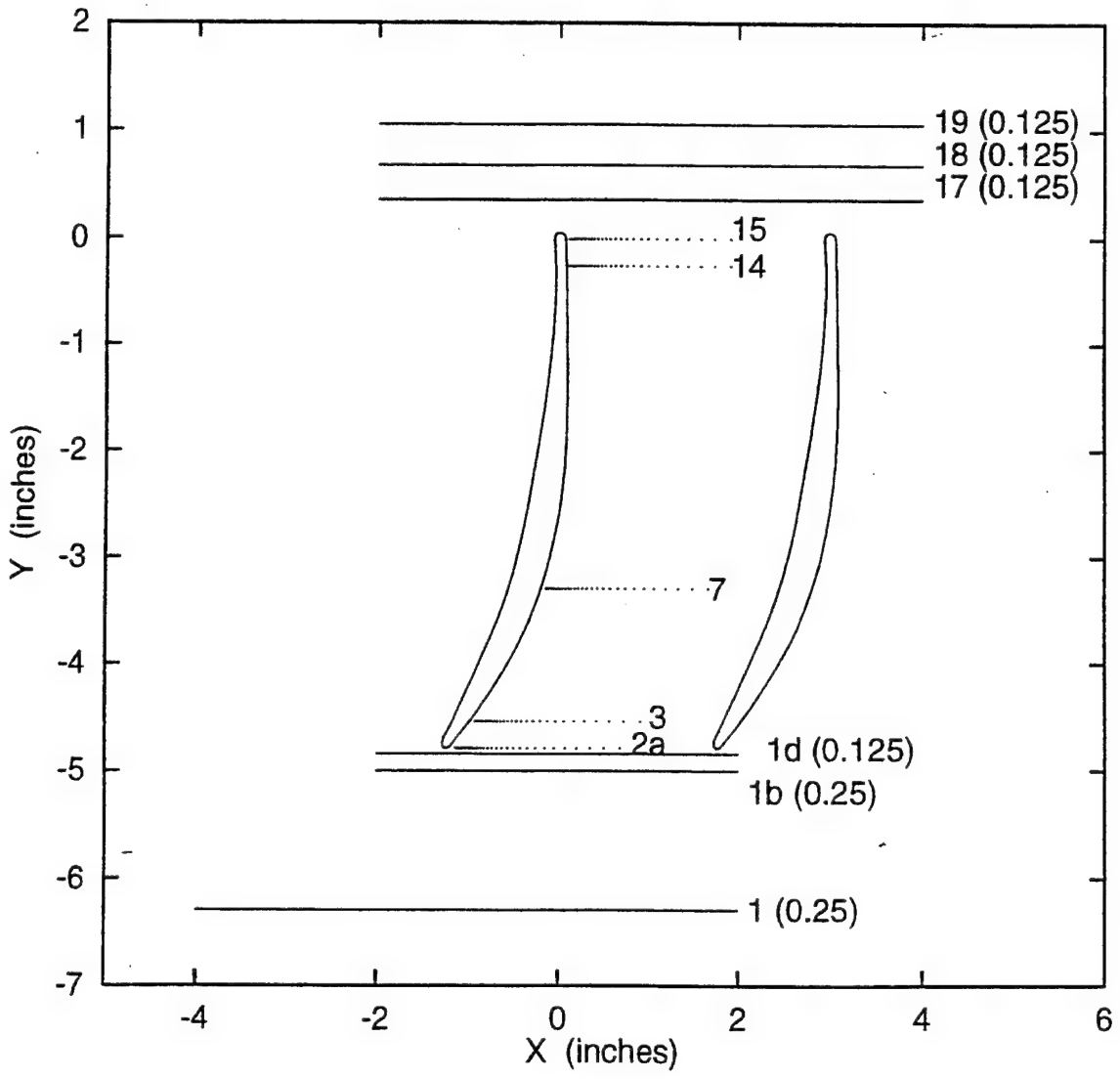

Figure 3. LDV Survey Stations Between Blades 6 and 7

Additionally, eleven specific locations were measured, with an increased number of data points, for power-spectrum and auto-correlation analyses. Table 2 below summarizes the measurements and the number of data points gathered for each point. Figure 4 depicts the stations at which these dedicated runs were performed. The points close to the blade were chosen to be within the intermittent reverse-flow region, and the outboard points were chosen to be outside the reverse-flow region.

Station	Point	Location	Number of Points Acquired
1	9	(0.0000, -6.2920)	3K, 30K, 50K
2a	1	(-1.1331, -4.7905)	3K, 30K
3	7	(-0.8394, -4.5420)	3K, 30K
7	3	(-0.1225, -3.2920)	3K, 30K
7	20	(0.3654, -3.2920)	3K, 30K
10	15	(0.3988, -1.7921)	30K
10	25	(1.0000, -1.7921)	30K
17	23	(0.2500, 0.3620)	30K
17	31	(1.5000, 0.3620)	30K
19	23	(0.2500, 1.0620)	30K
19	31	(1.2500, 1.0620)	30K

Table 2. LDV Power-Spectrum / Auto-Correlation Locations

The tunnel reference velocity (V_{ref}) for each run was computed as described by Elazar in Reference 1. The results are shown in Appendix B. The reference velocity was used to non-dimensionalize the data for comparison with previous studies.

Prior to each run, the probe volume was always referenced to the same location between the blades using an alignment tool. This allowed for a high confidence level in specifying station position for comparison with previous studies. The alignment procedure was developed and described in detail in Reference 1.

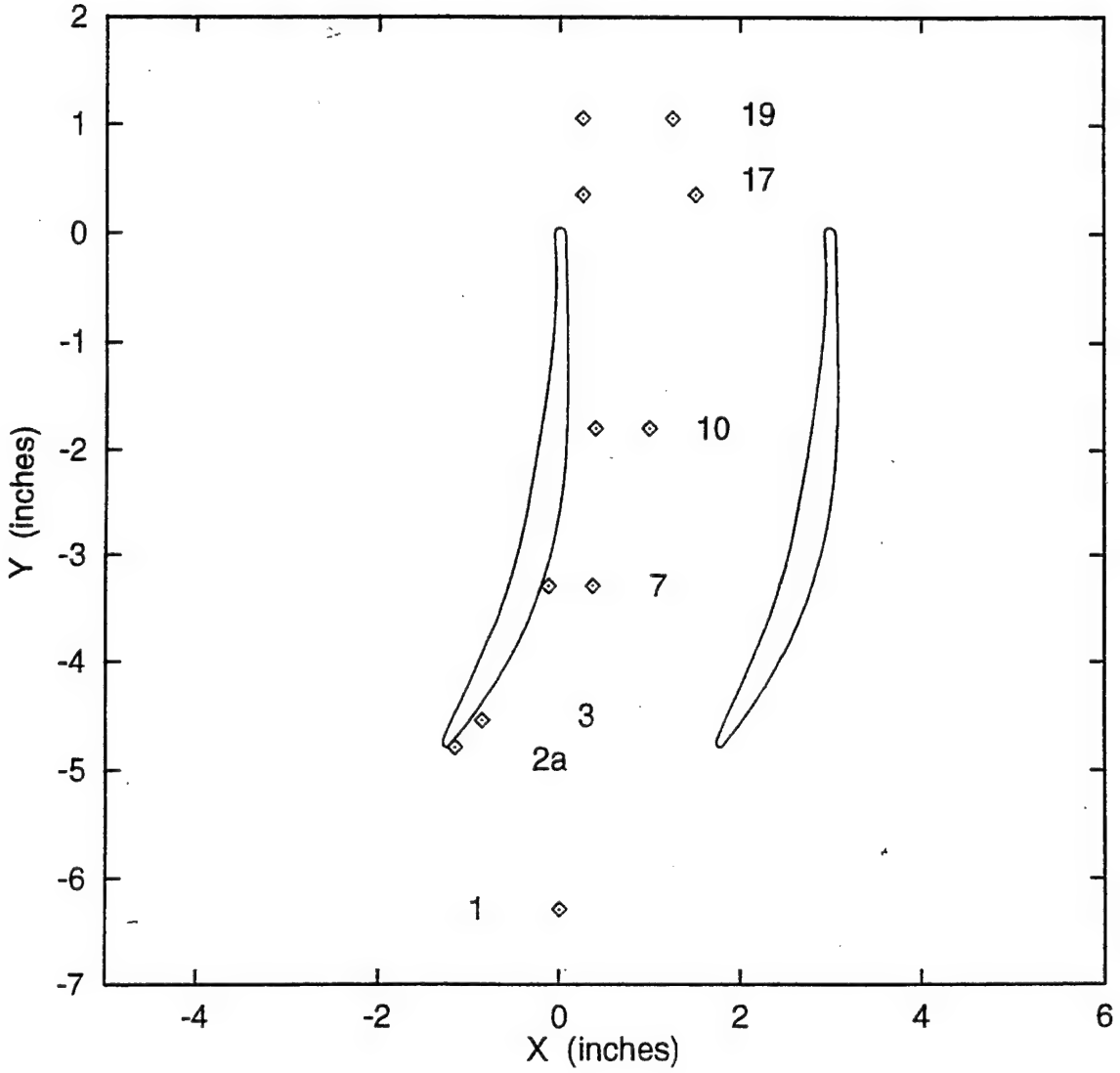

Figure 4. LDV Power-Spectrum / Auto-Correlation Locations

a. Inlet Surveys

The inlet region was surveyed across stations 1, 1b, and 1d (Figure 3). The survey spanned three and one-third passage widths in the pitchwise direction (-9 inches to +1 inch) for station 1, and one and one-third passage widths in the pitchwise direction (-2 inches to + 2 inches) for stations 1b and 1d. The laser beam system was horizontal when measuring at station 1. A 4 degree pitch-up of the LDV table was required for stations 1b and 1d to avoid blade shadowing of the vertical beam, and to achieve closer access to the leading edge. The potential problems due to pitching and yawing the LDV system were treated by Hobson and Shreeve in Reference 3. Their analysis showed the maximum spatial error due to probe volume orientation to be 0.3 mm, which is the minimum diameter of the measurement volume.

The optics were configured the same throughout the present study with the 488-nm blue beam measuring the horizontal (U) component and the 514.5-nm green beam measuring the vertical (V) component. Frequency shifting was performed as outlined in Reference 4 in order to capture the large reversed-flow velocities.

b. Passage Surveys

The passage surveys were performed between blades 6 and 7. All passage surveys extended 1.8 inches (approximately 60 % passage width) away from the suction-side surface of blade 6. The LDV system was pitched up 2 degrees and yawed 4 degrees left for stations 2a, 3 and 7 for better access to the suction side of the blade. Stations 10, 14 and 15 were measured with only 4 degrees of left yaw.

c. Wake Surveys

The LDV system was reset to zero pitch and zero yaw for measurements at stations 17, 18, and 19. The wake surveys were centered around blades 6 and 7 and spanned two passage widths (6 inches).

d. Laser Power-Spectrum / Auto-Correlation Measurements

It was desired to expand the analysis of several points throughout the flow field by collecting a larger amount of data points. Instead of the standard 3,000 points

gathered at each location, 30,000 data points were chosen for the locations listed in Table 2. This choice corresponded to the limiting number of data points that could be acquired at positions with low data rates such that the acquisition software reached its maximum timeout of 30 minutes. This corresponded to a minimum data rate of 16.7 Hz in order to collect 30,000 samples. Stations 2a and 3, near the separation-bubble region, were most affected by this limitation.

3. Flow Visualization

The laser-sheet flow visualization was photographed through the optical access window using a hand-held 8mm camera at 30 frames/second and a VHS camera at 60 frames/second. The filming was performed at night to reduce glare and optimize the flow field image contrast. A total of approximately 15 minutes of footage was obtained of the intermittent reversed flow inside the blade passage and of the flow near to the passage entrance, including the leading-edge separation bubble.

III. COMPUTATIONAL FLUID DYNAMICS

A. GRID GENERATION

The grid generation program employed was a modified version of GRAPE (GRids about Aerofoils using Poisson's Equation), [Ref. 11]. This version allowed for the generation of a periodic C-type grid for turbomachinery cascades. The namelist input file, along with a description of the effort put forth in refining the leading edge geometry for the grid, is described in Appendix E.

The grid, a portion of which is depicted in Figure 5, contained 240 grid points wrapped around the blade in the streamwise direction and 49 grid points in the blade-to-blade direction. The grid was much finer in the normal direction near the surface for improved viscous flow resolution, particularly of the leading edge separation bubble. The outer, or periodic, boundaries corresponded in size to the cascade wind tunnel as described in Experimental Setup. The inlet region was located 30% of an axial chord upstream of the leading edge. The wake region extended two chord lengths downstream of the trailing edge.

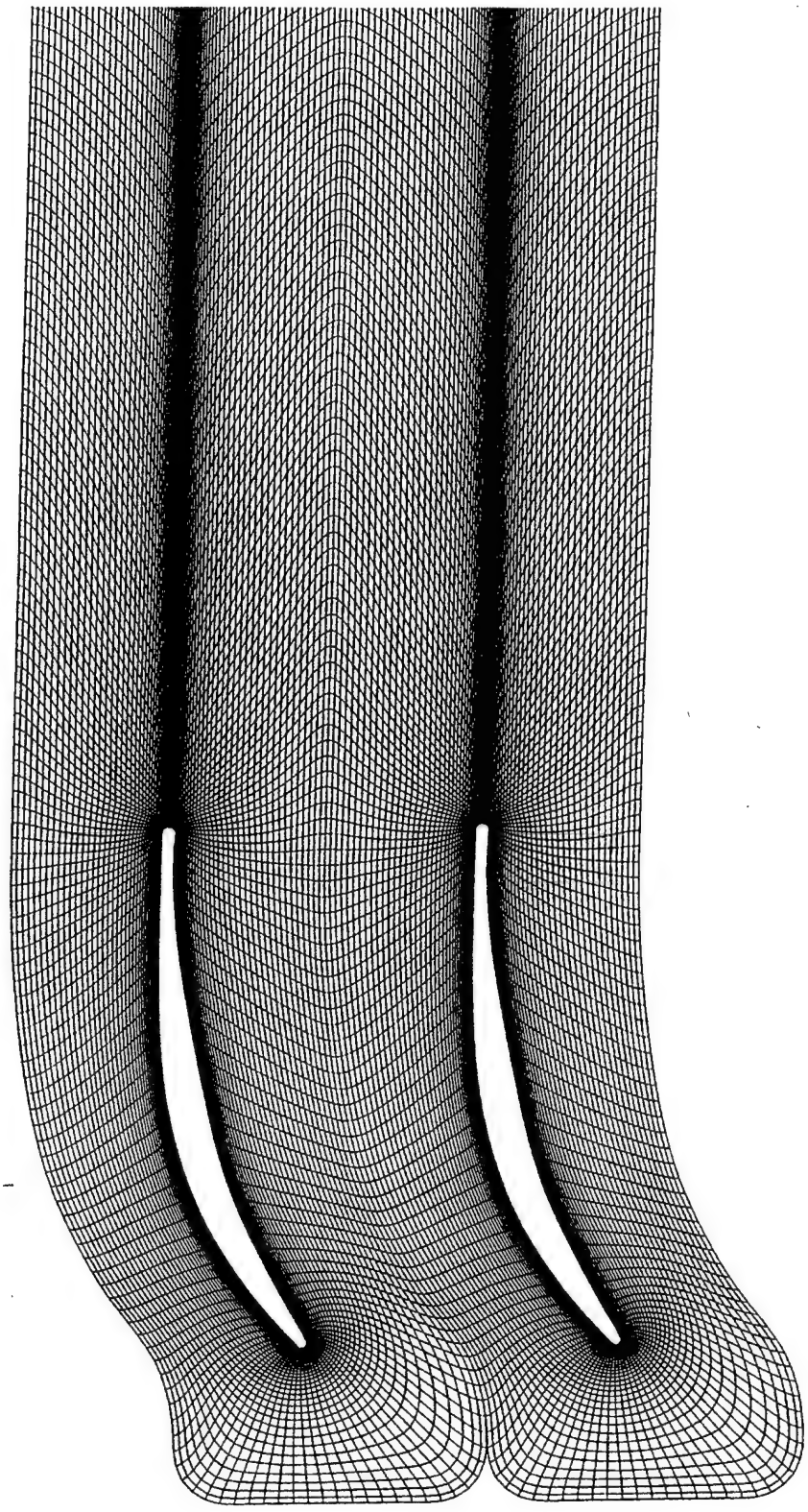

Figure 5. Two-Dimensional Periodic C-Grid

B. COMPUTATIONAL FLOW SOLVER

Numerical computations were made using Rotor Viscous Code Quasi-3D (RVCQ3D) of Reference 8. RVCQ3D solved the thin-layer Navier-Stokes equations by employing an explicit, multi-stage, Runge-Kutta algorithm. It could account for the effects of rotation, radius change and stream surface thickness variation in blade-to-blade turbomachinery flows. The Baldwin-Lomax algebraic eddy-viscosity model [Ref. 12] was used to characterize the turbulence within the flow field.

Computations were performed at the following inlet flow angles: 40, 43, 46, and 48 degrees. This was done to allow comparisons with existing experimental results. Validation of the computed results was achieved by comparing pressure coefficient distributions around the blade surface, leading-edge separation bubble sizes, and loss computations.

A typical namelist input file is shown in Appendix F. All solutions were run to 6,000 iterations and axial-velocity-density ratio (AVDR) was held at 6% for all computations. The AVDR was modeled by defining two stream surface points at the inlet and exit using the namelist 6 parameter 'NMN' as shown in Appendix F.

Although the inlet flow angle was specified initially, the flow solver computed to a new inlet condition based on the prescribed exit-static to inlet-stagnation pressure ratio. The inlet flow angle varied due to changes, primarily, in the tangential velocity component, as the axial velocity did not change due to continuity constraints.

Solutions were computed using the National Aerodynamic Simulation (NAS) Program CRAY C90 supercomputer and the NPS CRAY Y-MP EL98 supercomputer. CPU run time for the NAS C90 was between 3-4 minutes and the NPS EL98 required about 55 minutes. Analysis of the solution files was carried out using FAST graphics software [Ref. 13] and separate FORTRAN programs given in Appendices H (blade-surface pressure distribution) and I (computed inlet-region flow angle).

IV. RESULTS AND DISCUSSION

A. BLADE-SURFACE PRESSURE COEFFICIENT

A comparison of pressure coefficient around the blade surface between the present study and Reference 4 is shown in Figure 6. The results, after reconfiguring the tunnel, showed reasonable agreement with the pressure distributions obtained earlier at the leading edge; particularly on the pressure side. There was some difference near the trailing edge which was possibly due to a difference in setting of the tunnel's exit-plane tailboards. The setting of the tailboards significantly affected the exit static-pressure distribution.

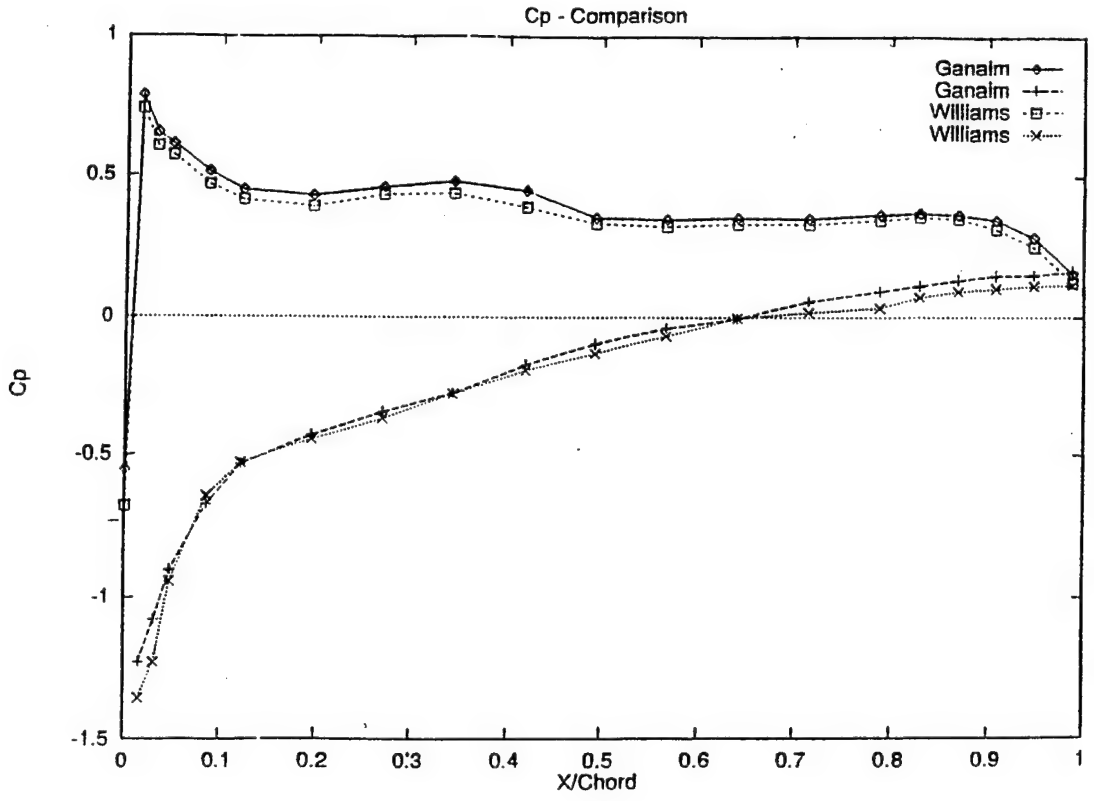

Figure 6. Pressure Distribution Comparison

B. LDV SURVEY COMPARISONS

The data analysis and comparisons which follow were performed without any refinement bounds for the velocity histograms. All the results from Reference 4 were re-analyzed in this manner.

1. Inlet Survey (Station 1)

Figures 7 and 8 show the non-dimensionalized mean velocity and turbulent intensities, respectively. The two studies showed variations in the mean velocity of less than 2% across three passage widths. The period in the variation in the mean velocity corresponded to the 3 inch blade separation, indicating that the blades were felt 30% of an axial chord ahead of the leading edge. The U and V turbulence-intensity levels were similar, and this indicated the turbulence was isotropic at the inlet. The increase in turbulence intensity from 2% to 4% over the extent of the survey is noted. This behavior was not observed at lower inlet-flow angles.

2. Passage Survey (Station 7)

Mean-flow results for station 7 are presented in Figure 9. There was good agreement across the passage which further established repeatability with Reference 4's results. The turbulence intensity in Figure 10 also agreed well and showed anisotropic behavior of the turbulence near the blade surface out to 50 % pitch. Beyond this point the turbulence became isotropic in the inviscid region, as the levels of turbulence in the U and V components were comparable. The data were presented as turbulence intensities, yet because the flow field was intermittently reversible the standard deviation of the histograms, given by the LDV, did not represent the turbulence in the flow. Rather, these should be looked upon as a measure of the unsteadiness in the flow, which was a combination of the random turbulence and intermittent reverse flow.

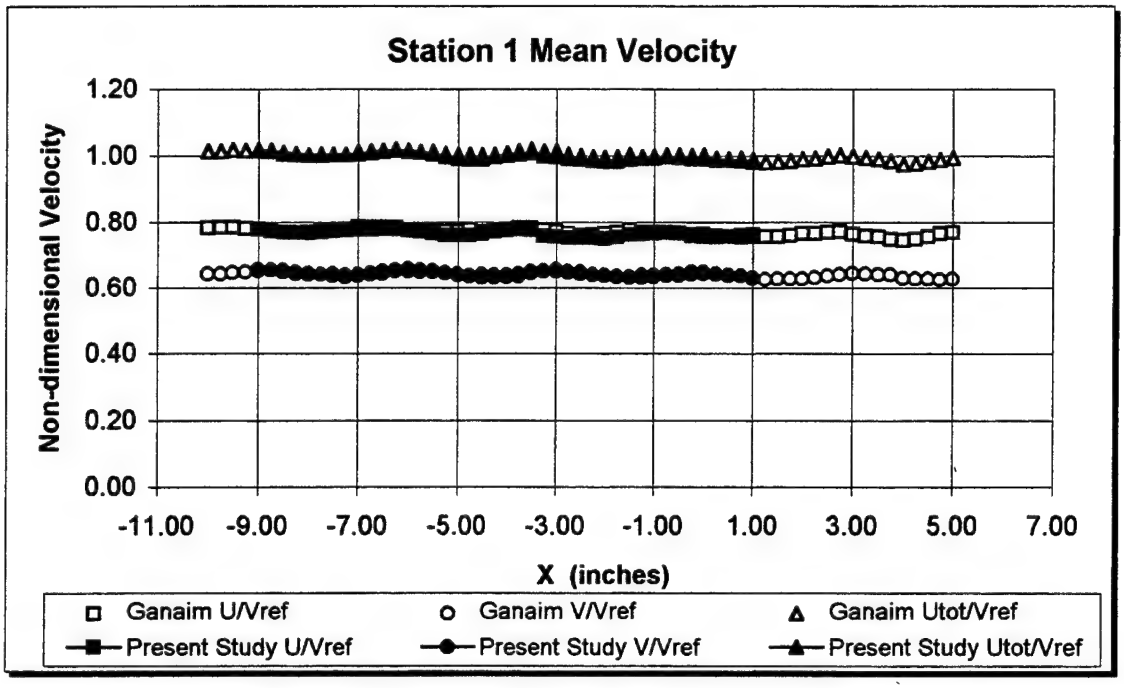

Figure 7. Velocity Comparison at Station 1

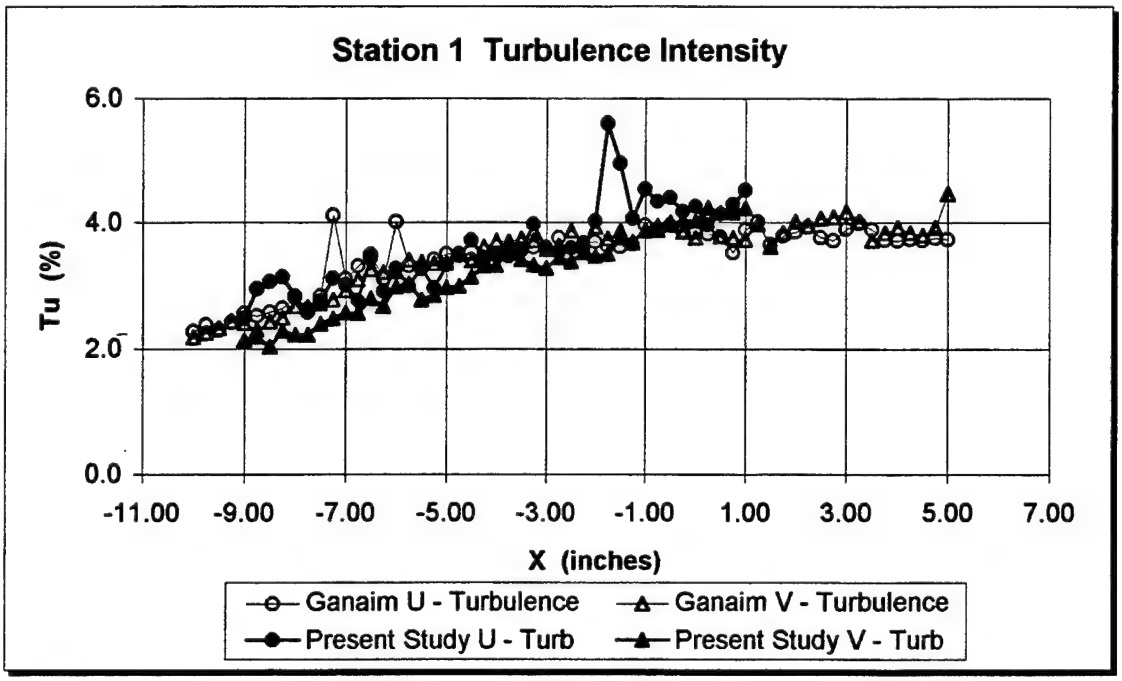

Figure 8. Turbulence Intensity Comparison at Station 1

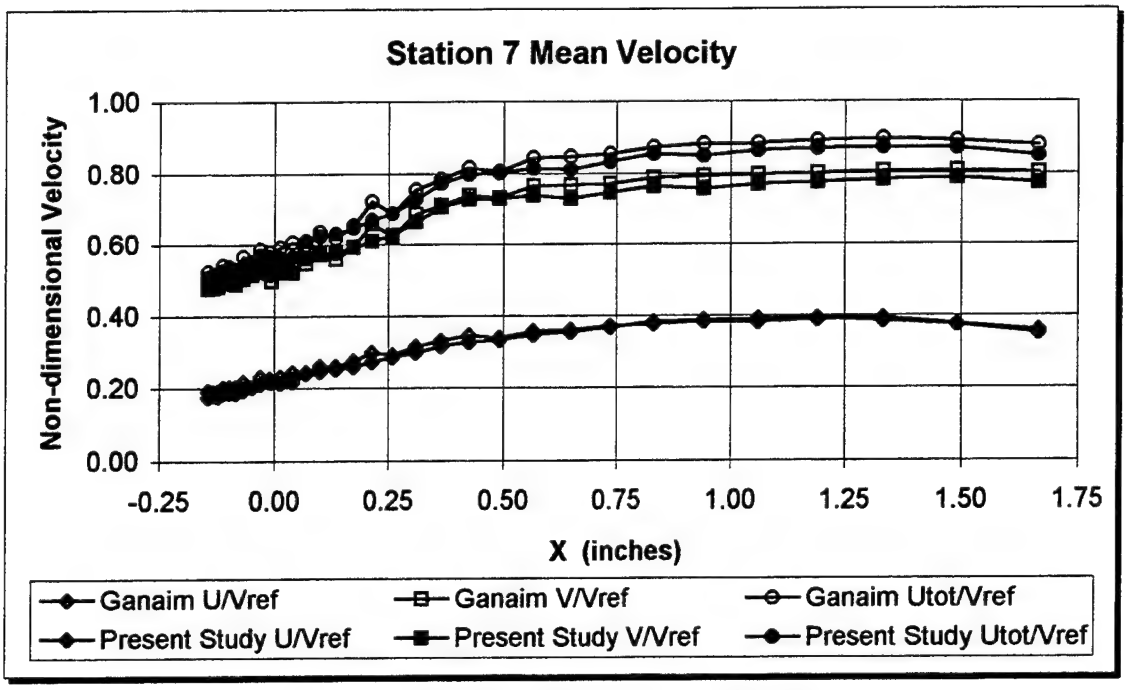

Figure 9. Velocity Comparison at Station 7

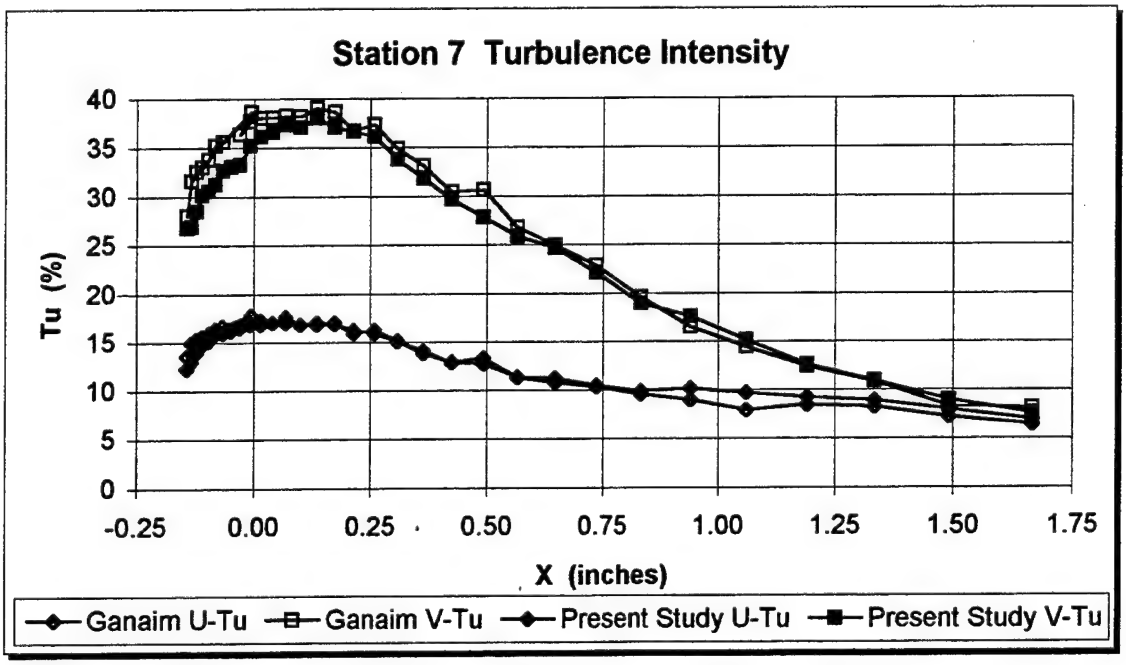

Figure 10. Turbulence Intensity Comparison at Station 7

Figures 11 and 12 separate the mean horizontal (U) and mean vertical (V) velocity components into their respective positive and negative mean values. The velocity histograms for each point across the passage were specially edited such that only negative velocities were retained and averaged to create a negative velocity trace and, likewise, only positive velocities were retained and averaged at each point to create a positive velocity trace. It was apparent from Figures 11 and 12 that the weighted average of the negative trace and positive trace would make up the mean velocity for each component across the passage as previously shown in Figure 9.

This analysis showed more of the character of the intermittent reversed flow than did a plot of the mean velocity. What occurred in the unsteady stalling process was not represented by the arithmetic mean. The envelope about the mean contained the positive and negative velocities that truly characterized the flow's behavior. Since the data were taken in coincidence mode, one disadvantage of this form of presentation was that during editing of the positive U velocity-component data, all of its negative points were discarded, as well as the corresponding V velocity-component data. The opposite but equivalent process occurred during editing of the V velocity component; such that all the data that were left were the velocity components in the first quadrant of a flow that was oscillating with components in all four quadrants. It was apparent from the figures that by 30 % pitch, the flow no longer exhibited reverse velocities in either the U or V components.

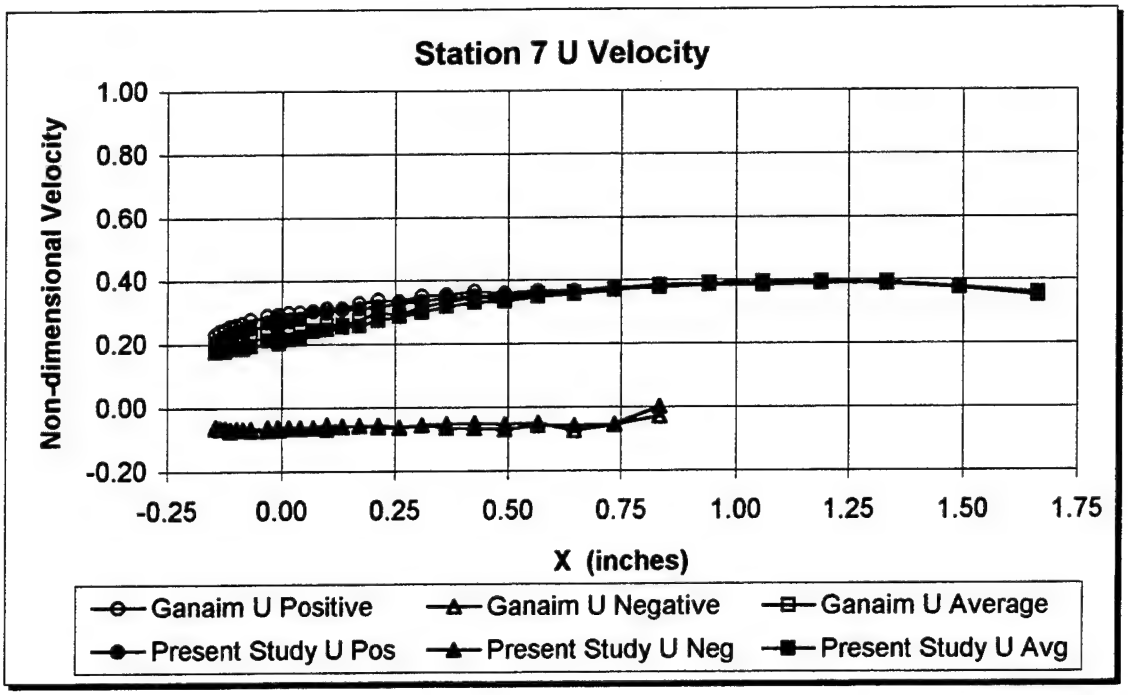

Figure 11. U Velocity Comparison at Station 7

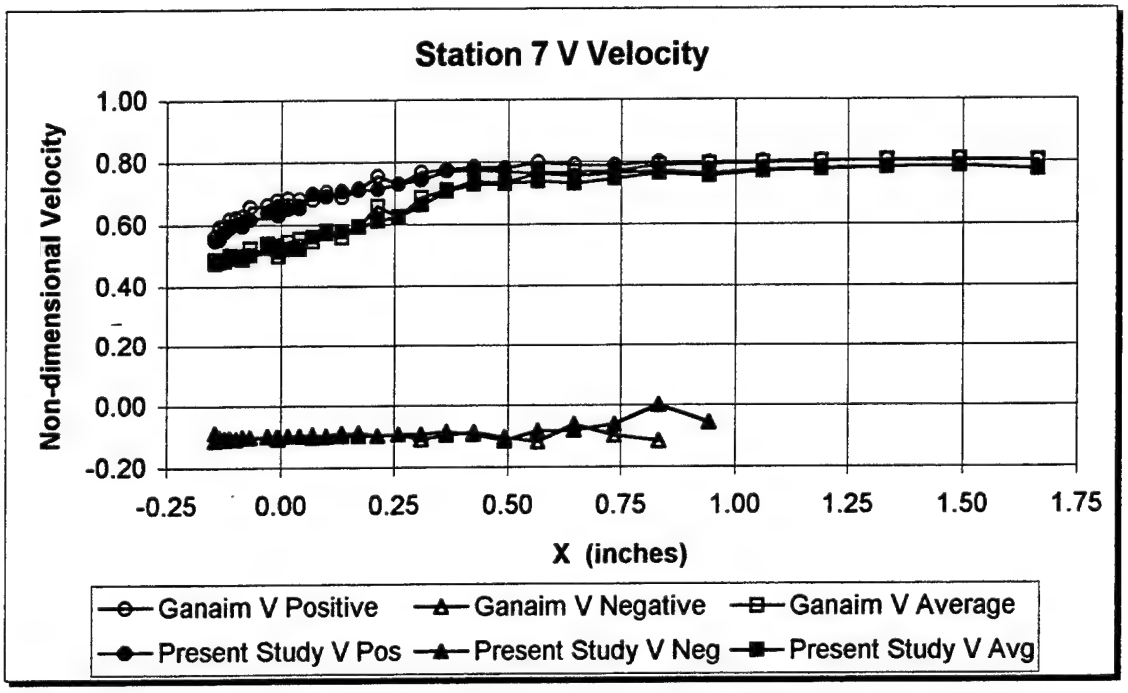

Figure 12. V Velocity Comparison at Station 7

3. Wake Survey (Station 19)

The wake surveys were compared at station 19. Figures 13 and 14 show the results and indicate good general agreement for the mean velocity and turbulence intensity/unsteadiness across two passage widths for the two studies. The periodic influence of the blades was strongly evident in the V component of Figure 13. Also, the asymmetry of the wake was especially apparent with the larger velocity deficit on the suction side of the blade. Figure 14 once again points out the anisotropic behavior of turbulence/unsteadiness in this same region.

Figures 15 and 16 are the results of the special editing as outlined for station 7 in Figures 11 and 12. It was of interest to note that the V-component reversed-flow velocities at station 19 were of the same magnitude as the V-component reversed-flow velocities at station 7.

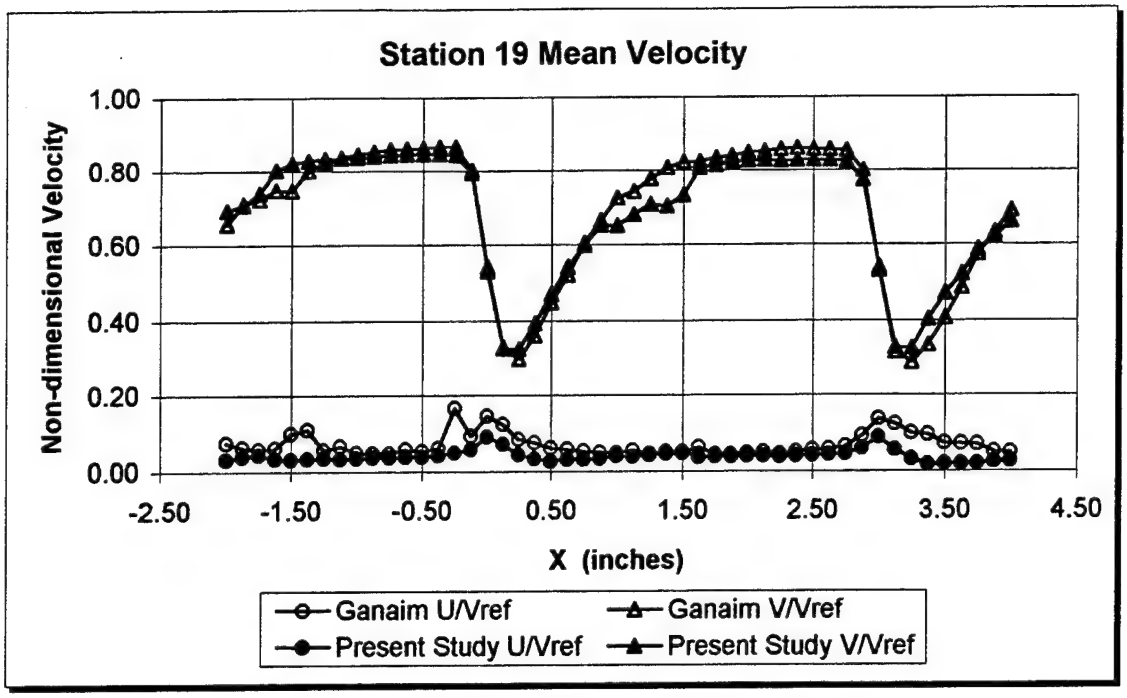

Figure 13. Velocity Comparison at Station 19

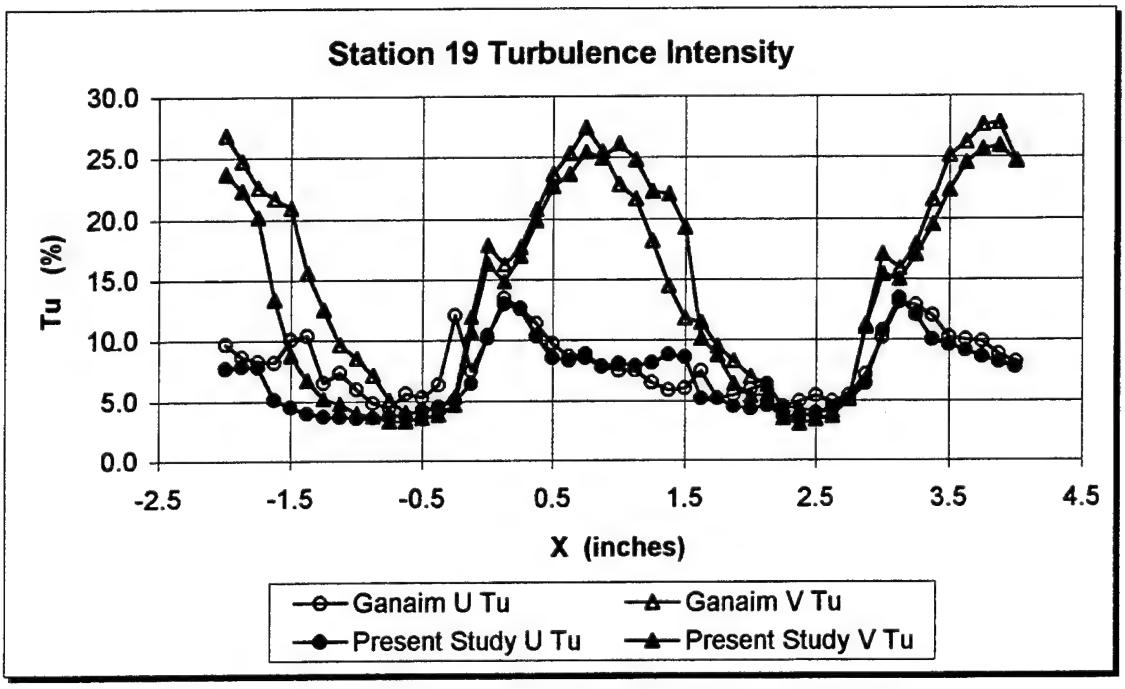

Figure 14. Turbulence Intensity Comparison at Station 19

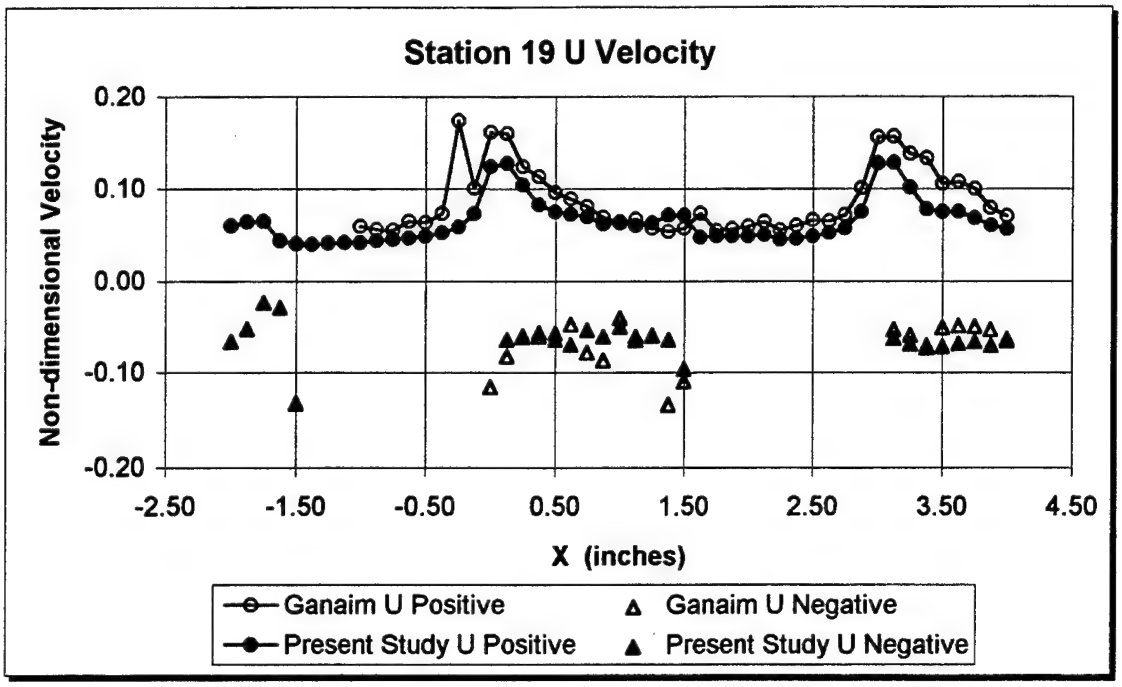

Figure 15. U Velocity Comparison at Station 19

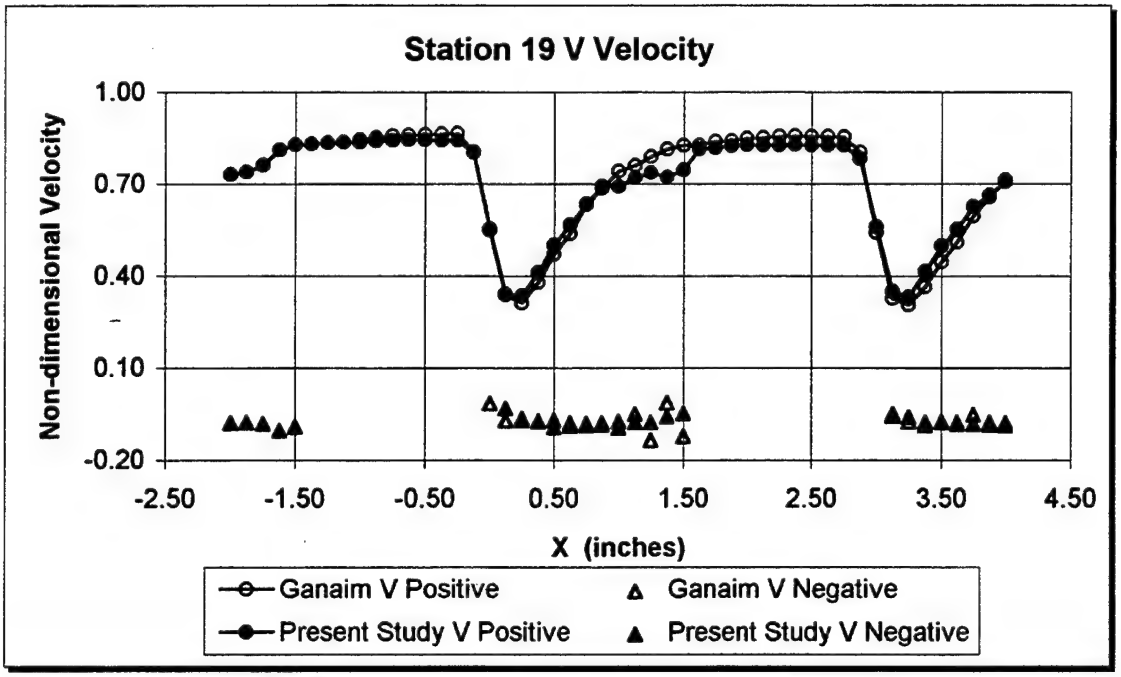

Figure 16. V Velocity Comparison at Station 19

C. PASSAGE SURVEY (STATION 3)

Measurements obtained at 32 locations at station 3 are shown in Figures 17-20. A detailed analysis to resolve the unsteady characteristics of the flow was made at the three locations (1, 7 and 20) shown in Figure 17 (U component of velocity) and Figure 19 (V component of velocity). The histograms of the U and V components of velocity at the three locations are shown in Figure 18 and Figure 20, respectively. Point 1 was located just off the blade surface. This was inside the leading-edge separation bubble, evidenced by the negative mean velocity of all the data points in the histogram (Figures 18a and 20a). The second location (point 7) was at 2.5 % pitch. This point was within the intermittent reversed-flow region, as indicated by the bi-modal velocity histograms (Figures 18b and 20b). The third location (point 20) was at 17 % pitch, and was outside the region of intermittent reversed-flow.

Figure 17 shows the mean pitchwise velocity along with the separate averages of the positive and negative components. The progression from a negative mean velocity to a positive mean velocity was apparent with the crossover distinctly evident in the bi-modal histogram at point 7. It was of interest to note that the arithmetic mean for the flow rarely occurred. The negative and positive velocity peaks were predominant, which was indicative of the unsteady stalled flow.

The streamwise and pitchwise velocity component behavior at station 3 appear to be similar because the blade surface was oriented at approximately 45 degrees to the two pairs of laser beams (X-Y axes for the velocity measurements). Figure 21 provides an alternate view of the previous data by plotting the pitchwise (U) and axial (V) velocity components together.

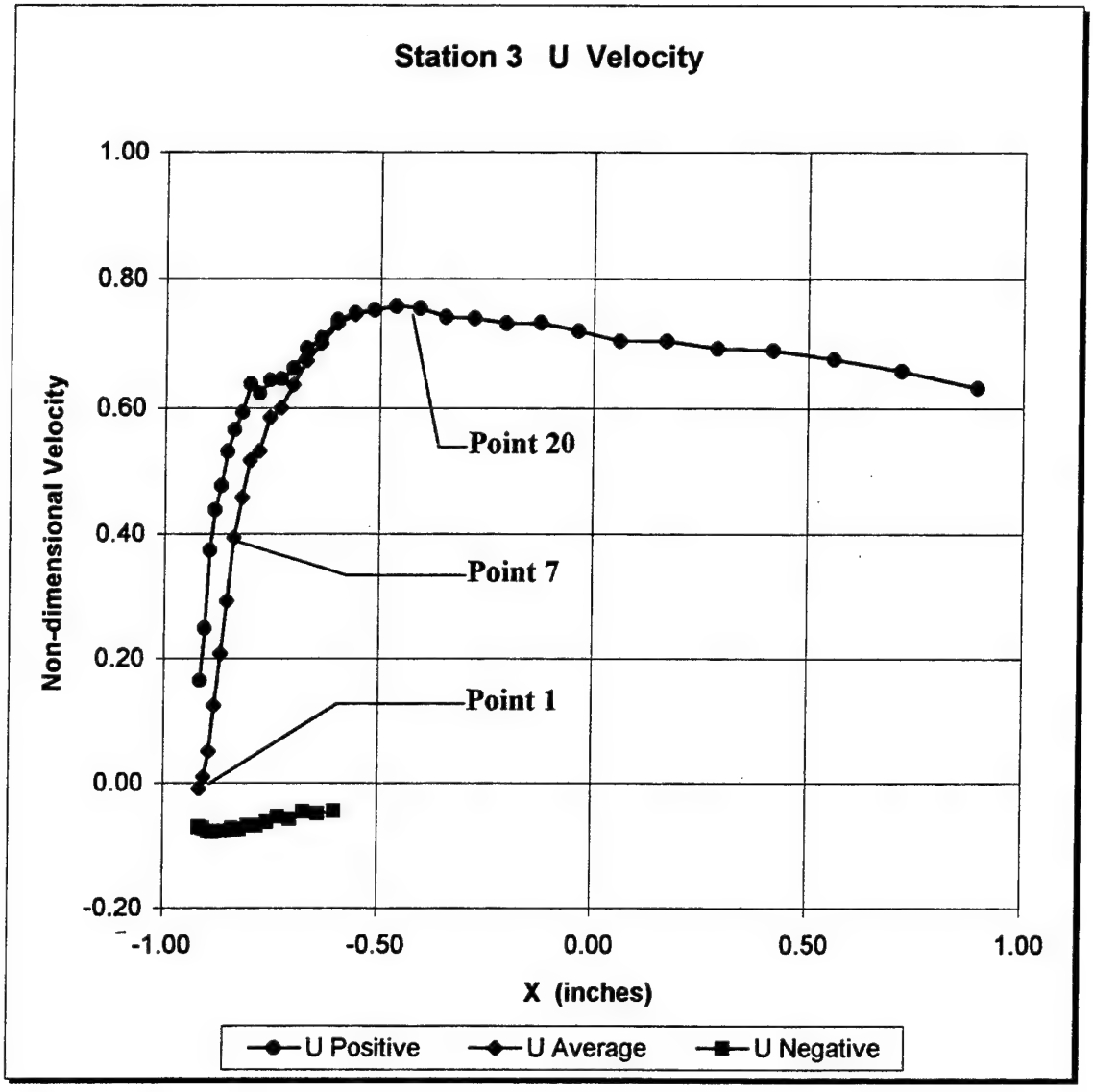

Figure 17. U Velocity Survey at Station 3

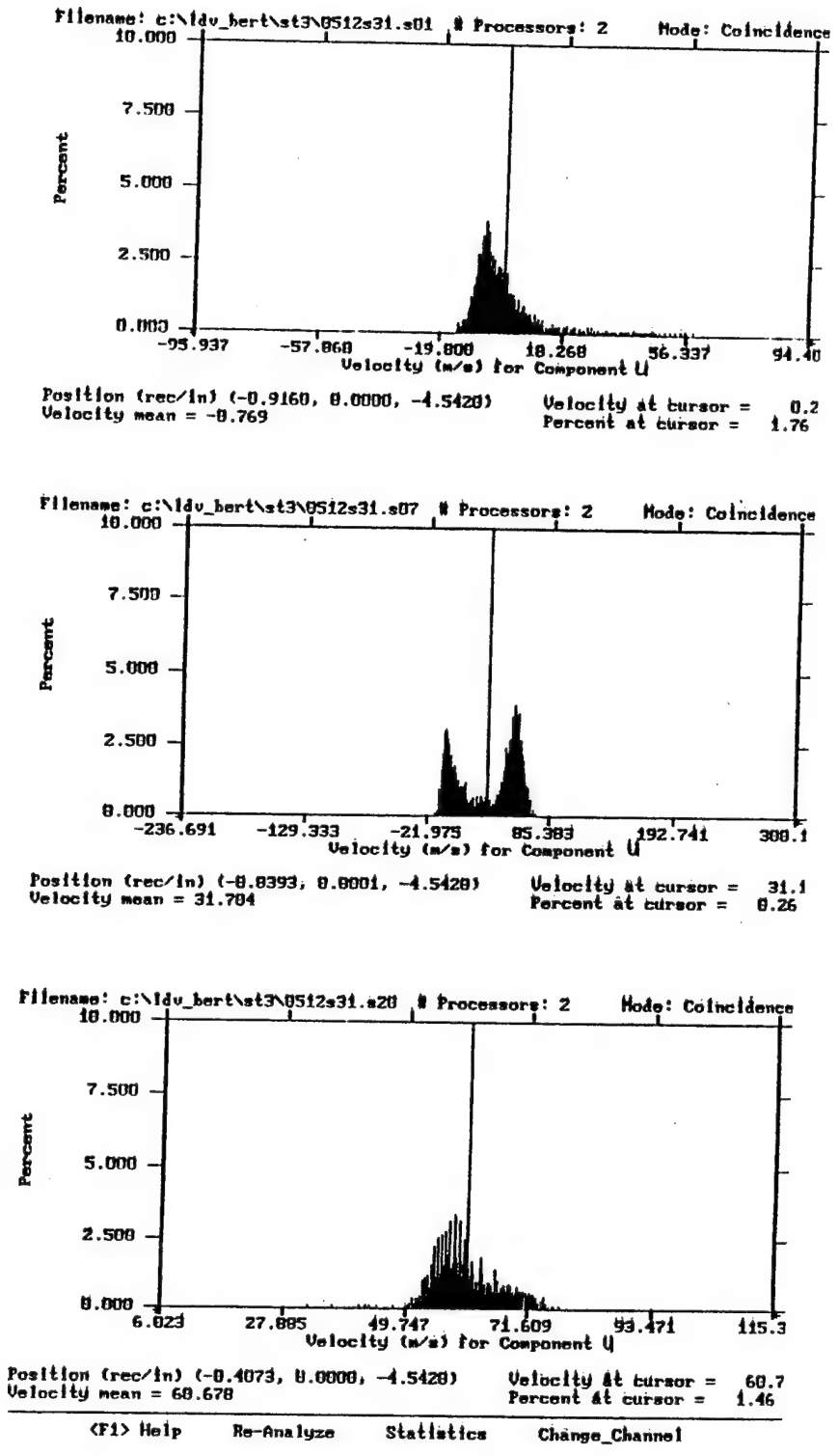

Figure 18. U Velocity Histograms at Station 3

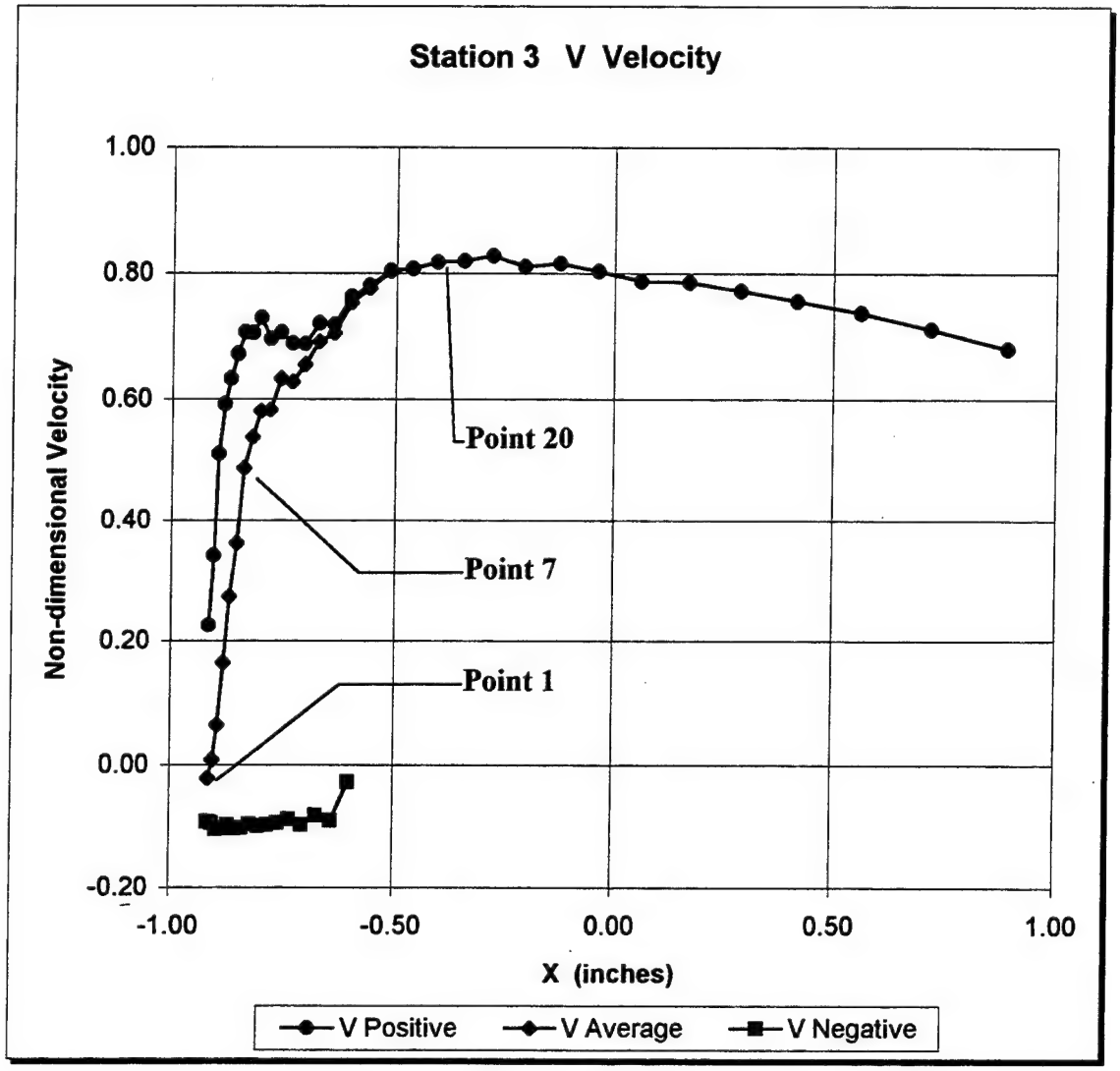

Figure 19. V Velocity Survey at Station 3

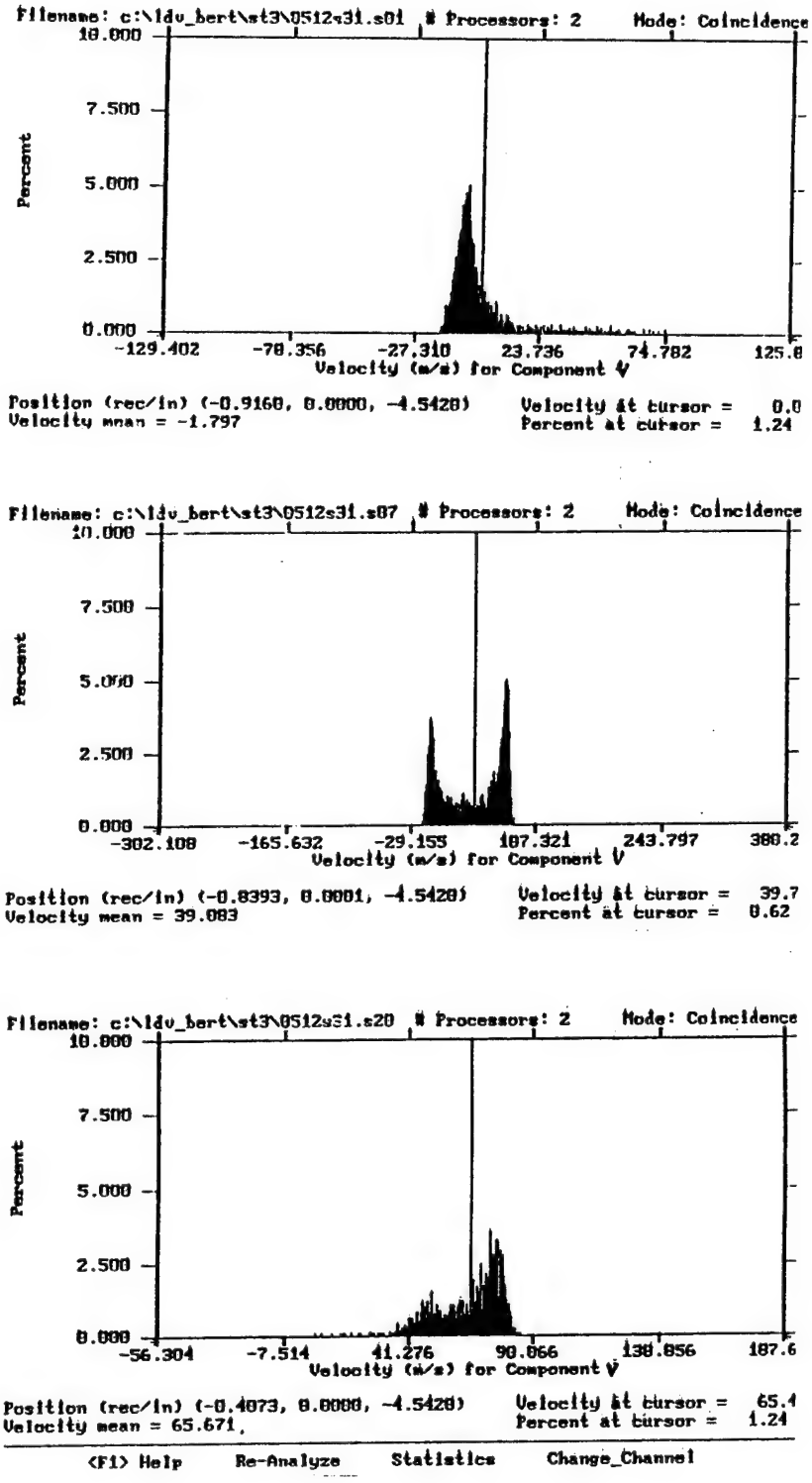

Figure 20. V Velocity Histograms at Station 3

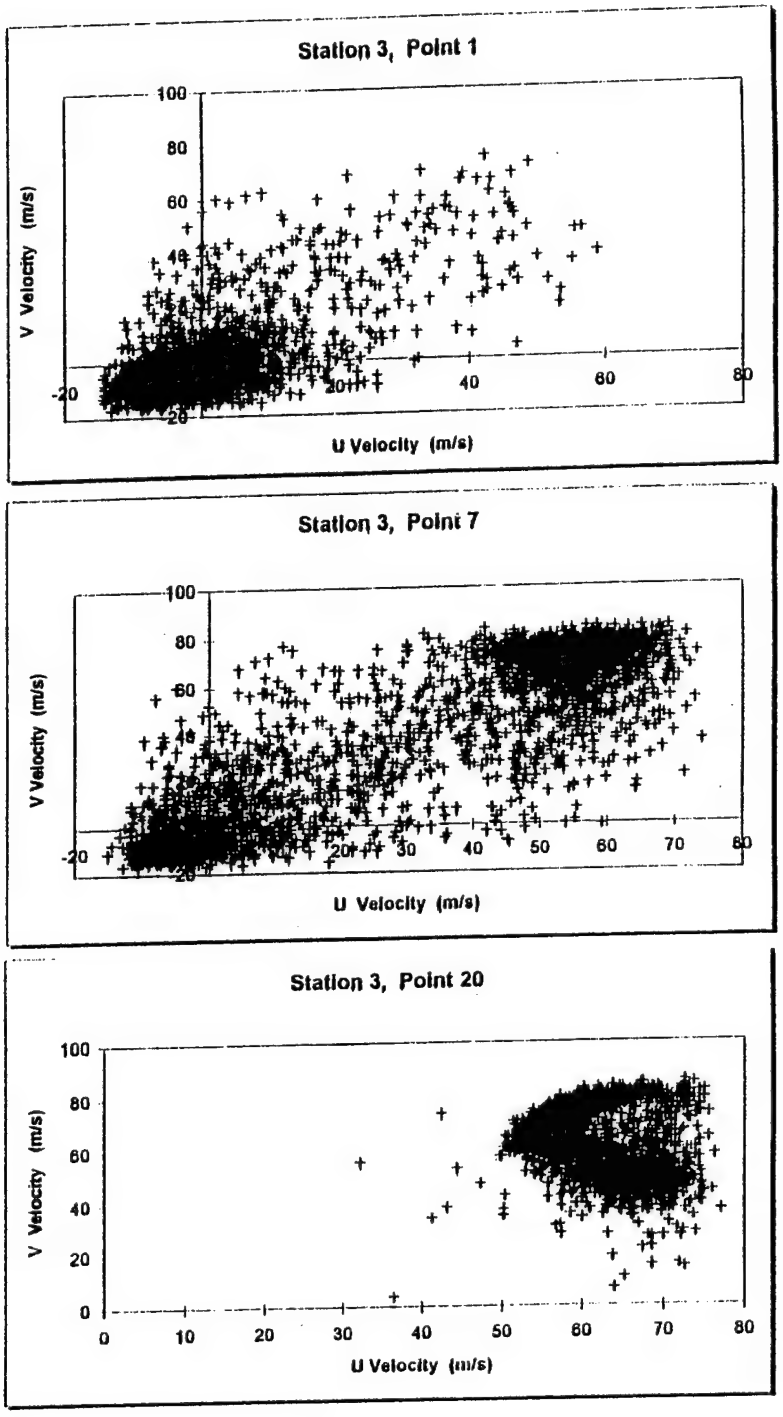

Figure 21. U - V Velocity Correlation Plot

D. POWER-SPECTRUM / AUTO-CORRELATION ANALYSIS

Power spectral density and auto-correlation analyses were performed on the data collected as previously indicated in Table 2. Only station 3 (point 7) and station 7 (points 3 and 20) have been included in Appendix C. Therein are contained the velocity histograms and time-history plots for these points. This analysis was performed using TSI's FIND software, version 4.03. The settings chosen for the analysis were the following: Window Type: *Hanning*; Fast Fourier Transform (FFT) Method: *Random Correlation*, and Correlation Type: *Random Correlation*. In all cases the default lagged-time slot ($\Delta\tau$) was used in order to satisfy the Nyquist sampling criterion.

It was initially believed that a large data set was required to properly carry out this type of analysis. The data sets acquired for station 3, point 7, included 3K and 30K data points. The comparison of the two sets showed similarity in their behavior. The same can be said for station 7, points 3 and 20, which were compared between 3K, 30K, and Ganaim's 3K data points. The only point of recurring significance throughout the power spectrum and auto-correlation plots was in the region between 20-25 Hz as shown in Figure 22 (30K points, present study), and Figure 23 (3K points, Reference 4) for station 7, point 3. No further interpretation of the results obtained was attempted due to the many limitations of discretely-sampled, randomly-arriving data points. Additionally, since this routine involved *averaging* the data over the lagged-time slot ($\Delta\tau$), there was some question whether the true character of the flow had been captured.

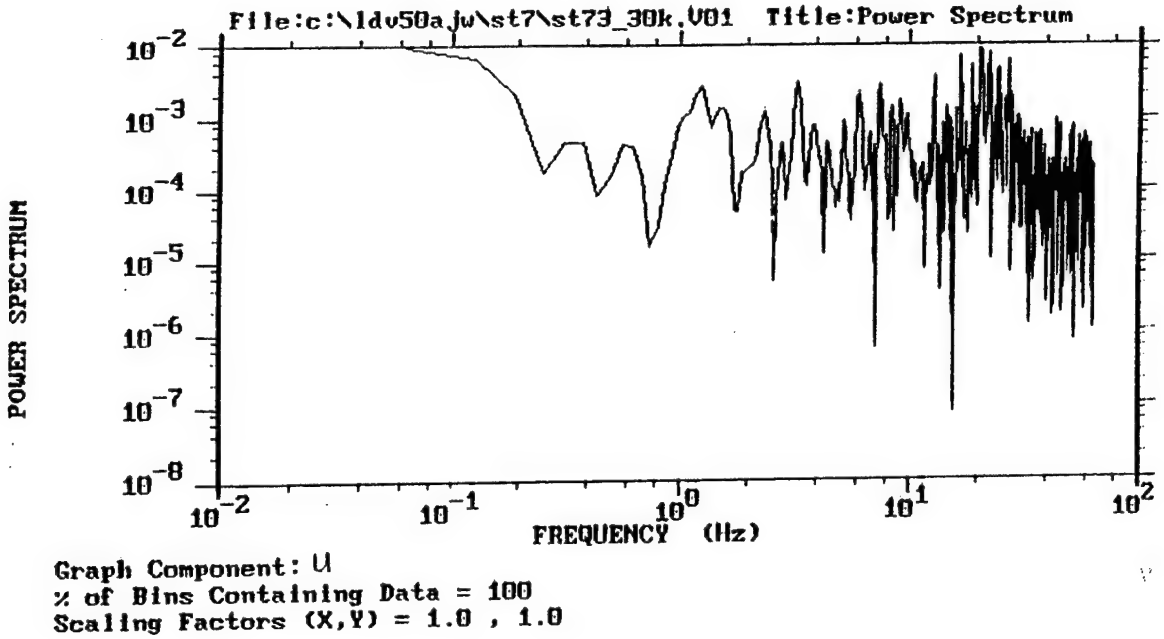

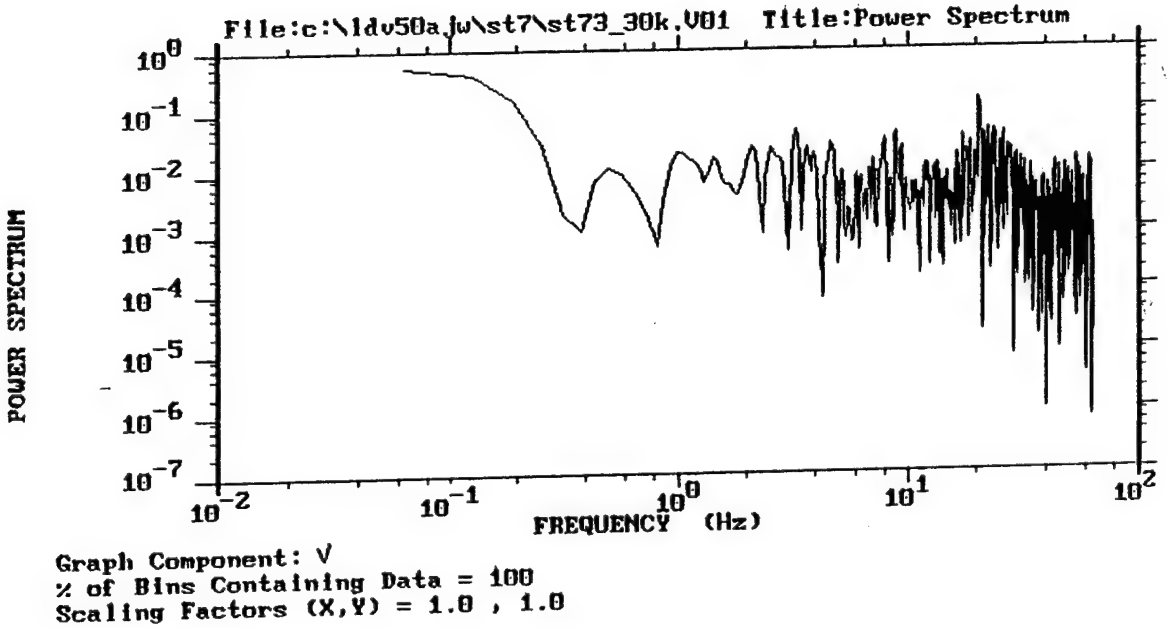

Figure 22. Power Spectrum for 30K Points

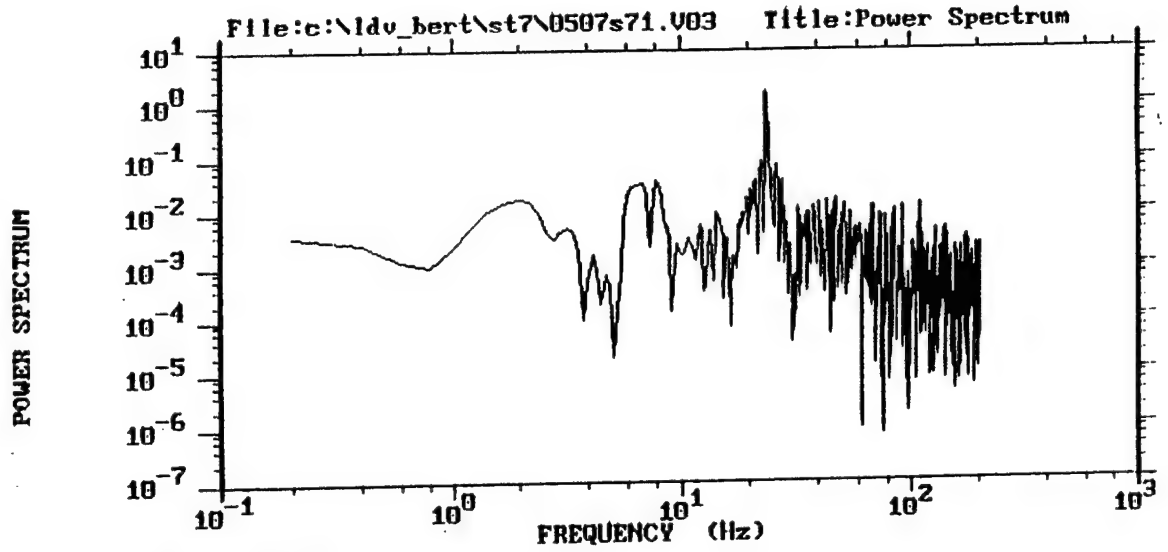

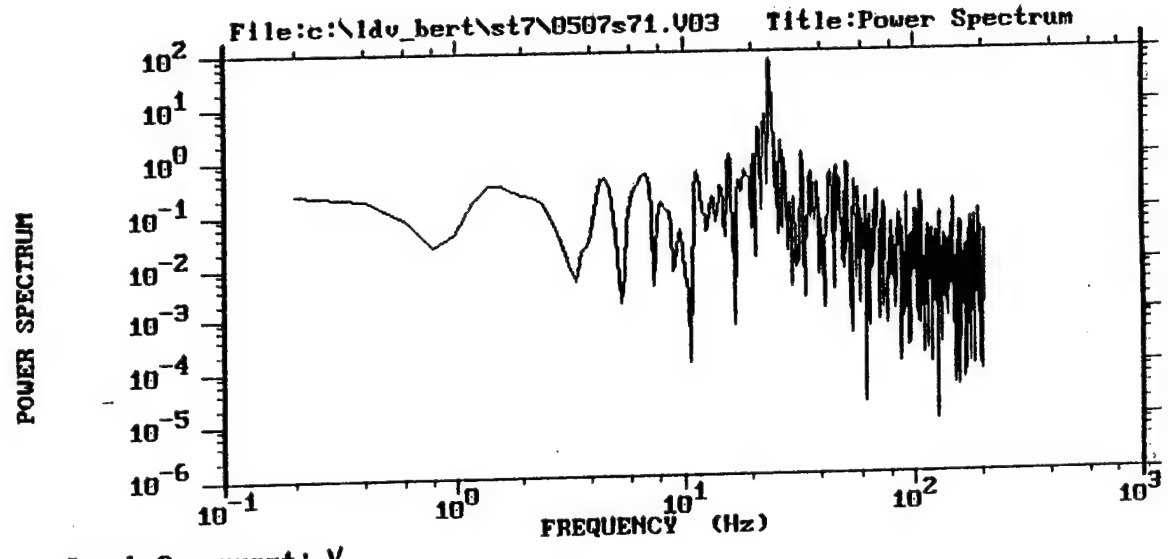

Figure 23. Power Spectrum for 3K Points

The use of larger data sets did not appear to be of significance in the final analysis. The primary limitation turned out to be the data sampling rate. The maximum frequency for spectral analysis was limited to 1/2 the data rate due to the Nyquist criterion, which prevents aliasing of the data. Table 3 shows the data rates and maximum frequencies for the spectral analysis plots of Appendix C.

Location	Number of Data Points	Data Rate (Hz)	Maximum Frequency (Hz)
Station 3, Point 7	3K	39	19
"	30K	49	24
Station 7, Point 3	3K	82	41
"	30K	127	63
"	3K (Ganaim)	606	303
Station 7, Point 20	3K	69	34
"	30K	71	35
"	3K (Ganaim)	613	306

Table 3. Spectral-Analysis Maximum Frequencies

E. FLOW VISUALIZATION

Visualization of reversed-flow velocities within a blade passage was documented on VHS videotape. The tunnel was run at a plenum chamber pressure of 12 inches H_2O to match the conditions during the LDV measurements. The shutter speeds for the 8mm recording were varied from 1/250th to 1/1000th and 1/4000th of a second with the rate of 30 frames/second remaining constant. It was found that the slower shutter speed of 1/250th of a second was better able to capture the streaklines of the intermittent reversed-flow due to longer particle traces for each image.

Upon replaying the videos at normal and slower speeds, several observations were made for both the present study and the flow visualization performed in Reference 4. The reversed-flow region appeared to be confined to the blade passage and did not extend upstream of the leading edge. The leading-edge separation bubble trapped and

accumulated seed particles, due to injection from the reversed flow. This seed within the bubble was able to sustain itself even after the fog was turned off. The bubble also appeared to pulsate in size in accordance with the intermittent reversed-flow. There was some three-dimensionality to the reversed flow evidenced by small spanwise velocity traces. Since the laser sheet was only projected between two blades, it was not possible to determine whether the cascade was experiencing intermittent stall from blade passage to blade passage, or if the entire cascade was stalling simultaneously.

F. COMPUTATIONAL RESULTS

1. Comparison of Blade-Surface Pressure Distributions

The predicted and experimental blade-surface pressure distributions are shown for 40, 43, 46, and 48 degrees in Figures 24-27 respectively. Experimental data for the 40 and 43 degree case were from Reference 14. The 46 degree case used Reference 15 experimental data and the 48 degree case used Reference 3 data. The AVDR parameter was held constant at 6% for all solutions, which showed good agreement for the first three cases. The 48 degree prediction over-estimated the experimental values aft of 60% chord. This was most probably due to under-estimating the stream-tube thickness variation at this inlet flow angle. Increasing the AVDR, as inlet flow angle increased, improved the agreement of the computational results; however, this was not the case experimentally, as documented in References 14, 16, and 17.

The computed static-pressure recovery far downstream of the trailing edge and that measured (from Reference 18) showed good agreement for the 40 and 43 degree cases. The computed value for 40 degrees was 0.313 as compared with a measured range of 0.32 - 0.34. The computed value for 43 degrees was 0.357 as compared with a measured range of 0.37 - 0.39. The computed static-pressure rise far downstream is relevant to accuracy in predicting the losses using viscous codes, and it was shown here to agree well with experiments near design incidence.

For $\beta_1 = 48$ degrees, the predicted flow field pressure contours between the blade rows are shown in Figure 28. The pressure field was continuous at the grid boundaries showing good periodicity; however, there was some indication of grid contamination of the pressure field at the trailing edge cut. The suction peak and stagnation point were both clearly evident. The static-pressure rise, or adverse-pressure gradient, towards the trailing edge on the suction side was also apparent. Investigation of the velocity field in this region showed that there was flow separation aft of mid-chord, followed by re-attachment prior to the blunt trailing edge. Similar behavior occurred for the 46 degree

solution. Experimentally this was not the case, as the flow remained attached on the aft section of the suction surface. This indicated that the code may be predicting incipient stall at 48 degrees (or at a lower inlet-flow angle of 46 degrees); whereas, experimentally this was only found at 50 degrees. It appeared that an unsteady solution may have been computed as evidenced by the climbing density residuals, which are shown in Appendix G, and the coalescence of the pressure contour lines throughout the flow field (Figure 28). The 40 and 43 degree solutions did not show any suction-side separation on the aft portion of the blade, in agreement with experiments.

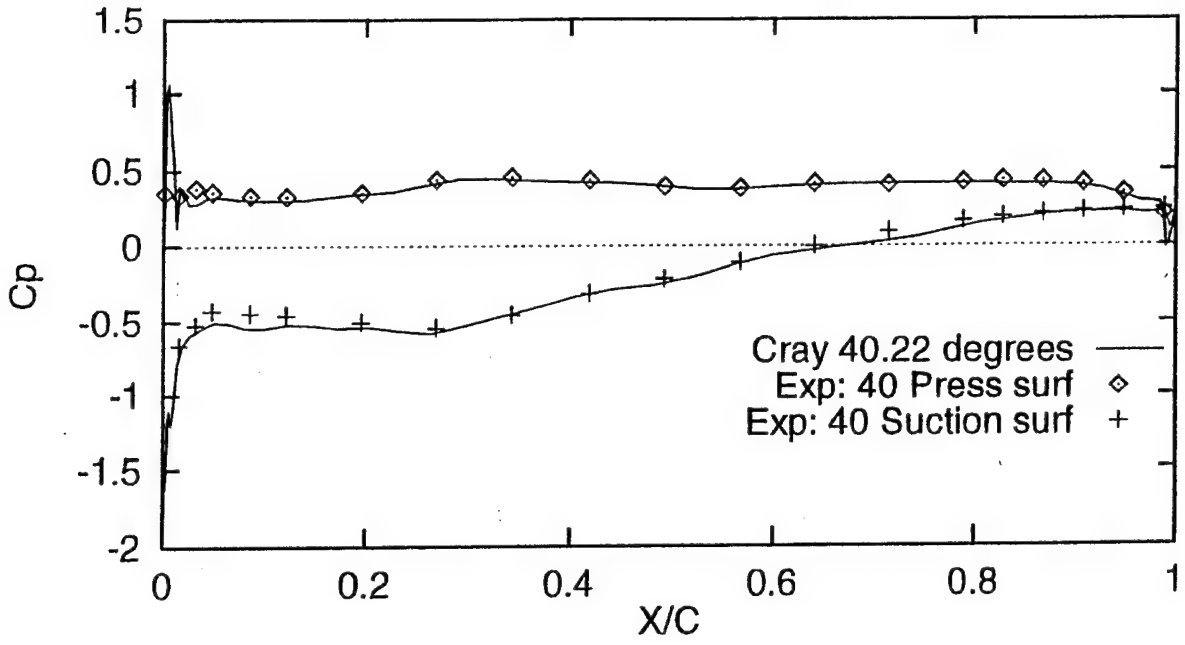

Figure 24. 40 Degree Pressure Distribution

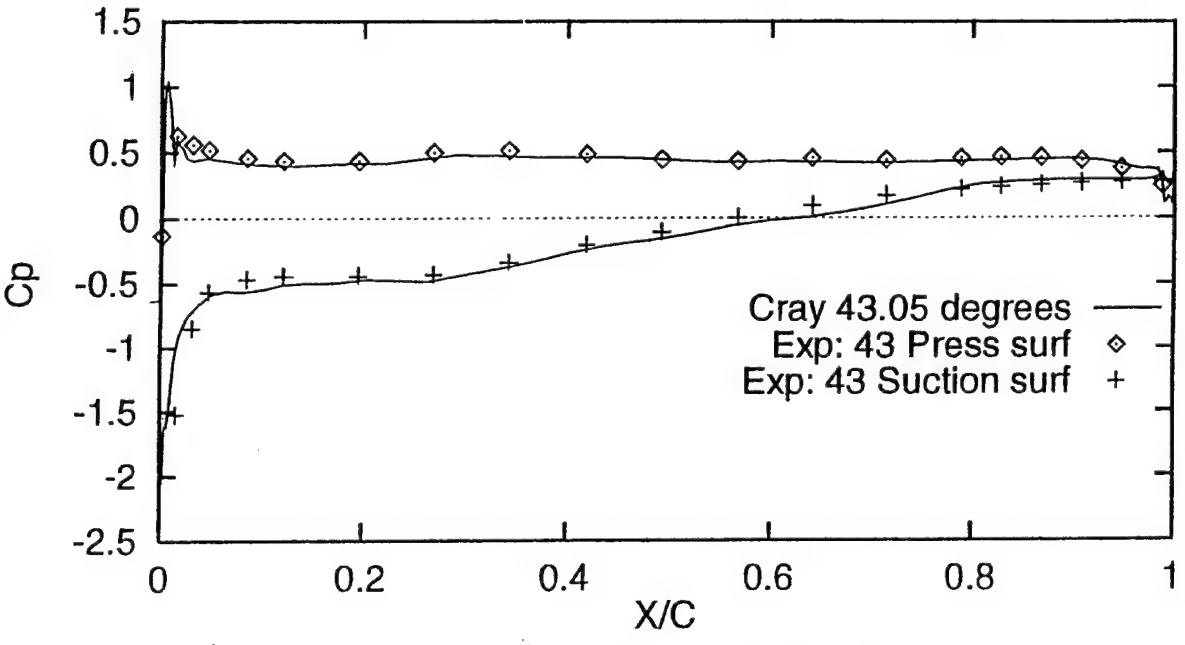

Figure 25. 43 Degree Pressure Distribution

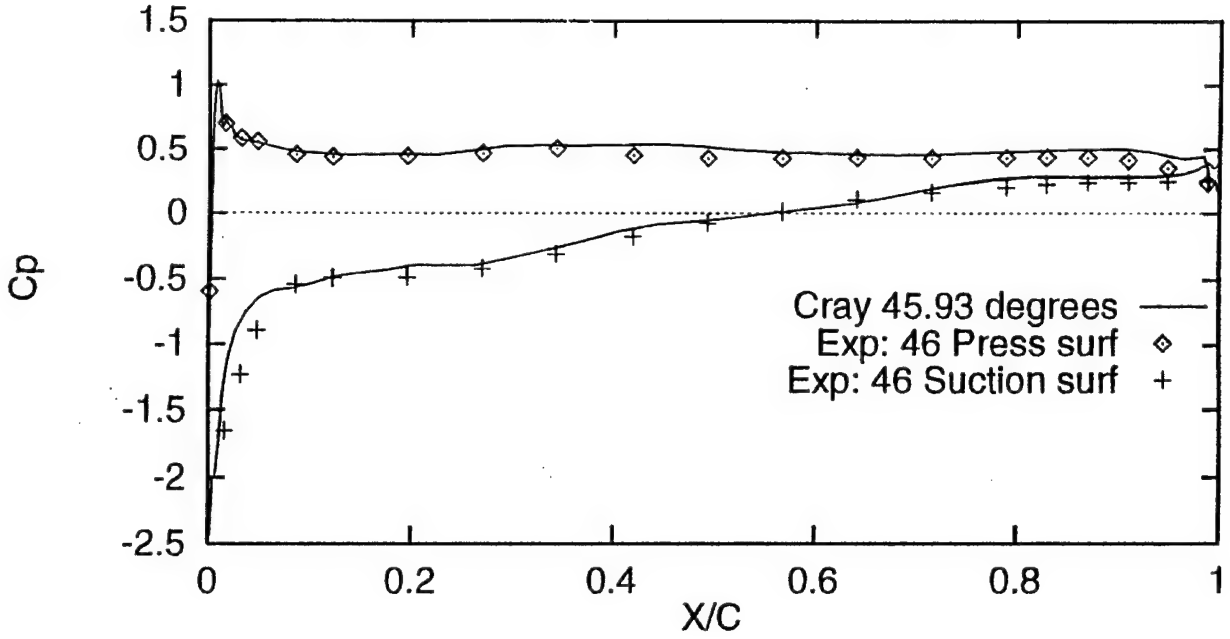

Figure 26. 46 Degree Pressure Distribution

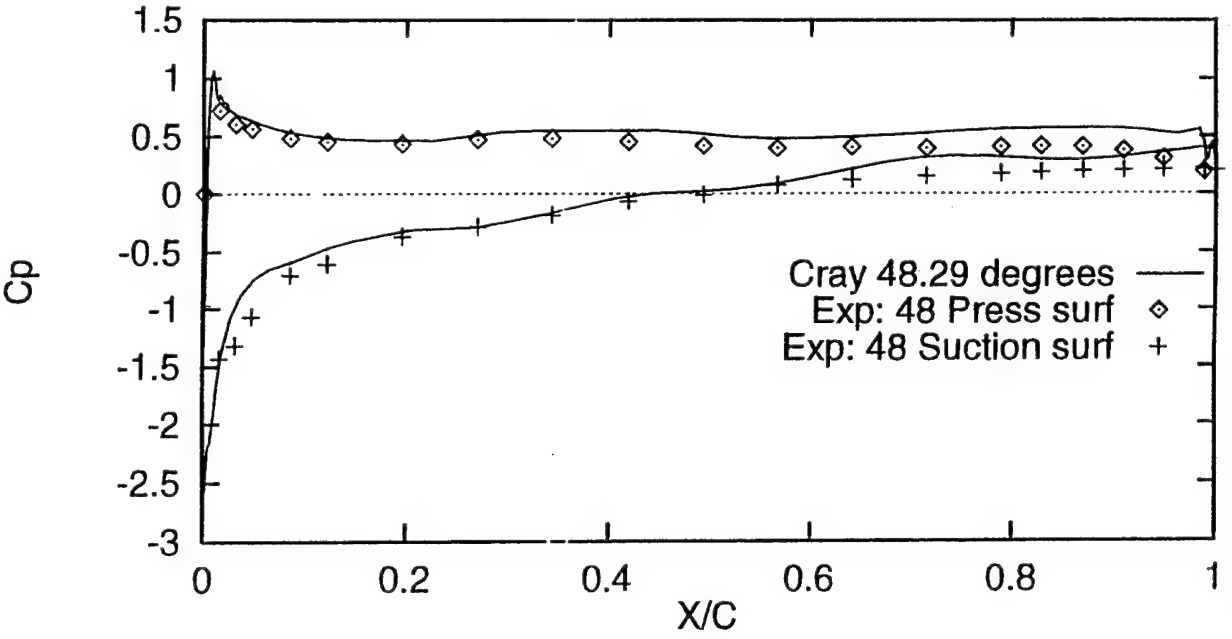

Figure 27. 48 Degree Pressure Distribution

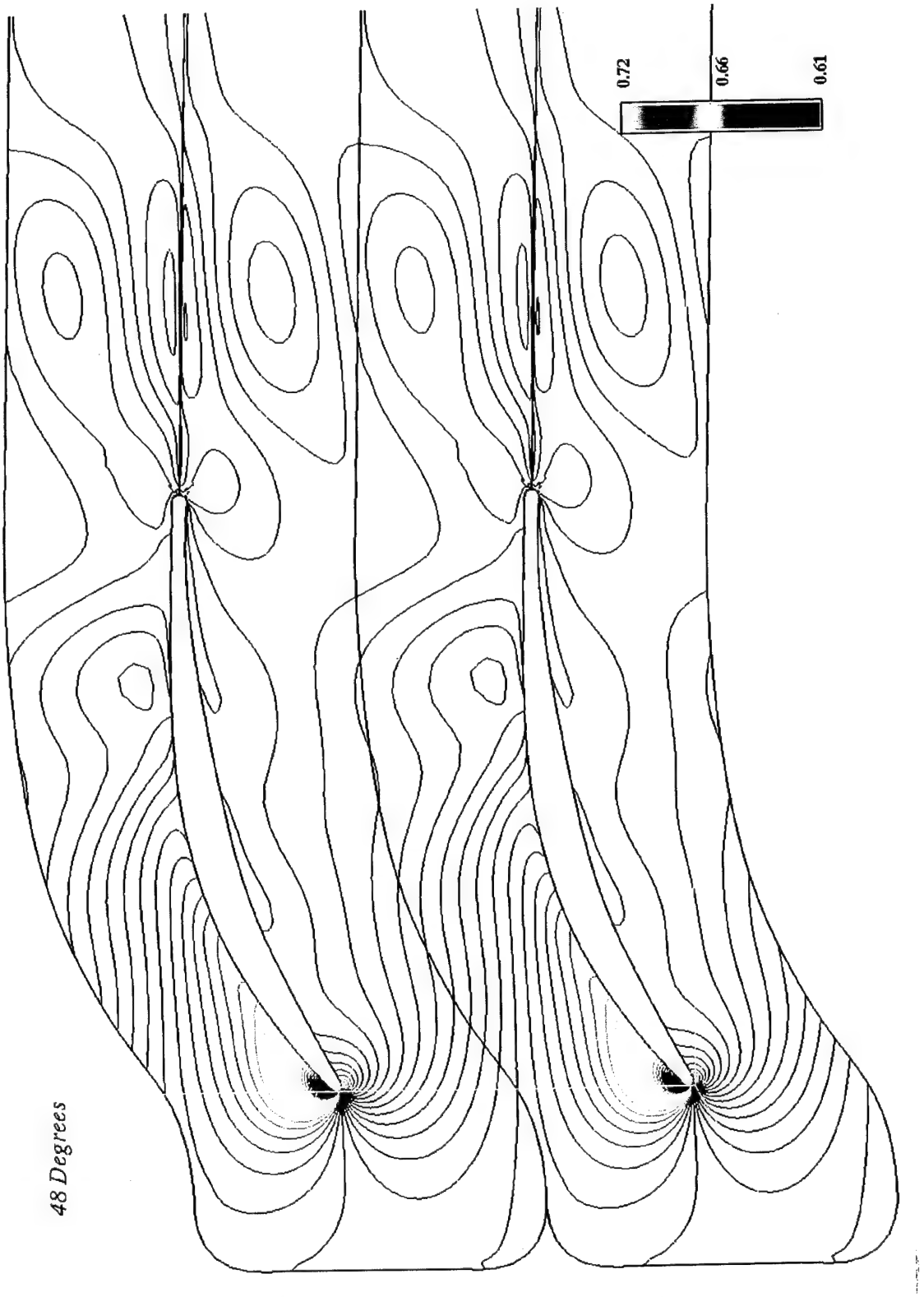

Figure 28. Non-Dimensional Pressure Contours for 48 Degrees

2. Leading-Edge Separation Bubble

A leading-edge separation bubble was predicted for all computational solutions. The location of the computed separation point was insensitive to varying inlet flow angle. The re-attachment point for each case was determined graphically. Figure 29 shows the bubble region for β_1 = 48 degrees in which the recirculating flow was evident. A comparison of computed and experimental re-attachment points is shown in Figure 30. The experimental data was from Reference 19, obtained using the china-clay technique. The plot showed an under-prediction of greater than 50% for the re-attachment locations, which is typical of bubble computations. The Baldwin-Lomax turbulence model does not account for freestream turbulence, which, as pointed out in Reference 3, is necessary in order to properly characterize the development of the blade surface boundary layer, or the occurrence of separation. The two most likely reasons for the shortcoming of the computations are firstly, the limitations of the Baldwin-Lomax turbulence model and secondly, the lack of grid refinement in the streamwise direction aft of the leading edge. The trend of increasing downstream distance for re-attachment, as inlet flow angle increased, appeared to be properly computed.

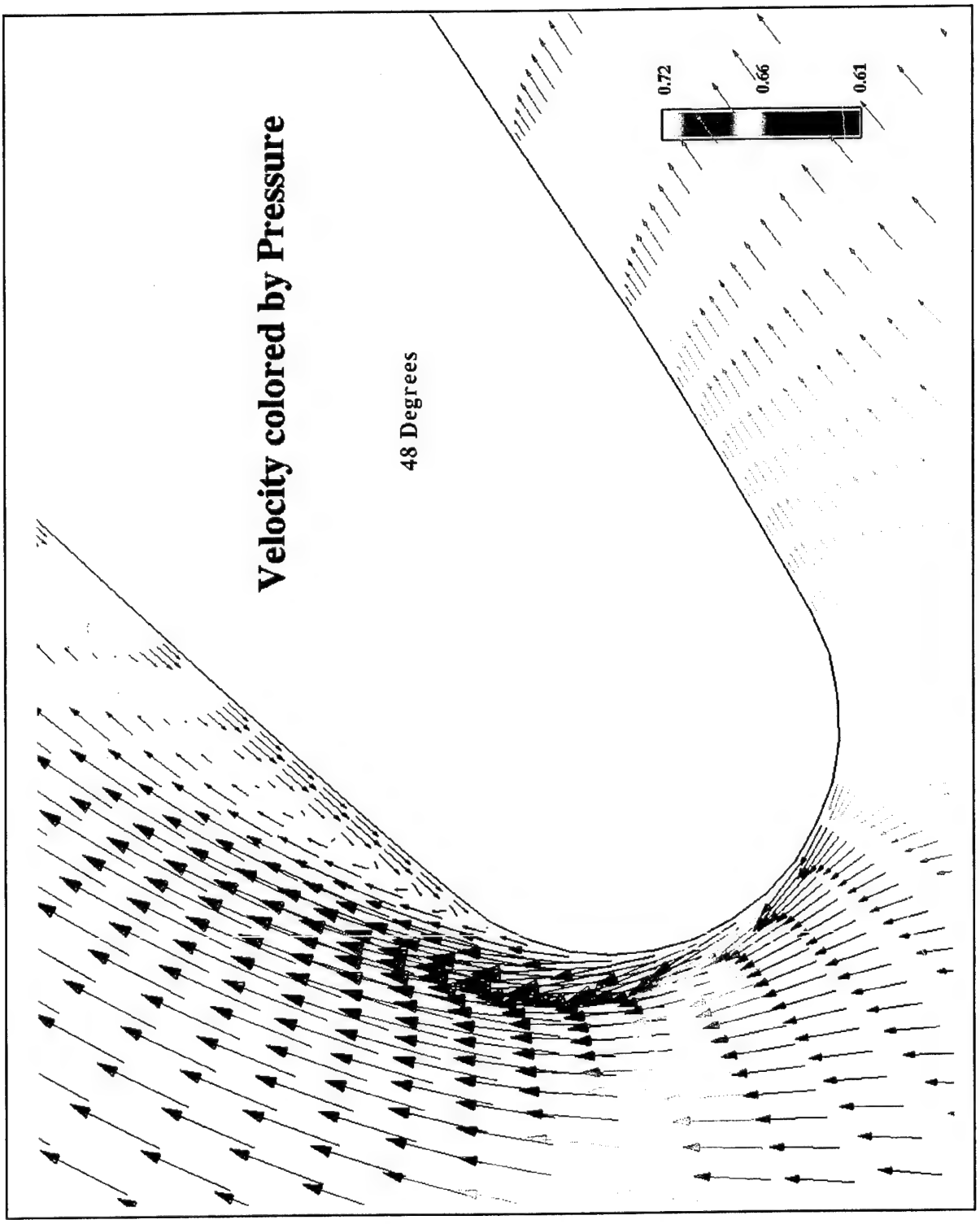

Figure 29. Leading-Edge Velocity Plot

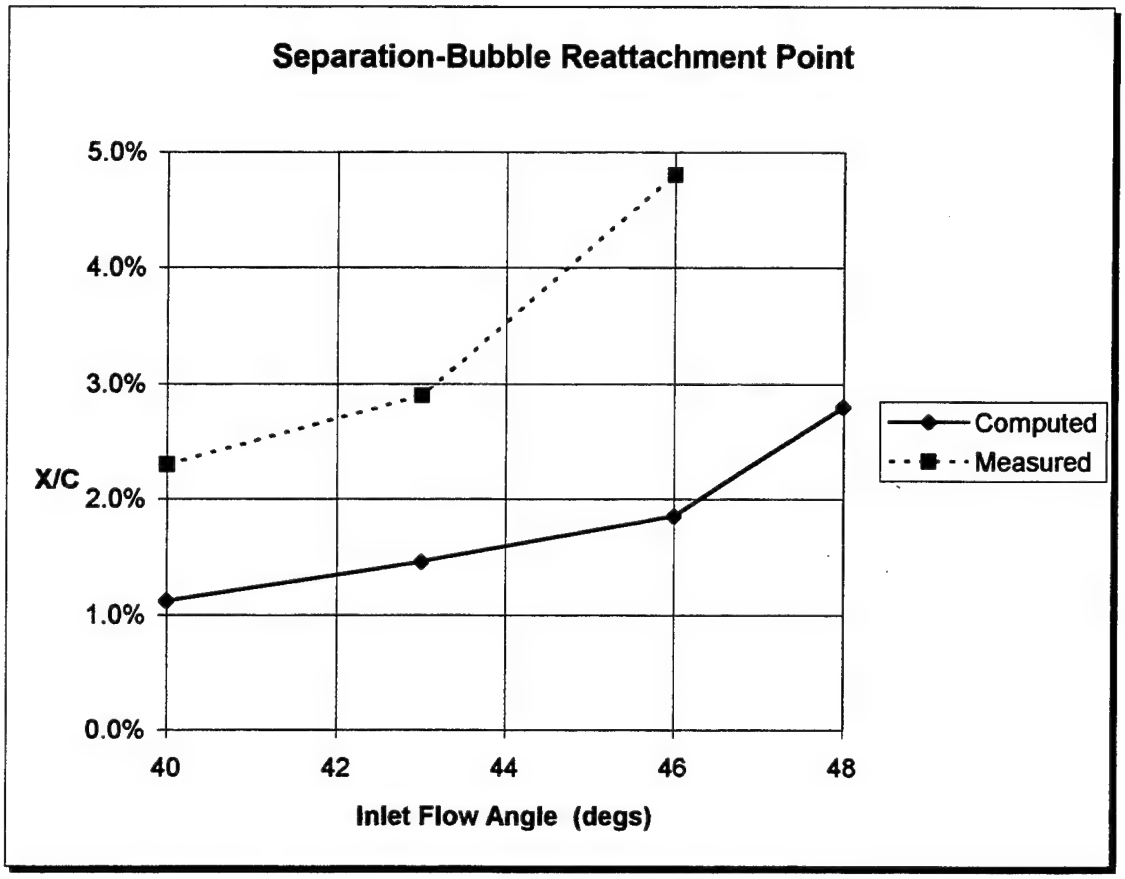

Figure 30. Separation-Bubble Reattachment

3. Losses

The final assessment of RVCQ3D was its loss-prediction capability. Figure 31 plots measured losses as reported in References 14, 16 and 17 with those computed in the present study. The first two computed cases of 40 and 43 degrees were within 5% of the measured results. The 46 degree case showed a sharp departure from the measured results, falling short by 45%. An attempt to increase the AVDR parameter for this case led to a small increase in the loss prediction but with a marked degradation of the blade pressure distribution.

The output file for each solution contained a listing of the Baldwin-Lomax turbulence-model behavior by printing values of turbulent eddy viscosity for each grid point. Upon interrogation of this output file, the behavior of the Baldwin-Lomax turbulence model was seen to exhibit certain characteristics. Firstly, for all cases the turbulence model turned on inside the separation bubble region. Secondly, for the 40 degree case, the model did not turn on until two grid points inside the bubble region, indicating a laminar region in the forward section of the bubble. The model then turned off again at the re-attachment point and turned back on further downstream. Thirdly, for 48 degrees the model turned on at the separation point and remained on past the re-attachment point to the trailing edge. The transition criteria used for all the computations was that once the turbulence model computed a turbulent eddy viscosity (μ_T) which was 14 times larger than the laminar viscosity (μ_L), this value of μ_T was used to compute an effective viscosity ($\mu_{eff} = \mu_L + \mu_T$). Otherwise the effective viscosity was simply the laminar viscosity.

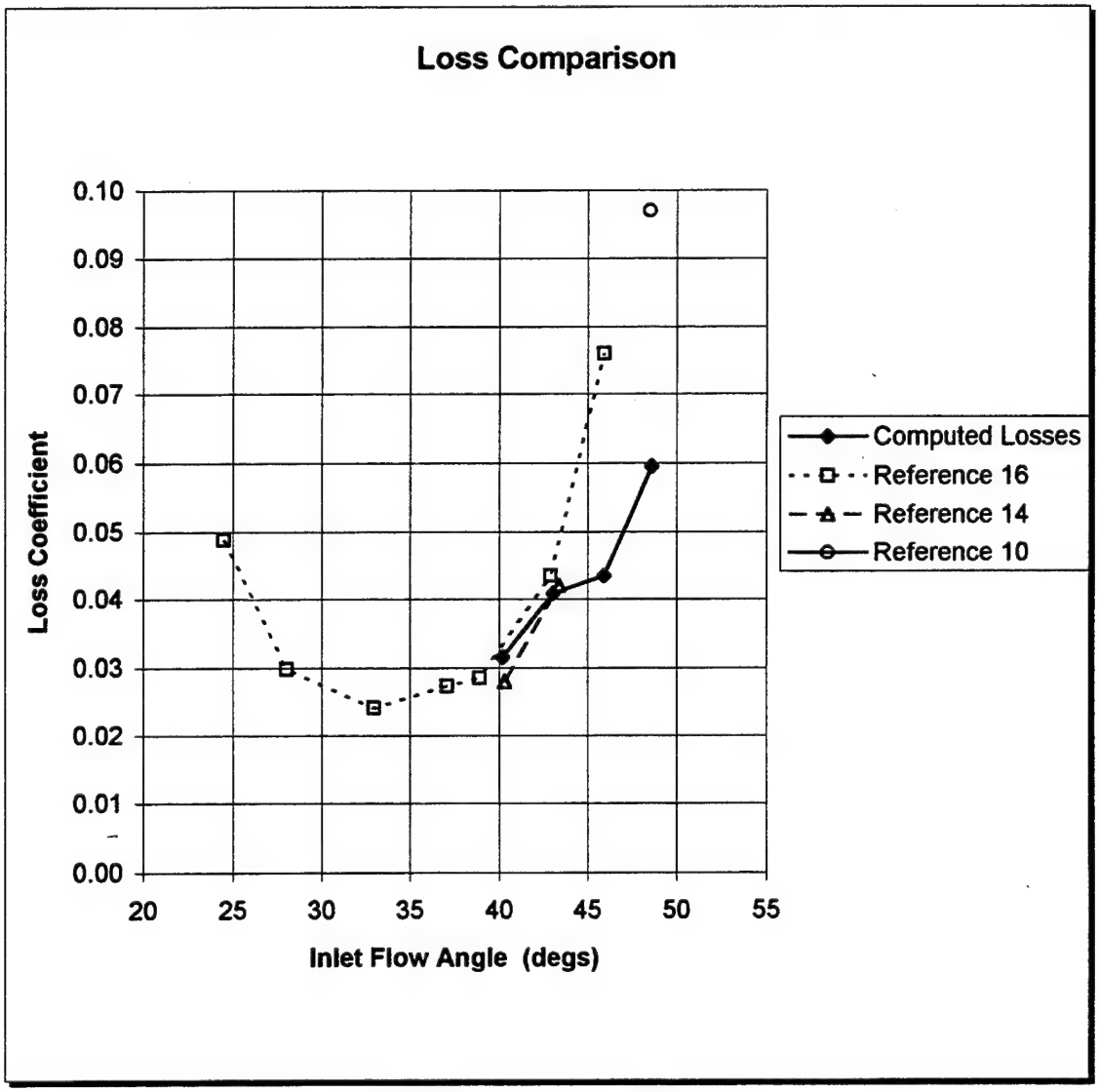

Figure 31. Loss Comparison

V. CONCLUSIONS AND RECOMMENDATIONS

Experimental flow field measurements near stall were successfully repeated for a controlled-diffusion compressor cascade using a two-dimensional laser-Doppler velocimeter system. The nominal inlet flow angle achieved was 50.05 degrees at a constant Mach number of 0.25 and Reynolds number of 700,000. The measurements were useful in that they showed repeatability with previous work by Ganaim, and validated a test case for two-dimensional unsteady separated flows.

Analysis of the data was presented through a unique editing process which captured the character of the intermittent reversed flow. This process more properly represented the stalling region as a combination of primarily positive and negative flow, since the time-mean velocity rarely occurred in the intermittent region.

Power-spectrum and auto-correlation calculations were completed on the data for eleven locations. Interpretation of these results was limited to their general behavior due to averaging of the data by the software package. Three locations were chosen for analysis and the results were found to depend greatly on the data acquisition rate. When expecting to perform power-spectrum analysis on experimental data, it is important to ensure that the data rate is high by repeated cleaning and proper re-fitting of the optical-access window.

Numerical computations showed good predictability of the blade pressure distribution up to 46 degrees (approximately 6 degrees above design incidence). The 48-degree case began to deviate by up to 50% from measured values aft of two-thirds chord. A case-by-case basis for adjusting AVDR may be necessary to bring the computed results into better agreement with the measurements at higher inlet flow angles.

A leading-edge separation bubble was formed in all computations in accordance with experiments. The extent of the computed bubble fell short of that seen in measurements. Computed losses agreed well at low incidence angles. As the inlet flow angle increased above 46 degrees, predicted losses deviated by 45% from the measurements. The use of a constant AVDR for numerical solutions greatly simplified the process. This was found to be acceptable for analyzing near on-design inlet flow angles.

Future computations of the flow through the cascade with a quasi-3d code should focus on achieving the following:

1. Continue numerical solutions to determine the optimum AVDR as inlet-flow angle varies, and compare with those measured in the cascade.

2. Quantify what effects adjusting AVDR to match pressure distributions has on the computed losses.

3. Increase the grid size in both the I and J directions for better characterization of the flow near the blade surface and around the leading edge separation bubble.

4. Replace the Baldwin-Lomax turbulence model with a two-equation turbulence model to account for freestream turbulence intensity.

5. Perform time-accurate solutions at higher incidence angles to see if unsteadiness is being properly modeled.

APPENDIX A: EXPERIMENTAL-MEASUREMENTS LOG

A detailed log of the atmospheric conditions, tunnel plenum chamber conditions and LDV traverse-mechanism geometry for each experimental run.

Station	Filename	Point(s)	Date	Time	Plenum Pressure (in H_2O)	Plenum Temp (°F)	Prandtl Probe (in H_2O)	Atmos. Pressure (psi)	LDV Pitch / Yaw
1	1114s1_a	1-41	11/14/94	17:00	11.9	65	17.0	14.70	0 / 0
				17:30	"	66	16.8	"	
	st1_3k	9	11/30/94	7:40	12.0	58	17.0	14.80	0 / 0
				7:50	"	59	"	"	
	st1_30k	9	11/30/94	7:55	12.0	59	17.0	14.80	0 / 0
				8:03	12.1	"	"	"	
	st1_50k	9	11/30/94	8:45	12.0	60	17.0	14.80	0 / 0
				8:55	"	"	"	"	
1b	1121s_1b	1-17	11/21/94	16:35	12.0	61	16.9	14.79	+4 / 0
				16:51	12.1	63	"	"	
1d	1122s_1d	1-33	11/21/94	16:55	12.1	64	16.9	14.79	+4 / 0
				17:19	"	65	17.1	"	
2a	1122s_2a	1-32	11/22/94	8:45	12.0	61	16.8	14.85	+2 / 4L
				9:35	11.9	64	16.6	"	
	st2a_3k	1	11/30/94	10:28	12.0	64	16.8	14.80	+2 / 4L
				10:35	"	"	"	"	
	st2a_30k	1	12/5/94	7:55	12.1	58	17.1	14.70	+2 / 4L
				8:27	12.2	60	17.3	14.69	
3	1123s_3	1-32	11/23/94	7:50	11.9	60	16.8	14.83	+2 / 4L
				8:45	11.8	66	16.7	14.84	
	st37_3k	7	11/30/94	10:03	12.0	61	16.8	14.80	+2 / 4L
				10:13	"	62	"	"	
	st37_30k	7	12/5/94	8:35	12.0	61	17.1	14.69	+2 / 4L
				9:07	"	62	"	14.70	
7	1123s_7	1-32	11/23/94	9:00	12.0	67	16.8	14.84	+2 / 4L
				9:24	"	68	"	"	
	st73_3k	3	11/30/94	9:40	12.1	60	17.0	14.80	+2 / 4L
				9:45	"	"	"	"	
	st73_30k	3	12/5/94	9:18	12.0	63	16.9	14.70	+2 / 4L
				9:25	"	"	17.0	"	
	st7_3k	20	11/30/94	8:05	12.1	59	17.0	14.80	0 / 0
				8:10	"	"	"	"	
	st7_30k	20	12/6/94	8:12	11.9	58	16.9	14.75	0 / 0
				8:25	"	60	"	"	
10	st10_edg	15	12/6/94	9:28	12.1	63	17.0	14.76	0 / 0
				9:43	"	"	"	"	
	st10_out	25	12/6/94	8:53	12.0	62	16.8	14.75	0 / 0
				8:58	12.1	"	"	"	
14	1127s_14	1-32	11/27/94	15:33	12.0	58	17.1	14.82	0 / 4L
				16:00	12.2	62	17.3	"	
15	1128s_15	1-32	11/28/94	8:00	12.0	60	17.0	14.84	0 / 4L
				8:35	12.1	62	"	"	
17	1128s_17	1-49	11/28/94	8:52	12.0	62	17.0	14.84	0 / 0
				9:48	12.2	64	"	"	
	st17_in	31	12/6/94	8:30	11.9	61	16.9	14.75	0 / 0
				8:37	"	"	"	"	
	st17_out	23	12/6/94	8:40	11.9	61	16.8	14.75	0 / 0
				8:48	"	62	"	"	

Station	Filename	Point(s)	Date	Time	Plenum Pressure (in H2O)	Plenum Temp (oF)	Prandtl Probe (in H2O)	Atmos. Pressure (psi)	LDV Pitch / Yaw
18	1128s 18	1-49	11/28/94	10:00	11.9	64	17.0	14.85	0 / 0
				10:43	"	66	"	"	
19	1128s 19	1-49	11/28/94	10:47	11.9	66	17.0	14.84	0 / 0
				11:40	12.1	68	"	"	
	st19 in	31	12/6/94	9:12	12.2	62	17.3	14.76	0 / 0
				9:24	12.3	"	"	"	
	st19 out	23	12/6/94	9:02	12.1	62	17.1	14.75	0 / 0
				9:09	12.1	"	17.2	14.76	

APPENDIX B: CALCULATION OF INLET-FLOW REFERENCE VELOCITY

CCCCCCCCCCCCCCCCCCCCCCCCCCCCCCCCCCCCCCCCCCCCCCCCCCCCCCCCCCCCCCCCCCCCCCCCCCCC

OUTPUT FROM PROGRAM CALIBRATE

CCCCCCCCCCCCCCCCCCCCCCCCCCCCCCCCCCCCCCCCCCCCCCCCCCCCCCCCCCCCCCCCCCCCCCCCCCCC

LEAST SQUARES STRAIGHT LINE CURVE FIT IS USED
TO DETERMINE TUNNEL CHARACTERISTICS AT DIFFERENT SPEEDS

NEWTON S METHOD IS USED TO DETERMINE THE REFERENCE VELOCITY
FROM THE RECORDED AMBIENT PRESSURE AND TUNNEL PLENUM
PRESSURE AND TEMPERATURE

BEGIN DETERMINING TUNNEL CHARACTERISTICS
FROM THE FOLLOWING MEASURED VALUES

AXIAL VEL. M PER SEC.	TANGENTIAL VEL. M PER SEC.	AMBIENT PRESS. INCHES MERCURY	PLENUM PRESS. INCHES WATER	PLENUM TEMP. DEG. C.
18.3100	22.1350	29.9702	1.7000	13.8888
32.4070	38.5280	29.9702	4.7000	13.8888
42.5440	50.1820	29.9702	8.1000	15.5555
47.2920	56.3530	29.9702	10.0000	16.6666
51.7870	61.9370	29.9702	12.1000	17.2222
55.3660	66.7010	29.9702	14.0000	18.3333

CALCULATED VALUES FOR THE TUNNEL CONFIGURATION

TOTAL VELOCITY	MACH NUMBER	MACH NUMBER FUNCT.	PRESSURE RATIO
0.28726543910E+02	0.37818777200E-01	0.49880294974E-02	0.43443528269E-02
0.50345013984E+02	0.66279705382E-01	0.15207192279E-01	0.11919477085E-01
0.65789247298E+02	0.86361830486E-01	0.25620261319E-01	0.20366465634E-01
0.73567614295E+02	0.96387235172E-01	0.31766759119E-01	0.25024235973E-01
0.80734660079E+02	0.10567615343E+00	0.38003966212E-01	0.30121036781E-01
0.86685739064E+02	0.11324925118E+00	0.43463396462E-01	0.34686726827E-01

CALLING LEAST SQUARES SUBROUTINE
TO DETERMINE THE PRESSURE RATIO AS A FUNCTION OF MACH NO. PARAM

PRESSURE RATIO = A1 * ANUX + A0

MATRIX EQUATION

0.60E+01 0.16E+00 A0 0.13E+00
0.16E+00 0.53E-02 A1 0.42E-02

A1 = 0.78899597626E+00 A0 = 0.16213280706E-03

REFERENCE CONDITIONS FOR EACH RUN

AMB PRESS INCHES Hg	PLENUM PRESS INCHES H2O	PLENUM TEMP DEGREES C	RUN NAME
29.9295	11.9000	18.3333	1114s1_A.PRN
30.1331	12.0000	14.4444	ST1_3K.PRN
30.1331	12.0500	14.4444	ST1_30K.PRN
30.1331	12.0000	15.5555	ST1_50K.PRN
30.1127	12.0500	16.6666	1121S_1B.PRN
30.1127	12.1000	18.3333	1121S_1D.PRN
30.2349	11.9500	16.9444	1122S_2A.PRN
30.1331	12.0000	17.7777	ST2A_3K.PRN
29.9295	12.1500	14.4444	ST2A_30K.PRN
30.1942	11.8500	17.2222	1123S_3.PRN
30.1331	12.0000	16.6666	ST37_3K.PRN
29.9295	12.0000	16.6666	ST37_30K.PRN
30.2145	12.0000	20.0000	1123S_7.PRN
30.1331	12.1000	15.5555	ST73_3K.PRN
29.9295	12.0000	17.2222	ST73_30K.PRN
30.1331	12.1000	14.4444	ST7_3K.PRN
30.0313	11.9000	14.4444	ST7_30K.PRN
30.0517	12.1000	17.2222	ST10_EDG.PRN
30.0313	12.0500	16.6666	ST10_OUT.PRN
30.1738	12.1000	15.5555	1127S_14.PRN
30.2145	12.0500	16.1111	1128S_15.PRN
30.2145	12.1000	17.2222	1128S_17.PRN
30.0313	11.9000	16.1111	ST17_IN.PRN
30.0313	11.9000	16.6666	ST17_OUT.PRN
30.2349	11.9000	18.3333	1128S_18.PRN
30.2145	12.0000	19.4444	1128S_19.PRN
30.0517	12.2500	16.6666	ST19_IN.PRN
30.0517	12.1000	16.6666	ST19_OUT.PRN

I = 1
PRESSURE RATIO = 0.02968 MACH NUMBER PARAMETER = 0.3741E-01
RUN NAME = 1114s1_A.PRN

BEGIN NEWTON ITERATION

ITERATION NUMBER 1 MACH NO. PARAM. = 0.105475 ERROR TERM = 0.6522E-03
ITERATION NUMBER 2 MACH NO. PARAM. = 0.104822 ERROR TERM = 0.1641E-05
ITERATION NUMBER 3 MACH NO. PARAM. = 0.104821 ERROR TERM = -0.3698E-09
ITERATION NUMBER 4 MACH NO. PARAM. = 0.104821 ERROR TERM = 0.8591E-13

VREF = 80.23415022742

.
.
.

I = 28
PRESSURE RATIO = 0.03004 MACH NUMBER PARAMETER = 0.3787E-01
RUN NAME = ST19_OUT.PRN

BEGIN NEWTON ITERATION

ITERATION NUMBER 1 MACH NO. PARAM. = 0.105777 ERROR TERM = 0.2921E-03
ITERATION NUMBER 2 MACH NO. PARAM. = 0.105485 ERROR TERM = 0.2872E-06
ITERATION NUMBER 3 MACH NO. PARAM. = 0.105485 ERROR TERM = -0.6810E-10

VREF = 80.51152210108

EXPERIMENT NUMBER	REFERENCE VELOCITY	FILE NAME
1	80.2342	1114s1_A.PRN
2	79.7607	ST1_3K.PRN
3	79.9273	ST1_30K.PRN
4	79.9146	ST1_50K.PRN
5	80.2627	1121S_1B.PRN
6	80.6606	1121S_1D.PRN
7	79.8038	1122S_2A.PRN
8	80.2216	ST2A_3K.PRN
9	80.5328	ST2A_30K.PRN
10	79.5598	1123S_3.PRN
11	80.0682	ST37_3K.PRN
12	80.3411	ST37_30K.PRN
13	80.4184	1123S_7.PRN
14	80.2481	ST73_3K.PRN
15	80.4180	ST73_30K.PRN
16	80.0935	ST7_3K.PRN
17	79.5615	ST7_30K.PRN
18	80.5887	ST10_EDG.PRN
19	80.3718	ST10_OUT.PRN
20	80.1937	1127S_14.PRN
21	80.0501	1128S_15.PRN
22	80.3705	1128S_17.PRN
23	79.7917	ST17_IN.PRN
24	79.8682	ST17_OUT.PRN
25	79.8265	1128S_18.PRN
26	80.3422	1128S_19.PRN
27	81.0107	ST19_IN.PRN
28	80.5115	ST19_OUT.PRN

APPENDIX C: VELOCITY HISTOGRAMS, TIME-HISTORY PLOTS, POWER-SPECTRUM PLOTS, AND AUTO-CORRELATION PLOTS

1. Station 3, Point 7

a. 3K Data Points

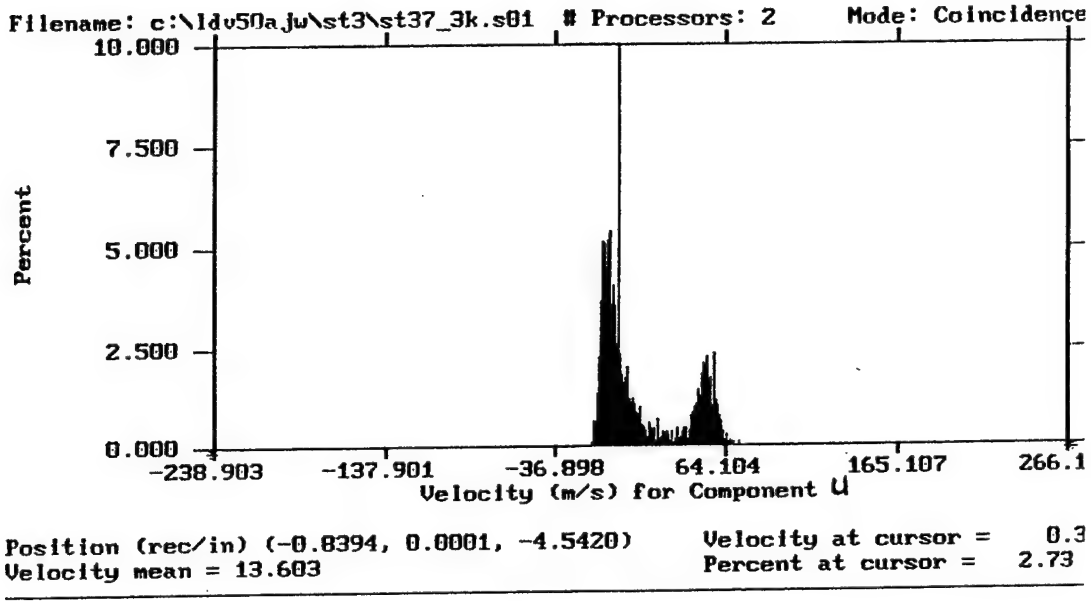

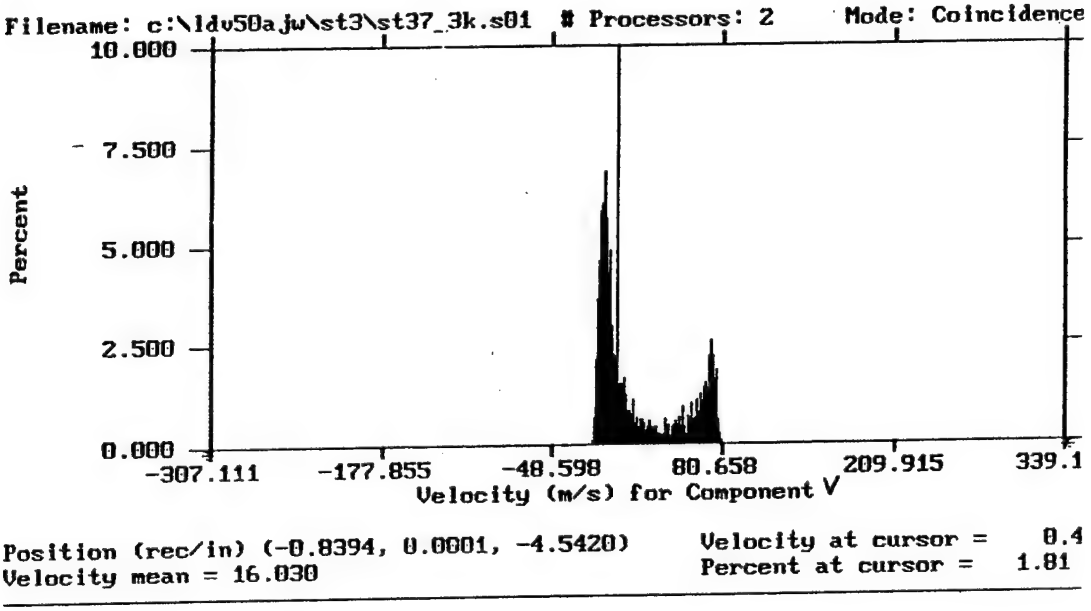

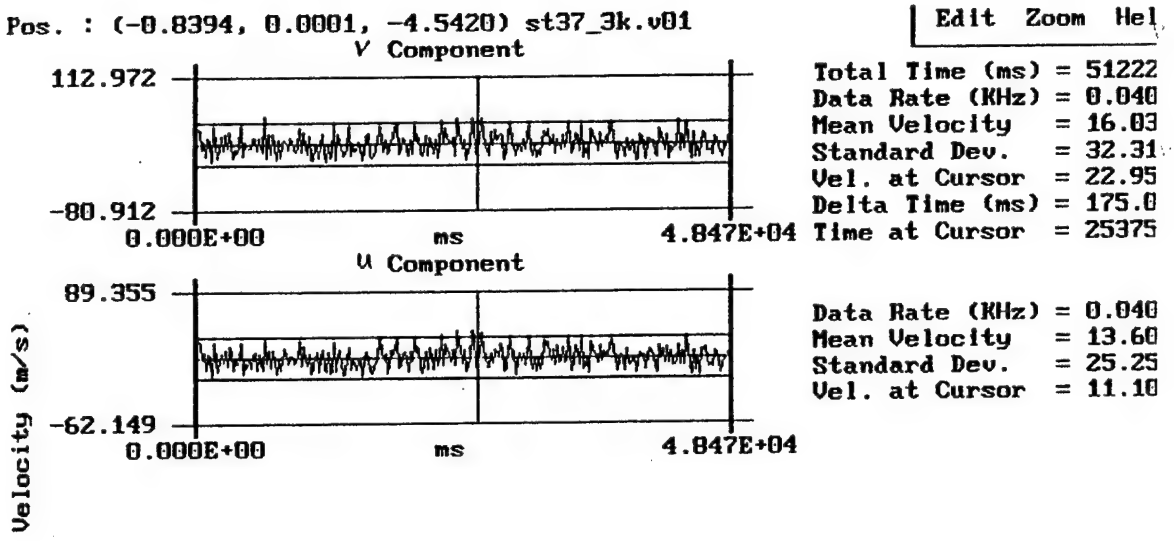
Pos. : (-0.8394, 0.0001, -4.5420) st37_3k.v01
Edit Zoom Hel
V Component
112.972
-80.912
0.000E+00
ms
4.847E+04
Total Time (ms) = 51222
Data Rate (KHz) = 0.040
Mean Velocity = 16.03
Standard Dev. = 32.31
Vel. at Cursor = 22.95
Delta Time (ms) = 175.0
Time at Cursor = 25375
U Component
89.355
-62.149
0.000E+00
ms
4.847E+04
Velocity (m/s)
Data Rate (KHz) = 0.040
Mean Velocity = 13.60
Standard Dev. = 25.25
Vel. at Cursor = 11.10

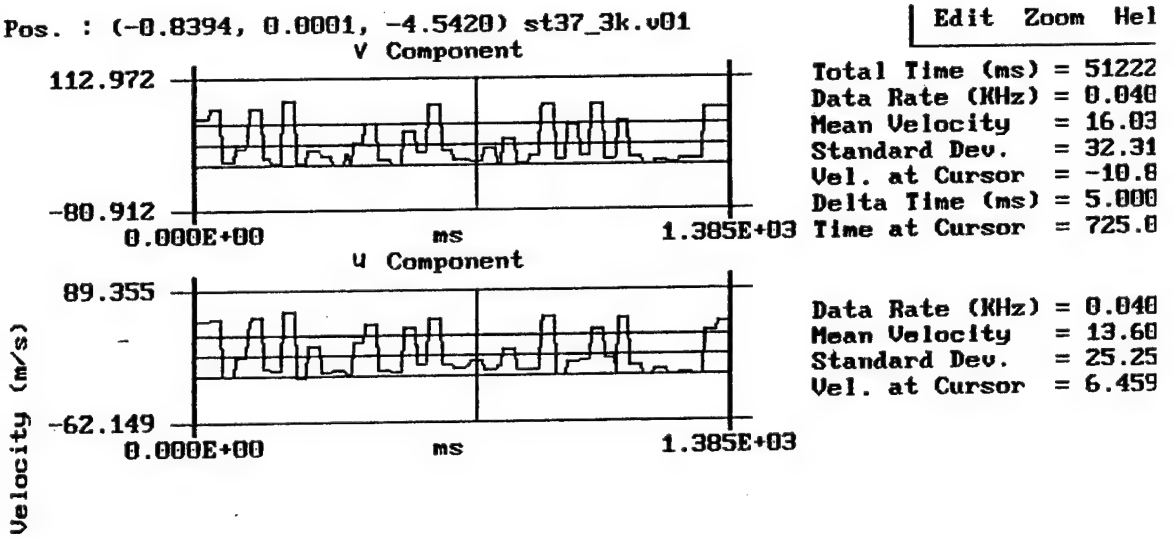
Pos. : (-0.8394, 0.0001, -4.5420) st37_3k.v01
Edit Zoom Hel
V Component
112.972
-80.912
0.000E+00
ms
1.385E+03
Total Time (ms) = 51222
Data Rate (KHz) = 0.040
Mean Velocity = 16.03
Standard Dev. = 32.31
Vel. at Cursor = -10.8
Delta Time (ms) = 5.000
Time at Cursor = 725.0
U Component
89.355
-62.149
0.000E+00
ms
1.385E+03
Velocity (m/s)
Data Rate (KHz) = 0.040
Mean Velocity = 13.60
Standard Dev. = 25.25
Vel. at Cursor = 6.459

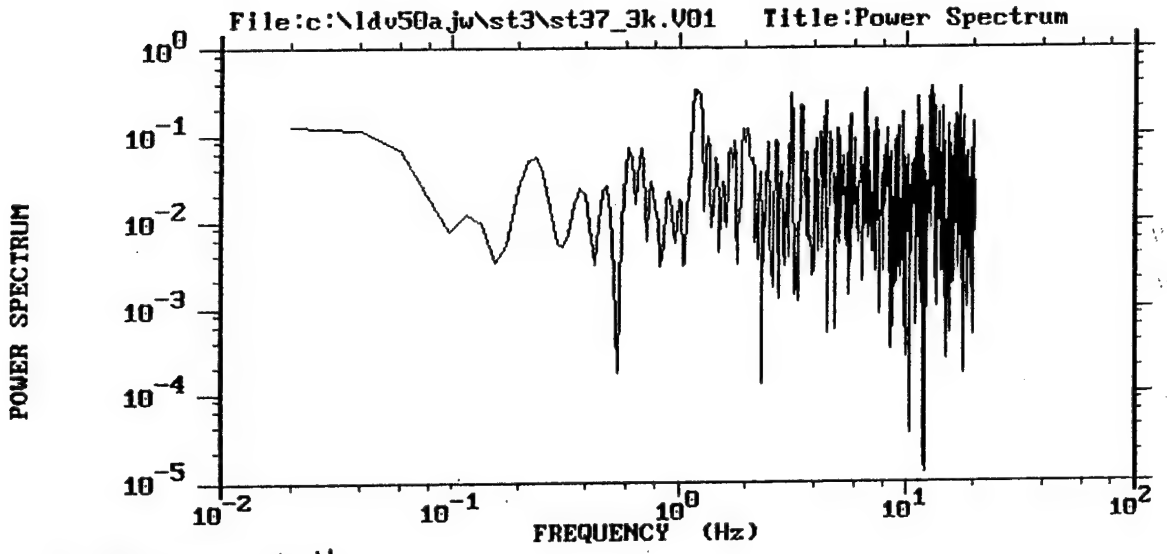

Graph Component: U
% of Bins Containing Data = 100
Scaling Factors (X,Y) = 1.0 , 1.0

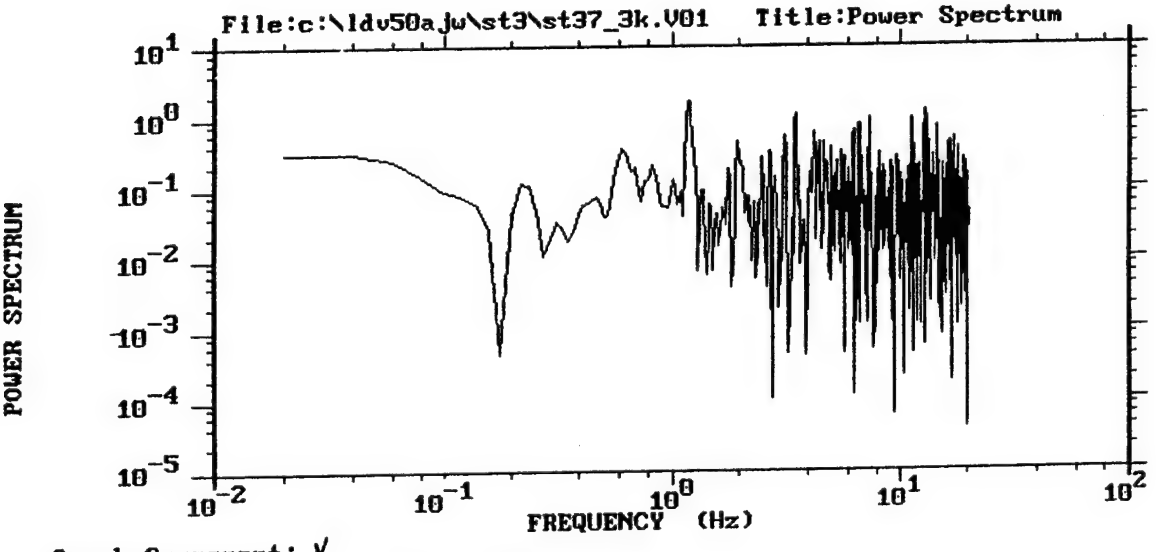

Graph Component: V
% of Bins Containing Data = 100
Scaling Factors (X,Y) = 1.0 , 1.0

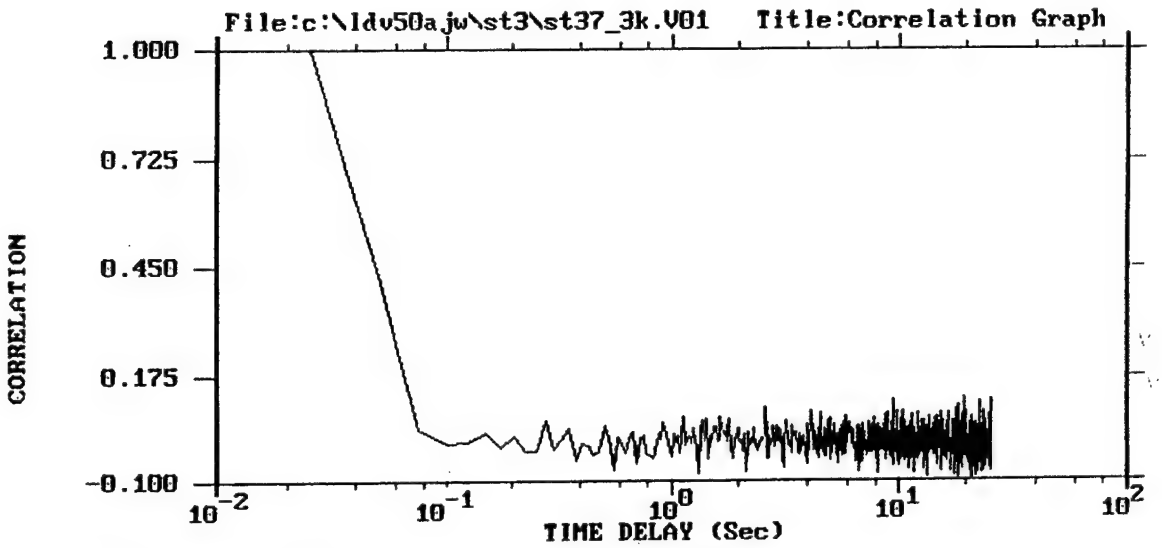

Graph Component: U
% of Bins Containing Data = 100
Scaling Factors (X,Y) = 1.0 , 1.0

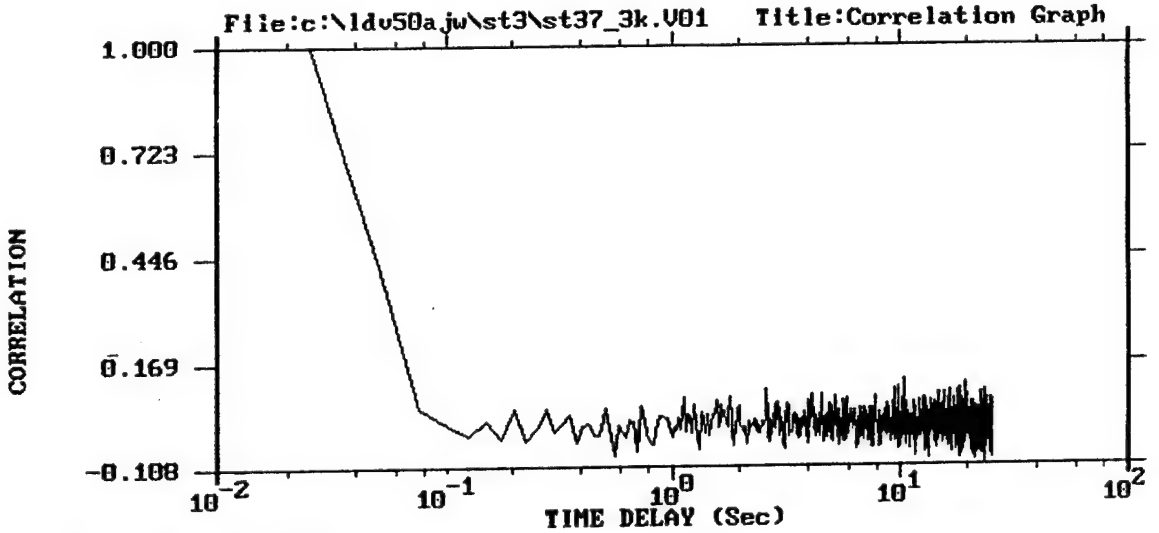

Graph Component: V
% of Bins Containing Data = 100
Scaling Factors (X,Y) = 1.0 , 1.0

b. 30K Data Points

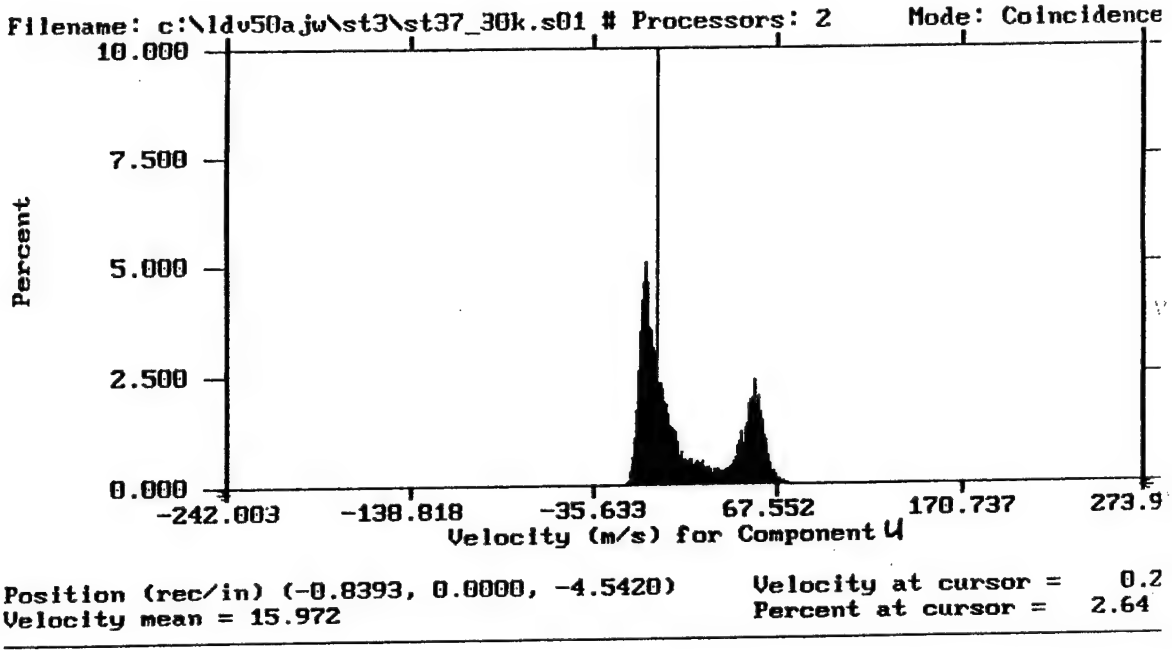

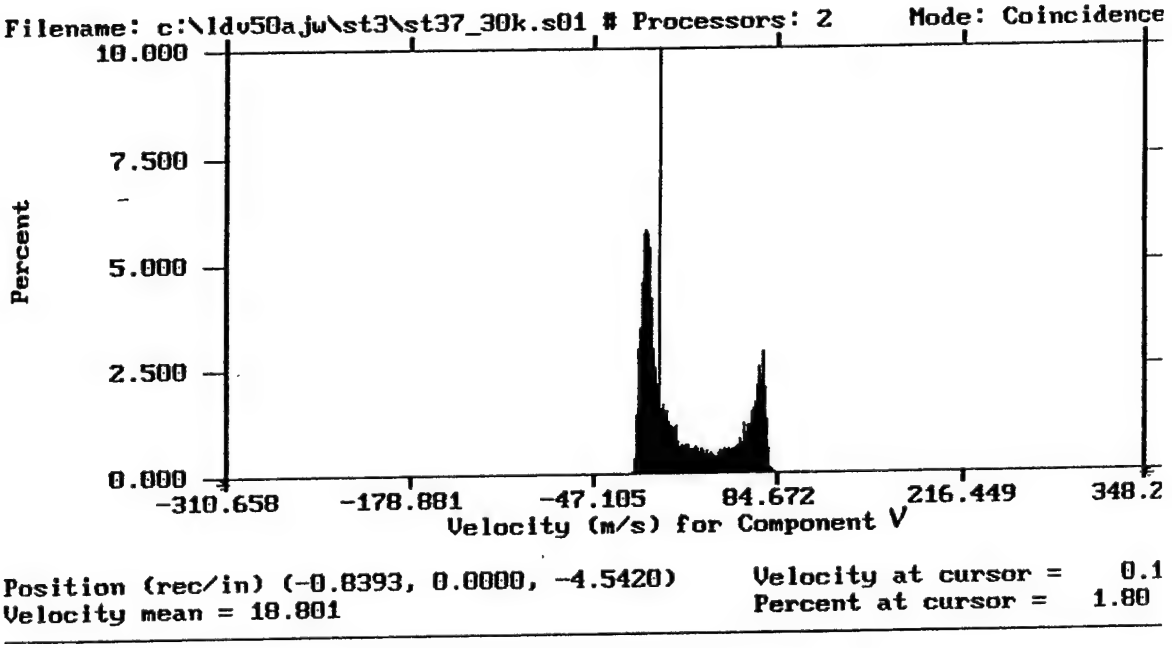

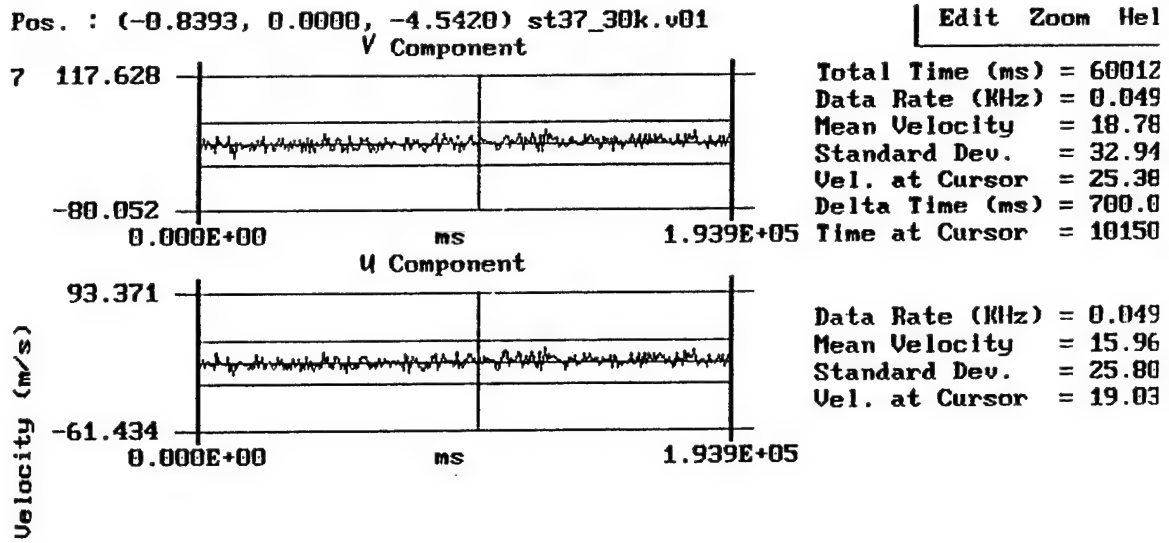
Pos. : (-0.8393, 0.0000, -4.5420) st37_30k.v01
Edit Zoom Hel
V Component
7 117.628
-80.052
0.000E+00
ms
1.939E+05
Total Time (ms) = 60012
Data Rate (KHz) = 0.049
Mean Velocity = 18.78
Standard Dev. = 32.94
Vel. at Cursor = 25.38
Delta Time (ms) = 700.0
Time at Cursor = 10150
U Component
93.371
-61.434
0.000E+00
ms
1.939E+05
Velocity (m/s)
Data Rate (KHz) = 0.049
Mean Velocity = 15.96
Standard Dev. = 25.80
Vel. at Cursor = 19.03

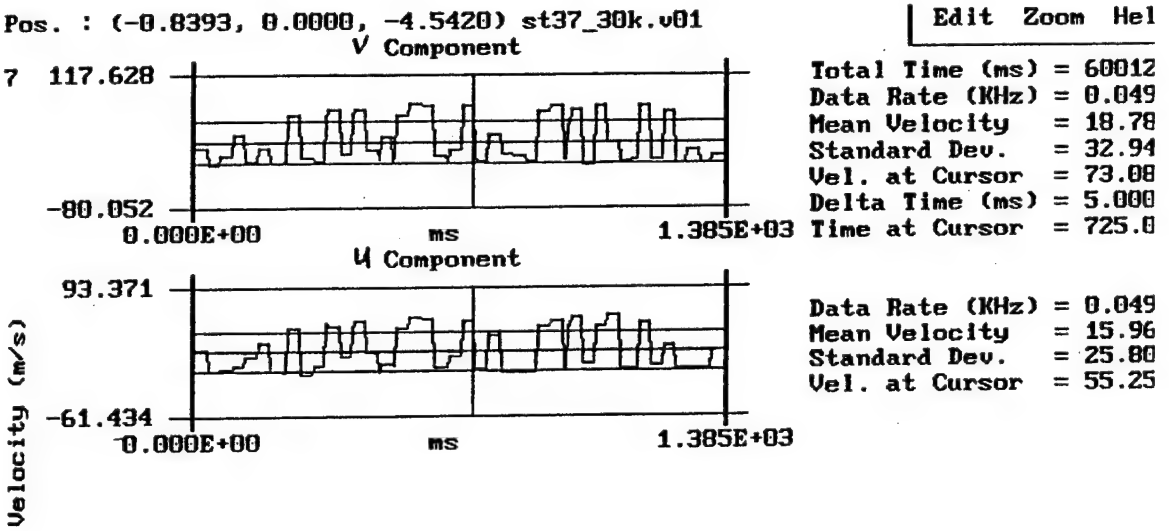
Pos. : (-0.8393, 0.0000, -4.5420) st37_30k.v01
Edit Zoom Hel
V Component
7 117.628
-80.052
0.000E+00
ms
1.385E+03
Total Time (ms) = 60012
Data Rate (KHz) = 0.049
Mean Velocity = 18.78
Standard Dev. = 32.94
Vel. at Cursor = 73.08
Delta Time (ms) = 5.000
Time at Cursor = 725.0
U Component
93.371
-61.434
0.000E+00
ms
1.385E+03
Velocity (m/s)
Data Rate (KHz) = 0.049
Mean Velocity = 15.96
Standard Dev. = 25.80
Vel. at Cursor = 55.25

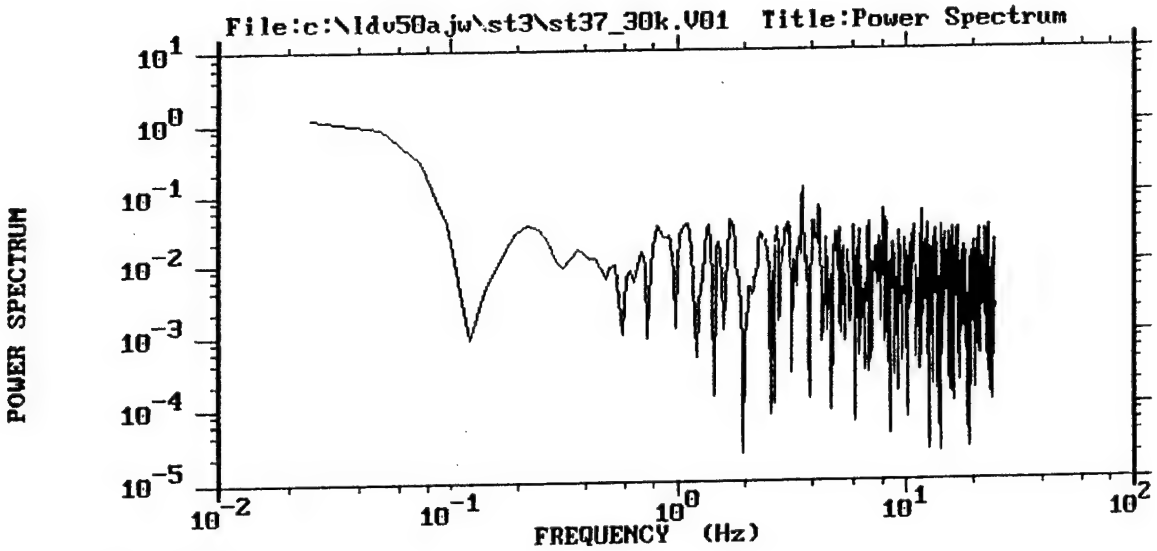

Graph Component: U
% of Bins Containing Data = 100
Scaling Factors (X,Y) = 1.0 , 1.0

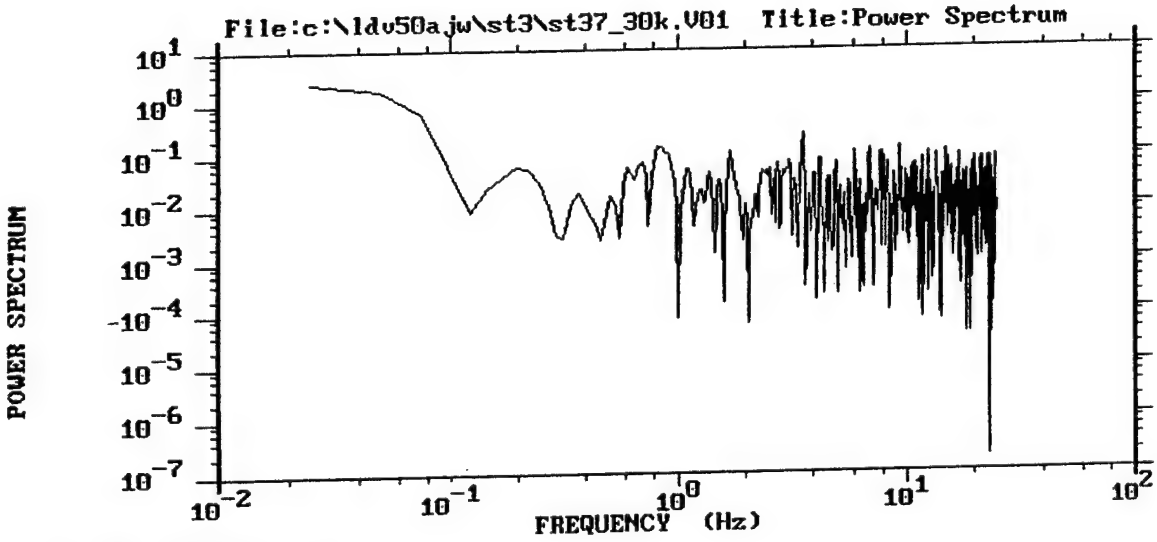

Graph Component: V
% of Bins Containing Data = 100
Scaling Factors (X,Y) = 1.0 , 1.0

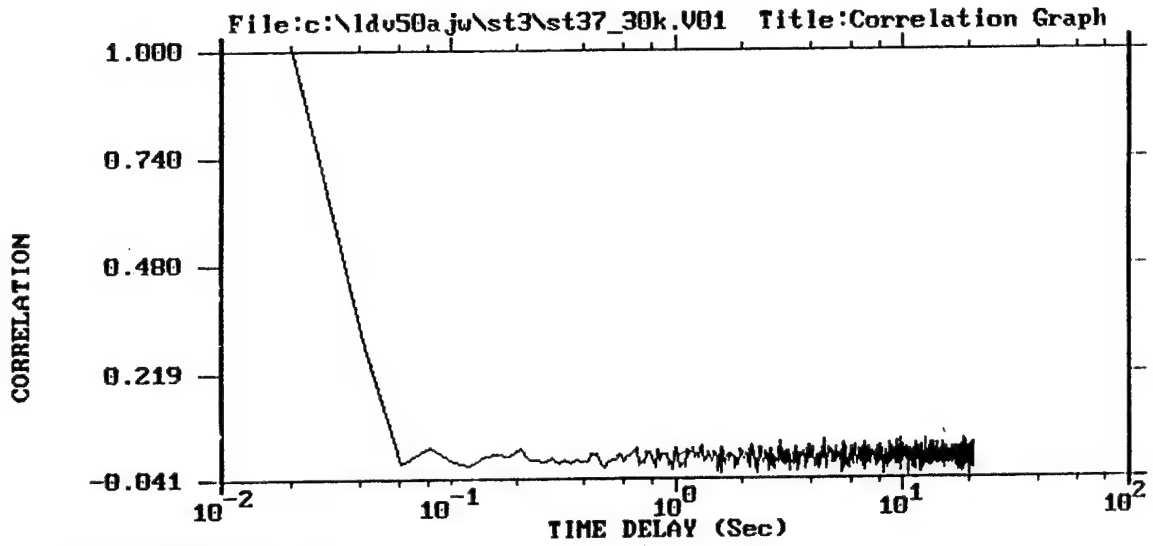

Graph Component: U
% of Bins Containing Data = 100
Scaling Factors (X,Y) = 1.0 , 1.0

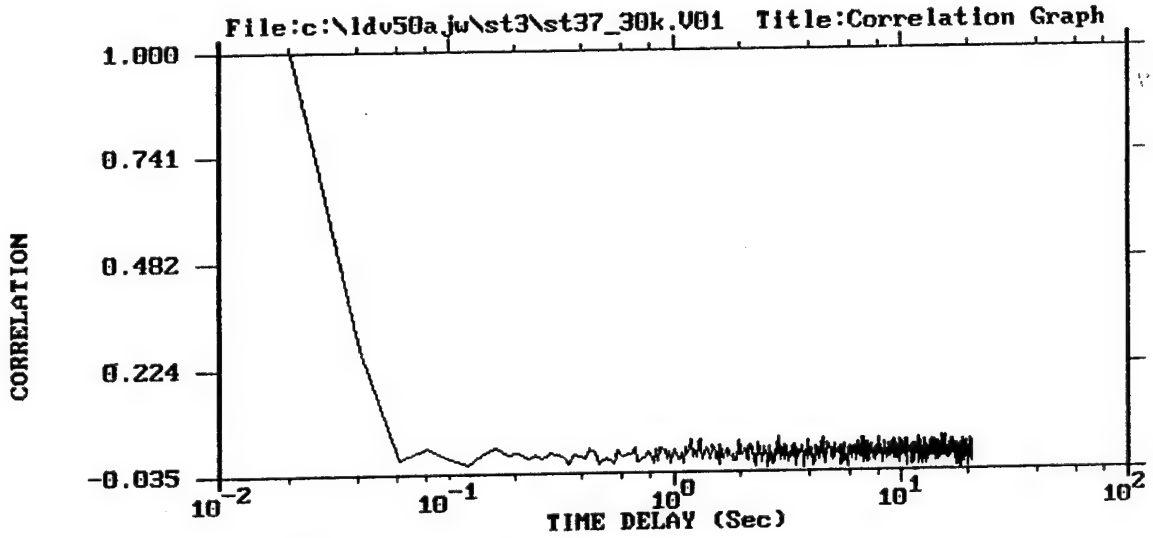

Graph Component: V
% of Bins Containing Data = 100
Scaling Factors (X,Y) = 1.0 , 1.0

2. Station 7, Point 3

a. 3K Data Points

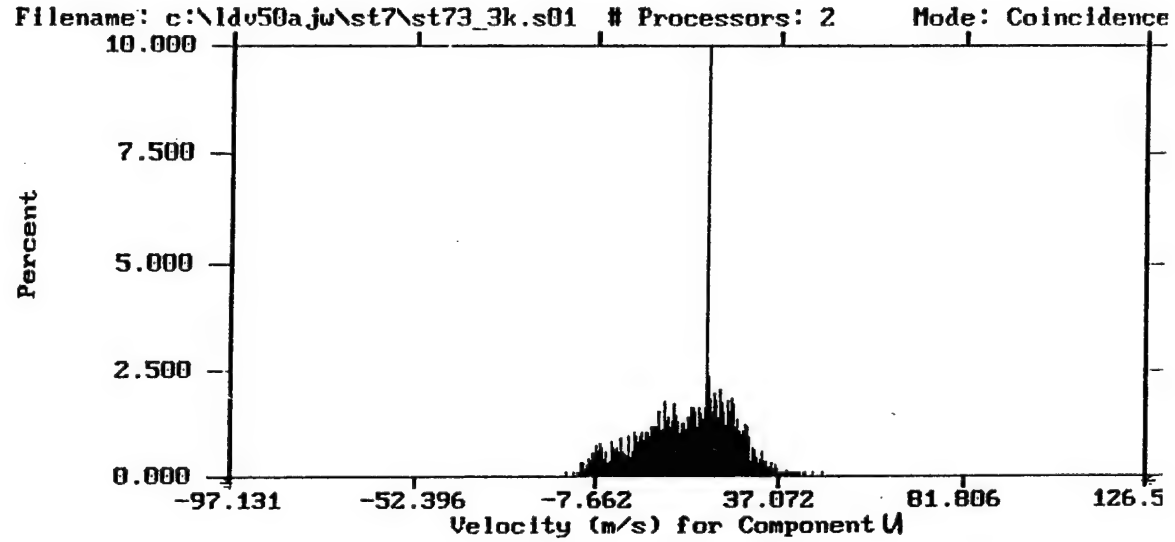

Position (rec/in) (-0.1225, 0.0000, -3.2921) Velocity at cursor = 19.6
Velocity mean = 14.785 Percent at cursor = 1.63

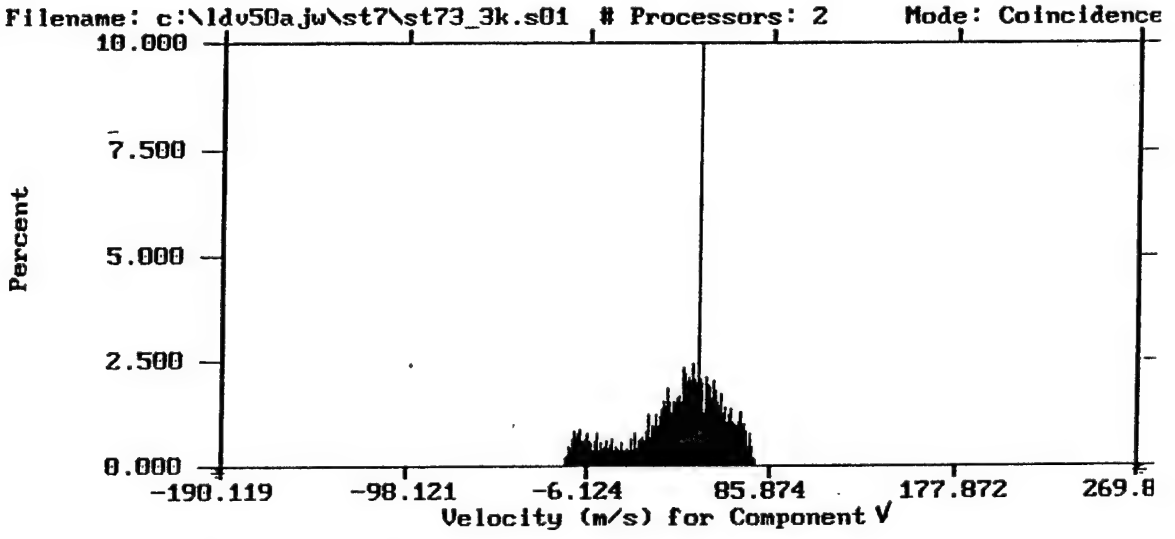

Position (rec/in) (-0.1225, 0.0000, -3.2921) Velocity at cursor = 50.0
Velocity mean = 39.875 Percent at cursor = 2.57

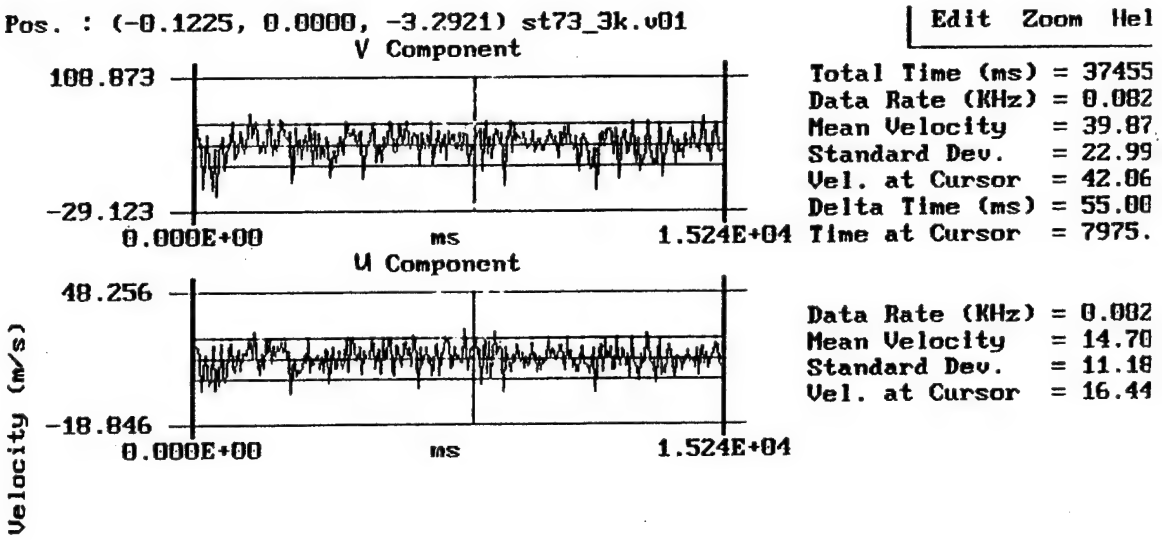
Pos. : (-0.1225, 0.0000, -3.2921) st73_3k.v01
Edit Zoom Hel
V Component
108.873
-29.123
0.000E+00
ms
1.524E+04
Total Time (ms) = 37455
Data Rate (KHz) = 0.082
Mean Velocity = 39.87
Standard Dev. = 22.99
Vel. at Cursor = 42.06
Delta Time (ms) = 55.00
Time at Cursor = 7975.
U Component
48.256
-18.846
0.000E+00
ms
1.524E+04
Velocity (m/s)
Data Rate (KHz) = 0.082
Mean Velocity = 14.70
Standard Dev. = 11.18
Vel. at Cursor = 16.44

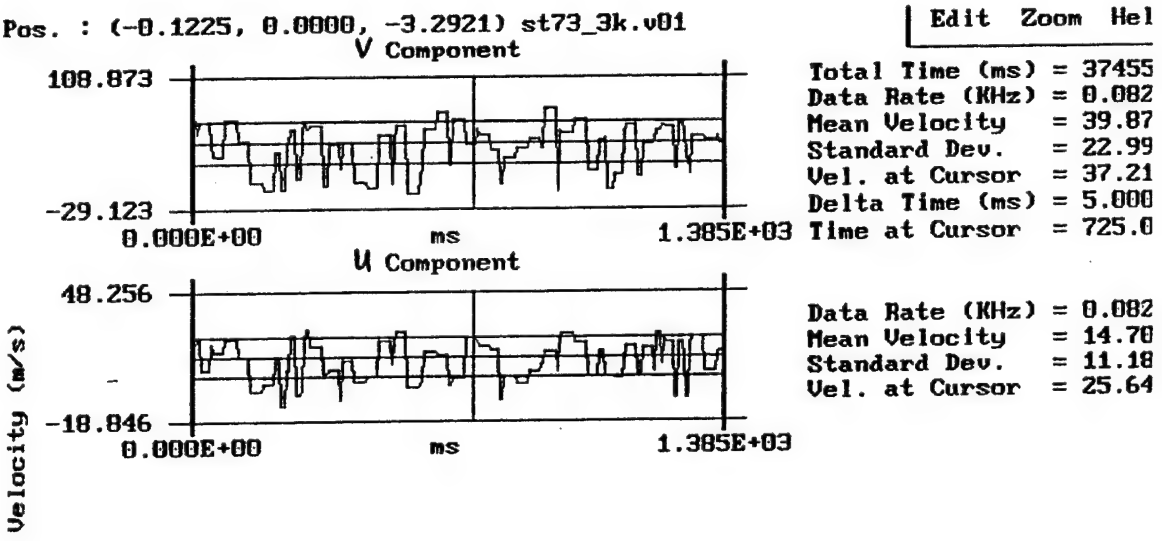
Pos. : (-0.1225, 0.0000, -3.2921) st73_3k.v01
Edit Zoom Hel
V Component
108.873
-29.123
0.000E+00
ms
1.385E+03
Total Time (ms) = 37455
Data Rate (KHz) = 0.082
Mean Velocity = 39.87
Standard Dev. = 22.99
Vel. at Cursor = 37.21
Delta Time (ms) = 5.000
Time at Cursor = 725.0
U Component
48.256
-18.846
0.000E+00
ms
1.385E+03
Velocity (m/s)
Data Rate (KHz) = 0.082
Mean Velocity = 14.70
Standard Dev. = 11.18
Vel. at Cursor = 25.64

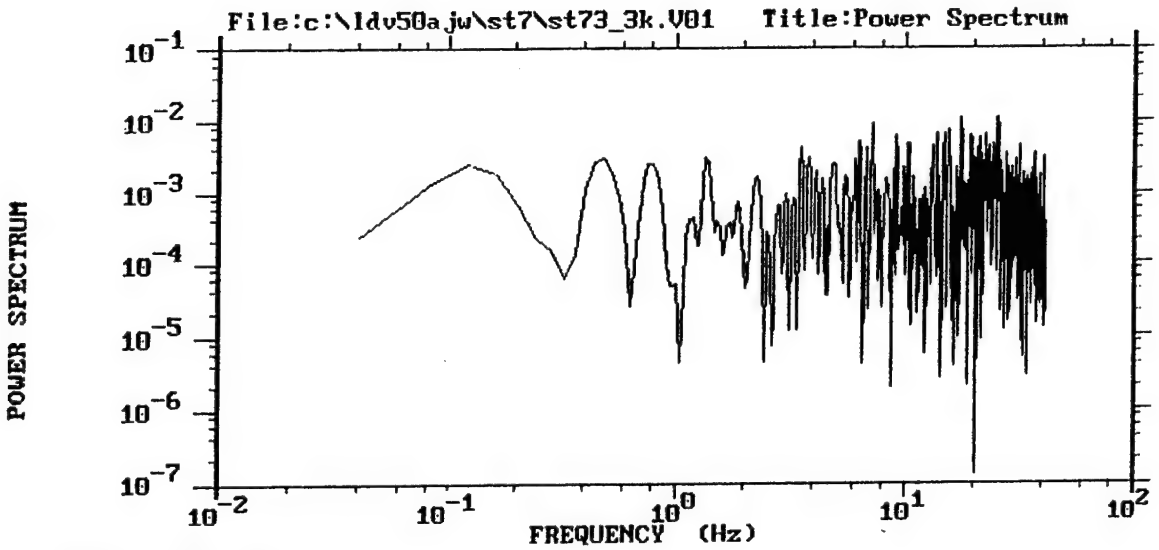

Graph Component: U
% of Bins Containing Data = 100
Scaling Factors (X,Y) = 1.0 , 1.0

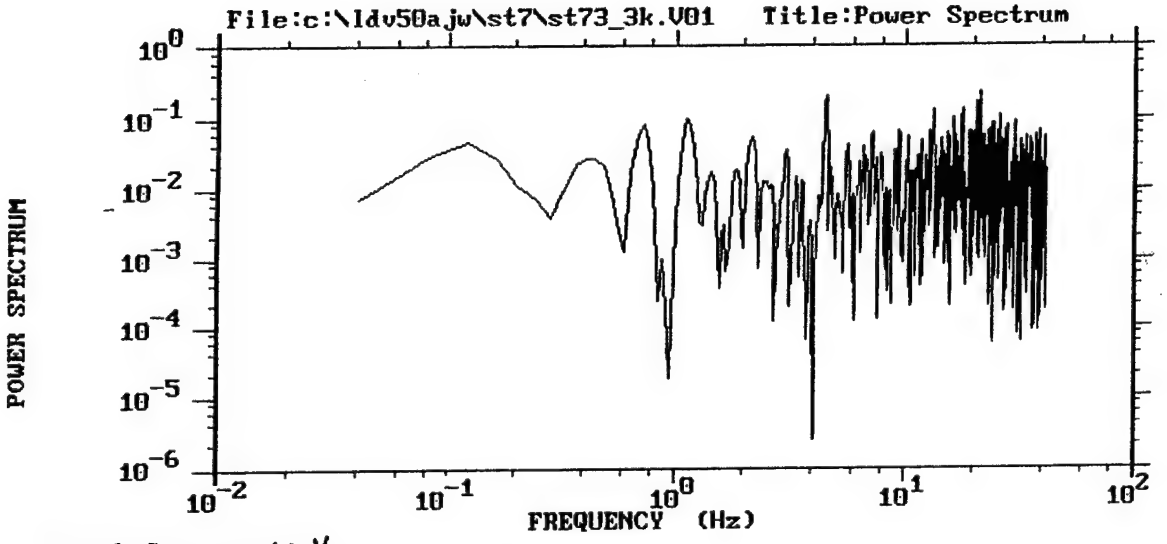

Graph Component: V
% of Bins Containing Data = 100
Scaling Factors (X,Y) = 1.0 , 1.0

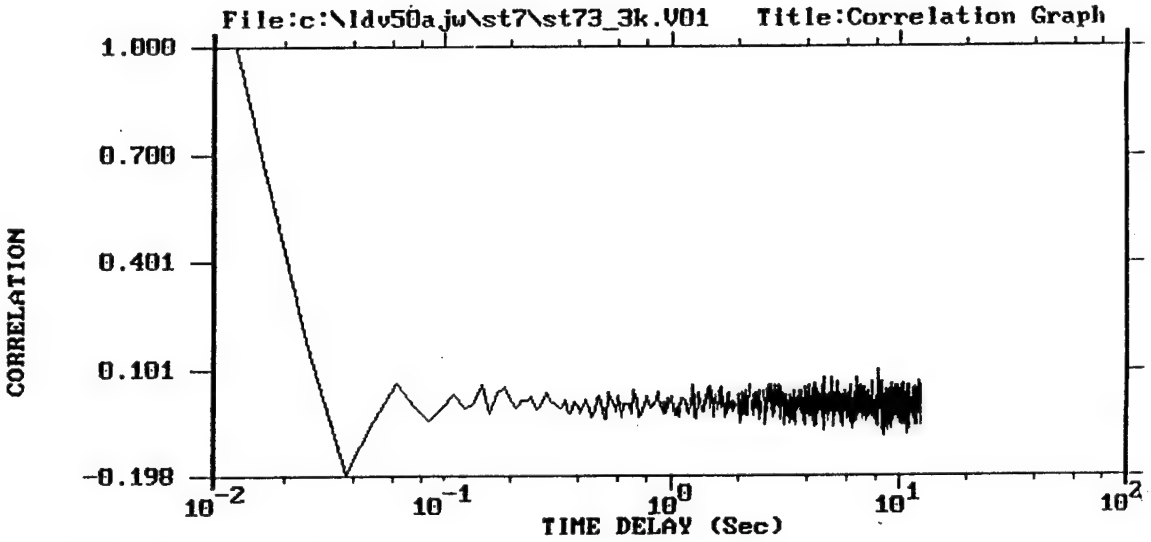

Graph Component: U
% of Bins Containing Data = 100
Scaling Factors (X,Y) = 1.0 , 1.0

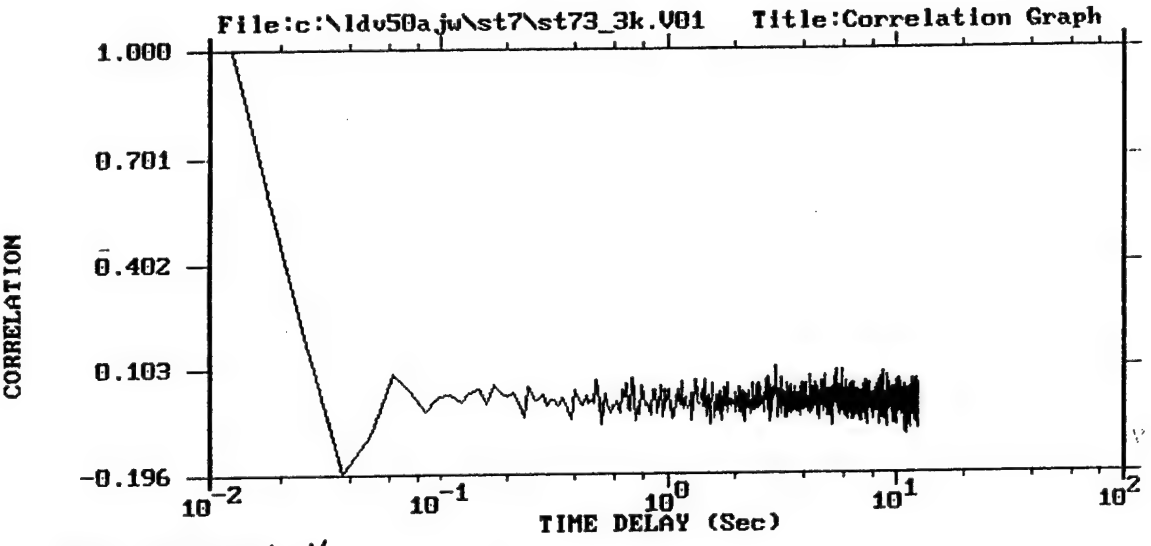

Graph Component: V
% of Bins Containing Data = 100
Scaling Factors (X,Y) = 1.0 , 1.0

b. 30K Data Points

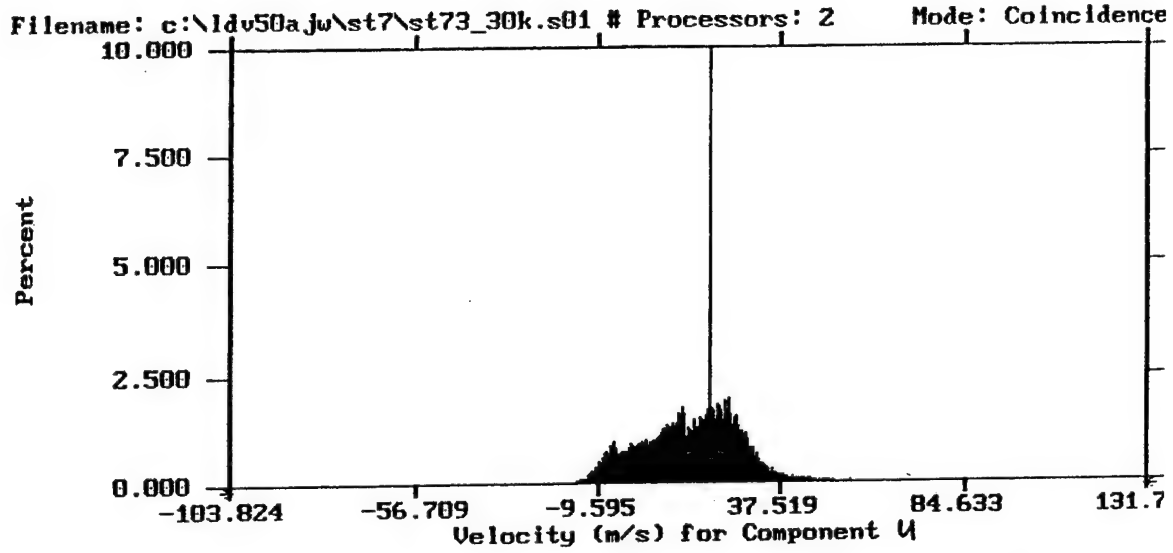

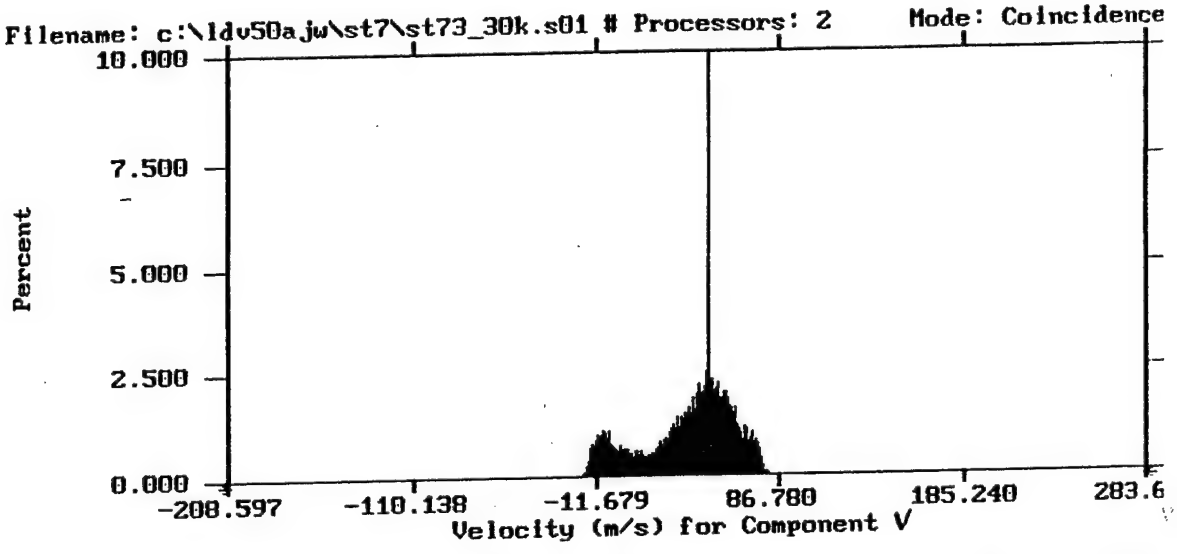

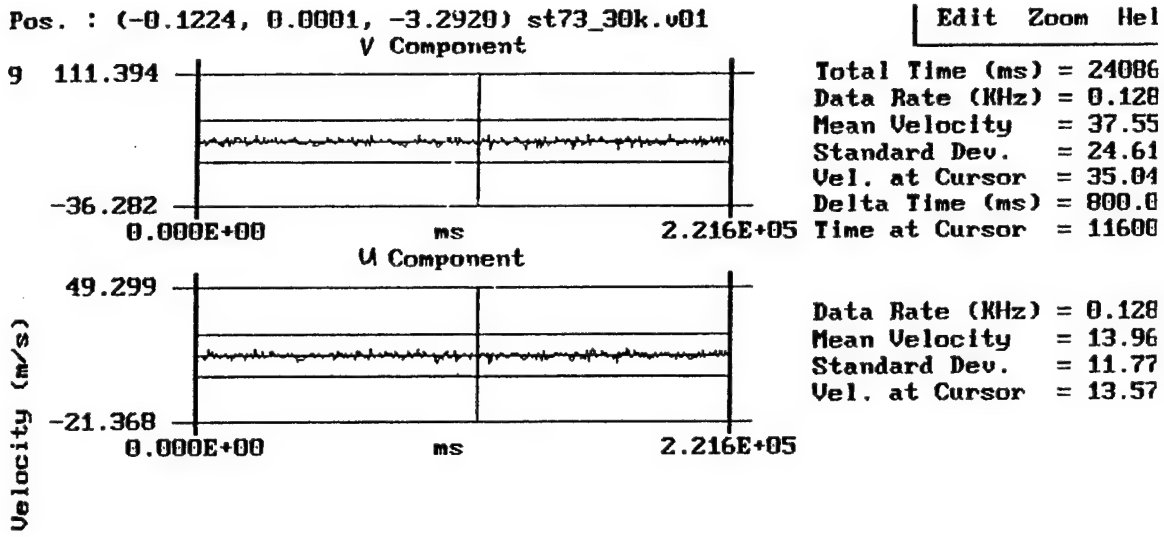
Pos. : (-0.1224, 0.0001, -3.2920) st73_30k.v01
Edit Zoom Hel
V Component
9 111.394
-36.282
0.000E+00
ms
2.216E+05
Total Time (ms) = 24086
Data Rate (KHz) = 0.128
Mean Velocity = 37.55
Standard Dev. = 24.61
Vel. at Cursor = 35.04
Delta Time (ms) = 800.0
Time at Cursor = 11600
U Component
49.299
-21.368
0.000E+00
ms
2.216E+05
Velocity (m/s)
Data Rate (KHz) = 0.128
Mean Velocity = 13.96
Standard Dev. = 11.77
Vel. at Cursor = 13.57

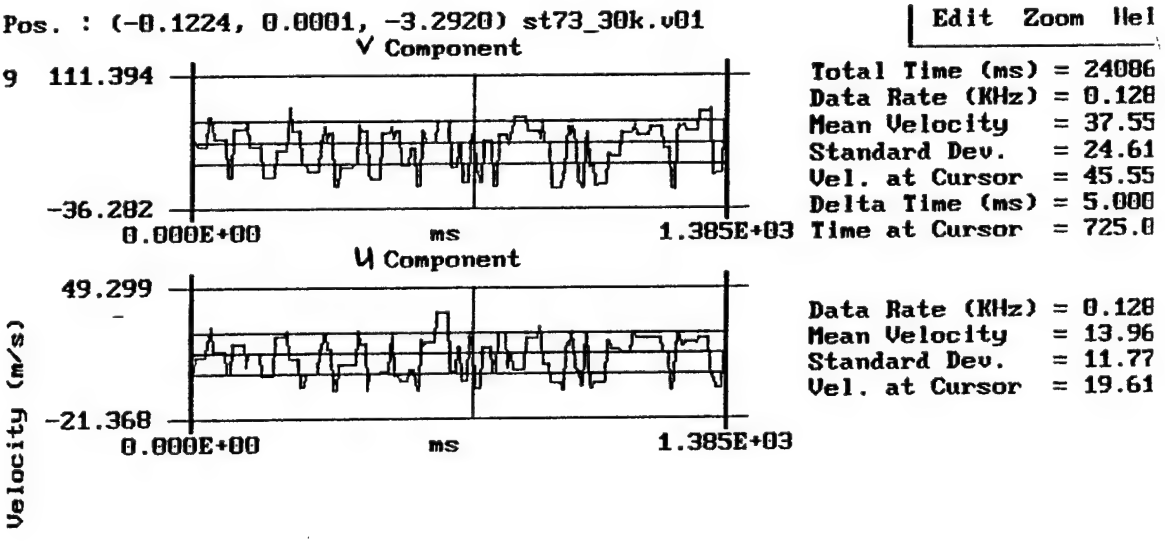
Pos. : (-0.1224, 0.0001, -3.2920) st73_30k.v01
Edit Zoom Hel
V Component
9 111.394
-36.282
0.000E+00
ms
1.385E+03
Total Time (ms) = 24086
Data Rate (KHz) = 0.128
Mean Velocity = 37.55
Standard Dev. = 24.61
Vel. at Cursor = 45.55
Delta Time (ms) = 5.000
Time at Cursor = 725.0
U Component
49.299
-21.368
0.000E+00
ms
1.385E+03
Velocity (m/s)
Data Rate (KHz) = 0.128
Mean Velocity = 13.96
Standard Dev. = 11.77
Vel. at Cursor = 19.61

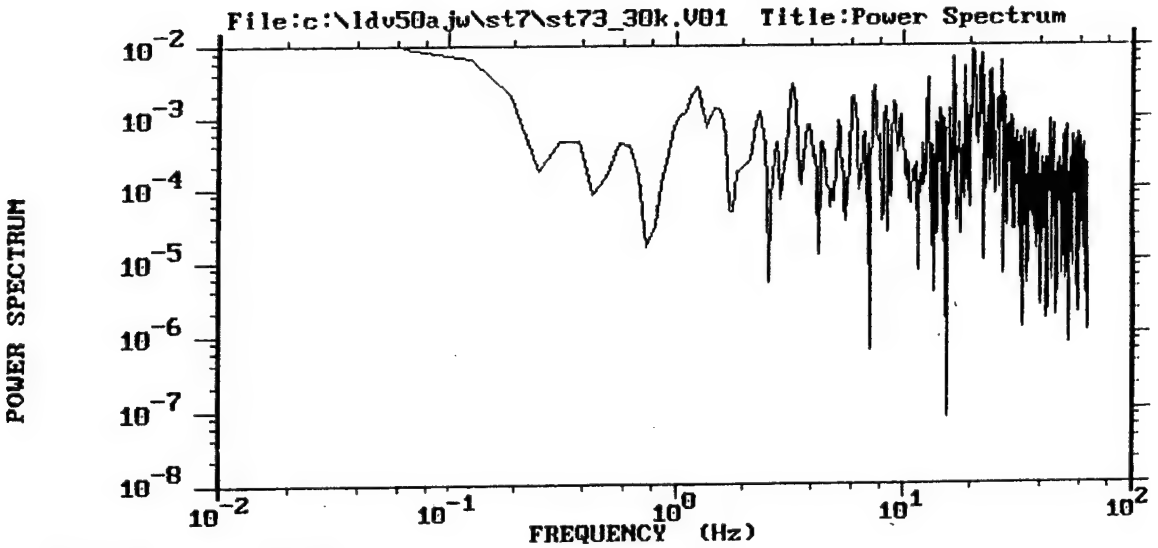

Graph Component: U
% of Bins Containing Data = 100
Scaling Factors (X,Y) = 1.0 , 1.0

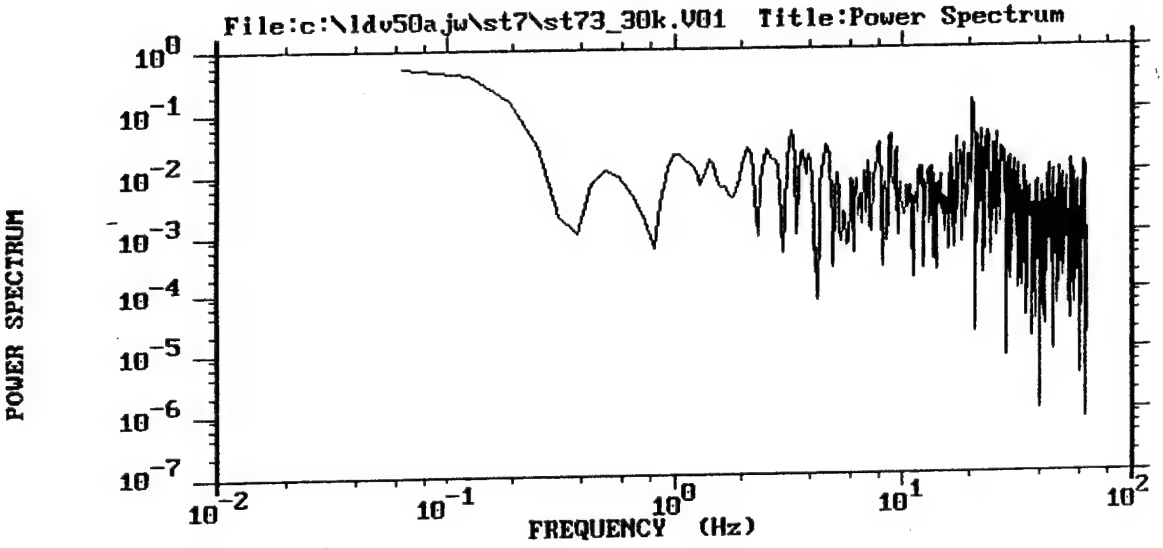

Graph Component: V
% of Bins Containing Data = 100
Scaling Factors (X,Y) = 1.0 , 1.0

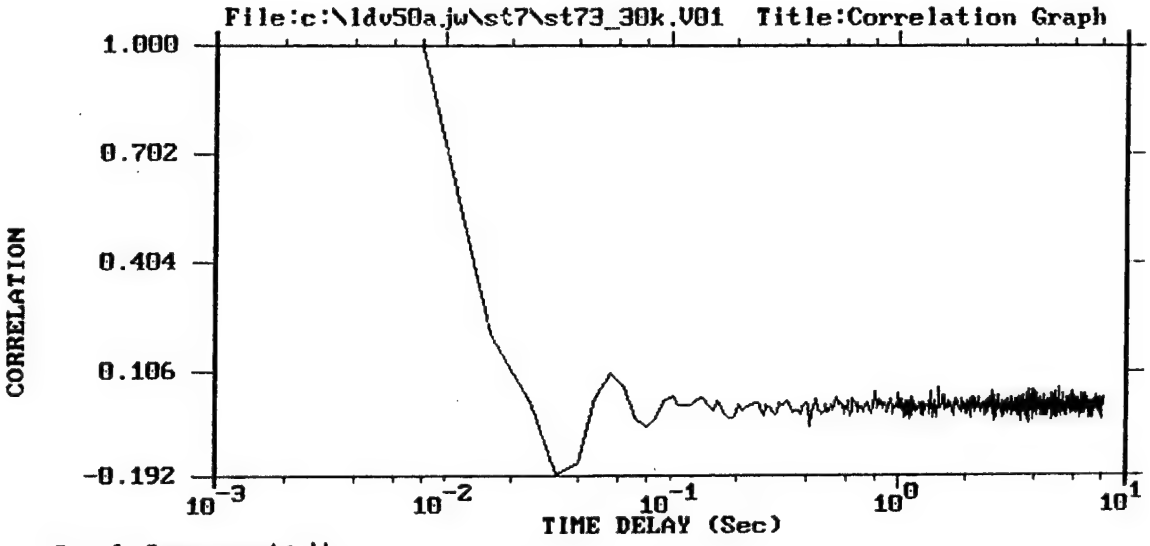

Graph Component: U
% of Bins Containing Data = 100
Scaling Factors (X,Y) = 1.0 , 1.0

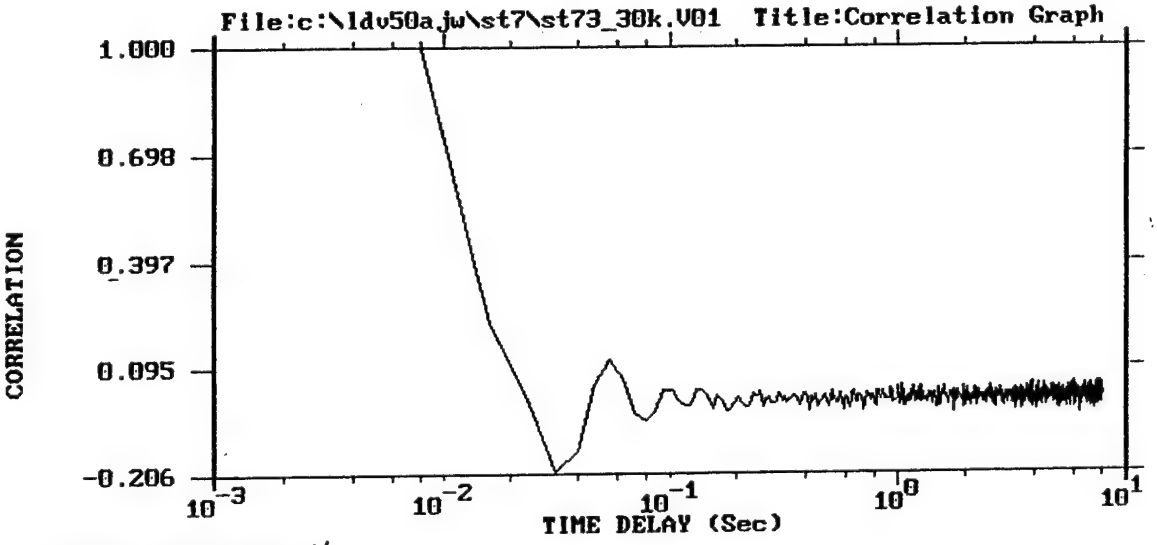

Graph Component: V
% of Bins Containing Data = 100
Scaling Factors (X,Y) = 1.0 , 1.0

c. Ganaim 3K Data Points

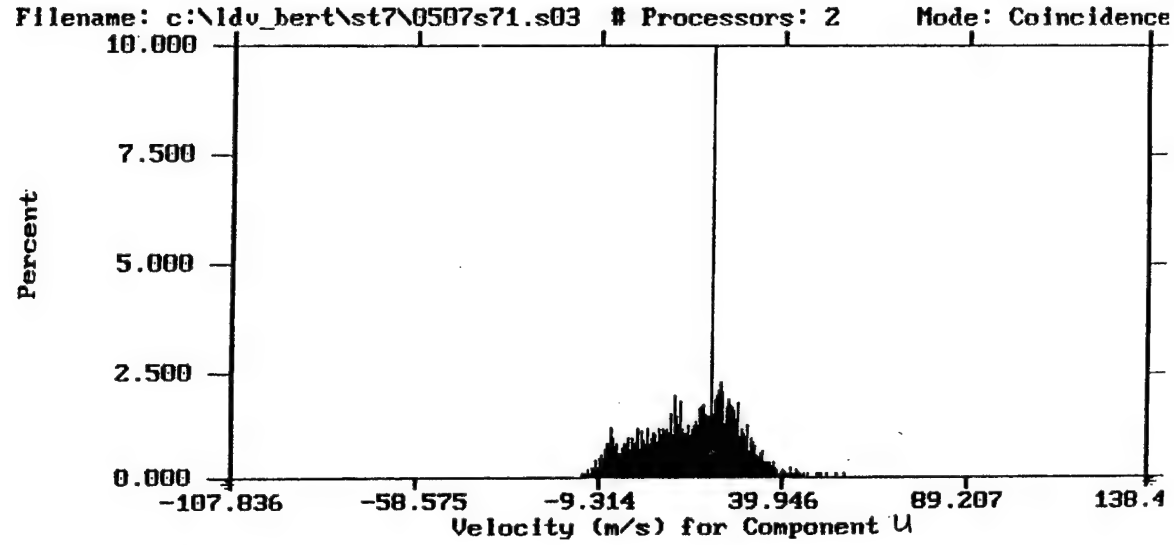

Position (rec/in) (-0.1224, 0.0000, -3.2921) Velocity at cursor = 20.7
Velocity mean = 15.316 Percent at cursor = 1.20

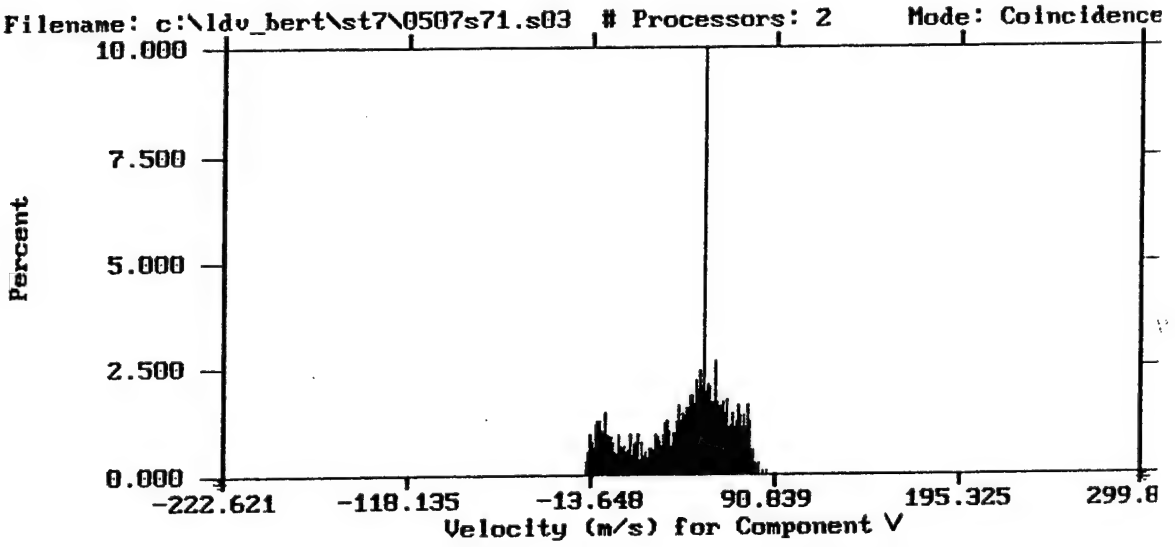

Position (rec/in) (-0.1224, 0.0000, -3.2921) Velocity at cursor = 50.0
Velocity mean = 38.608 Percent at cursor = 2.41

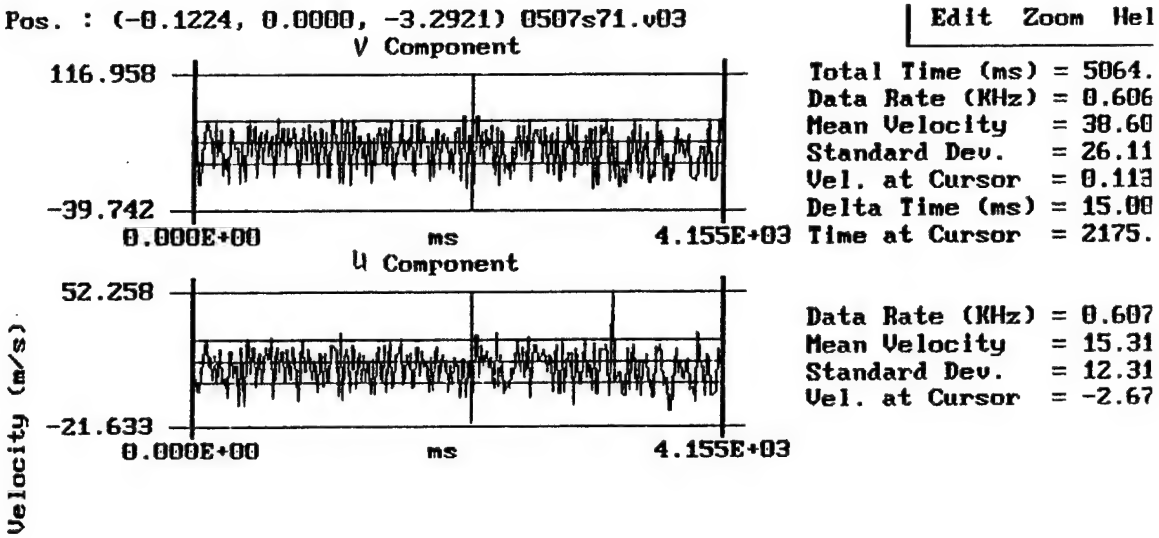
Pos. : (-0.1224, 0.0000, -3.2921) 0507s71.v03
Edit Zoom Hel
V Component
116.958
-39.742
0.000E+00
ms
4.155E+03
Total Time (ms) = 5064.
Data Rate (KHz) = 0.606
Mean Velocity = 38.60
Standard Dev. = 26.11
Vel. at Cursor = 0.113
Delta Time (ms) = 15.00
Time at Cursor = 2175.
U Component
52.258
-21.633
0.000E+00
ms
4.155E+03
Data Rate (KHz) = 0.607
Mean Velocity = 15.31
Standard Dev. = 12.31
Vel. at Cursor = -2.67
Velocity (m/s)

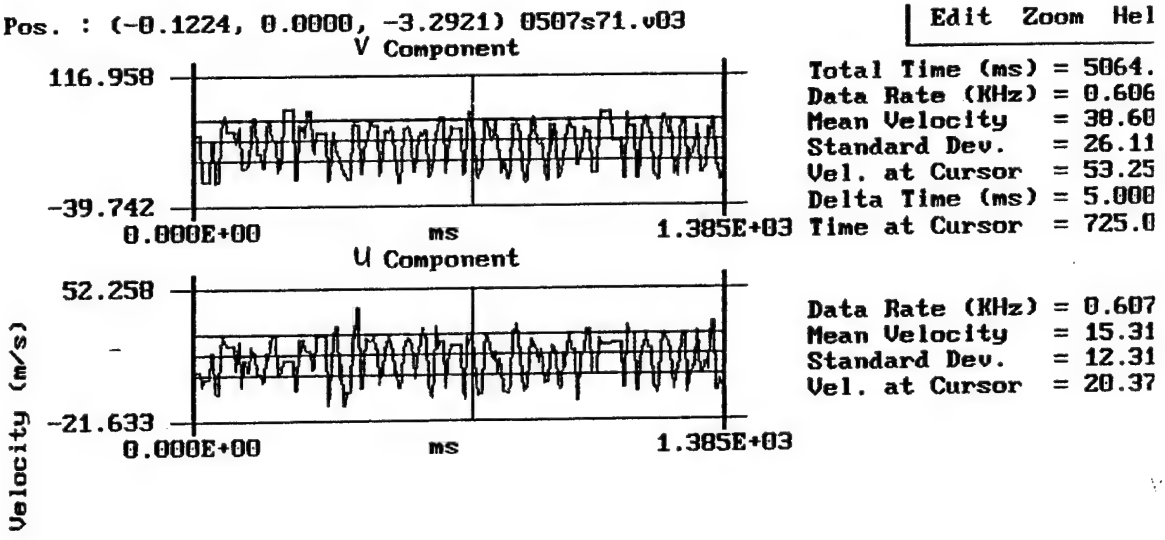
Pos. : (-0.1224, 0.0000, -3.2921) 0507s71.v03
Edit Zoom Hel
V Component
116.958
-39.742
0.000E+00
ms
1.385E+03
Total Time (ms) = 5064.
Data Rate (KHz) = 0.606
Mean Velocity = 38.60
Standard Dev. = 26.11
Vel. at Cursor = 53.25
Delta Time (ms) = 5.000
Time at Cursor = 725.0
U Component
52.258
-21.633
0.000E+00
ms
1.385E+03
Data Rate (KHz) = 0.607
Mean Velocity = 15.31
Standard Dev. = 12.31
Vel. at Cursor = 20.37
Velocity (m/s)

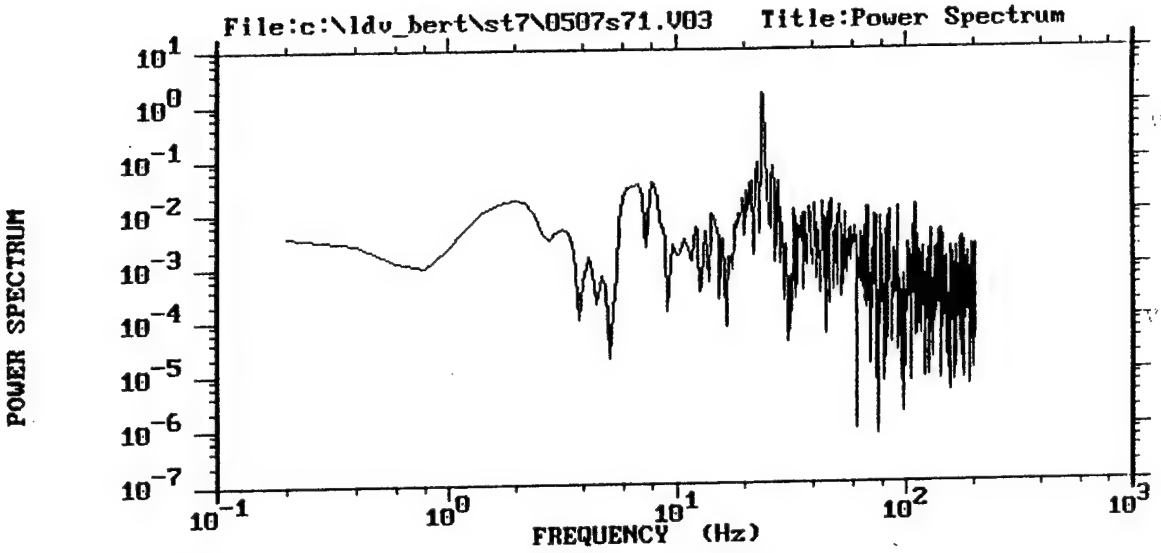

Graph Component: U
% of Bins Containing Data = 100
Scaling Factors (X,Y) = 1.0 , 1.0

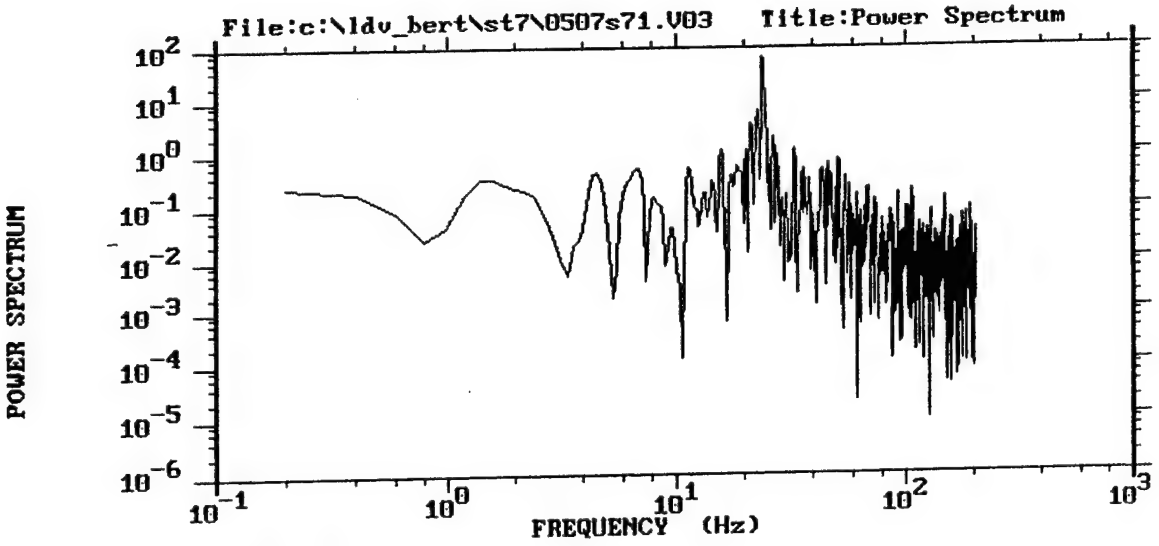

Graph Component: V
% of Bins Containing Data = 100
Scaling Factors (X,Y) = 1.0 , 1.0

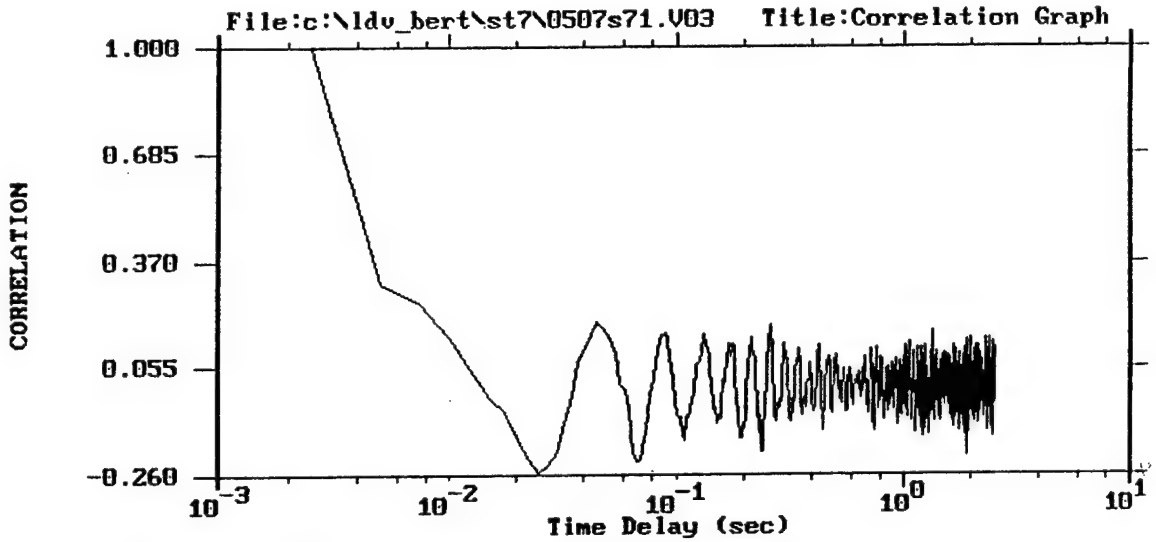

Graph Component: U
% of Bins Containing Data = 100
Scaling Factors (X,Y) = 1.0 , 1.0

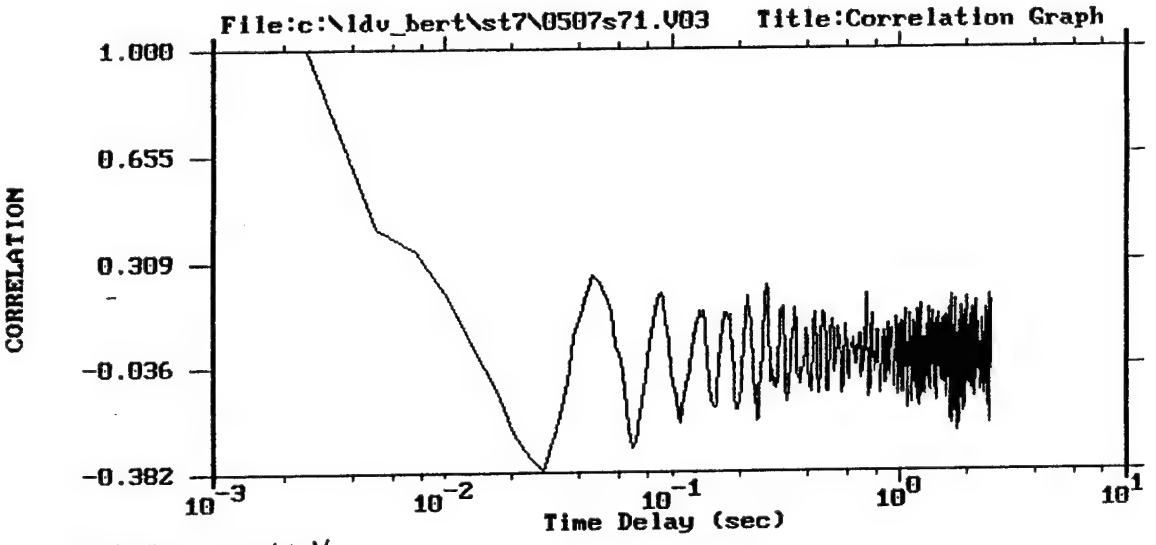

Graph Component: V
% of Bins Containing Data = 100
Scaling Factors (X,Y) = 1.0 , 1.0

3. Station 7, Point 20

a. 3K Data Points

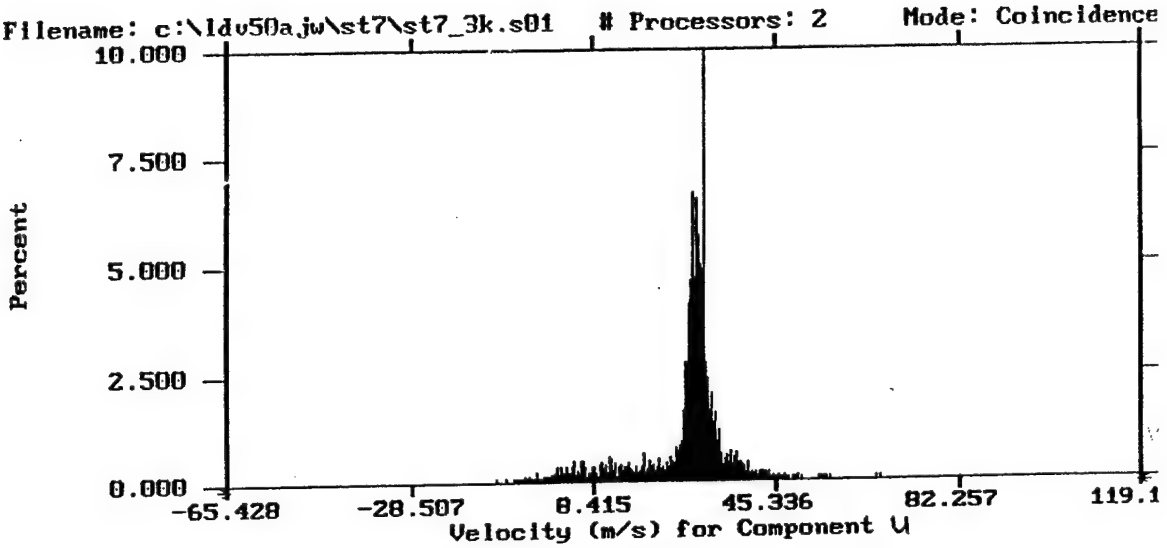

Position (rec/in) (0.3654, 0.0000, -3.2920)
Velocity mean = 26.884

Velocity at cursor = 30.9
Percent at cursor = 3.22

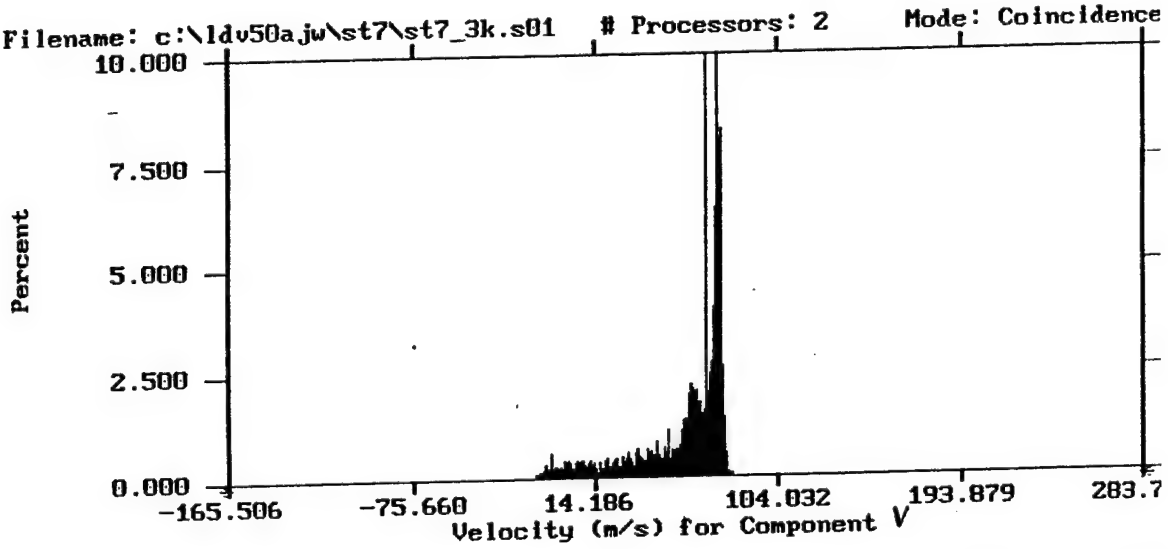

Position (rec/in) (0.3654, 0.0000, -3.2920)
Velocity mean = 59.130

Velocity at cursor = 68.9
Percent at cursor = 1.73

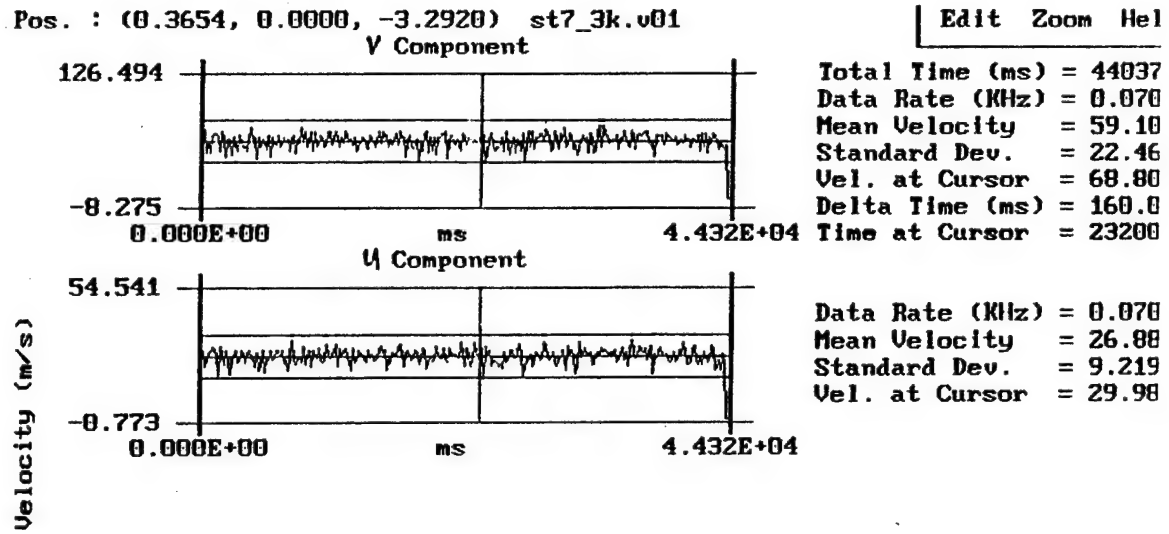
Pos. : (0.3654, 0.0000, -3.2920) st7_3k.v01
Edit Zoom Hel
V Component
126.494
-8.275
0.000E+00
ms
4.432E+04
Total Time (ms) = 44037
Data Rate (KHz) = 0.070
Mean Velocity = 59.10
Standard Dev. = 22.46
Vel. at Cursor = 68.80
Delta Time (ms) = 160.0
Time at Cursor = 23200
U Component
54.541
-0.773
0.000E+00
ms
4.432E+04
Velocity (m/s)
Data Rate (KHz) = 0.070
Mean Velocity = 26.88
Standard Dev. = 9.219
Vel. at Cursor = 29.98

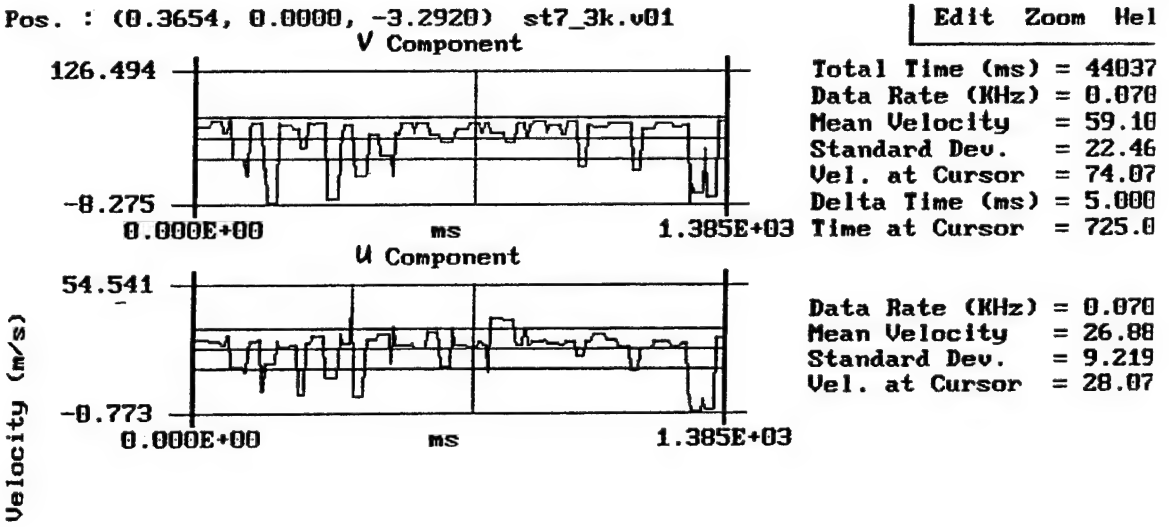
Pos. : (0.3654, 0.0000, -3.2920) st7_3k.v01
Edit Zoom Hel
V Component
126.494
-8.275
0.000E+00
ms
1.385E+03
Total Time (ms) = 44037
Data Rate (KHz) = 0.070
Mean Velocity = 59.10
Standard Dev. = 22.46
Vel. at Cursor = 74.07
Delta Time (ms) = 5.000
Time at Cursor = 725.0
U Component
54.541
-0.773
0.000E+00
ms
1.385E+03
Velocity (m/s)
Data Rate (KHz) = 0.070
Mean Velocity = 26.88
Standard Dev. = 9.219
Vel. at Cursor = 28.07

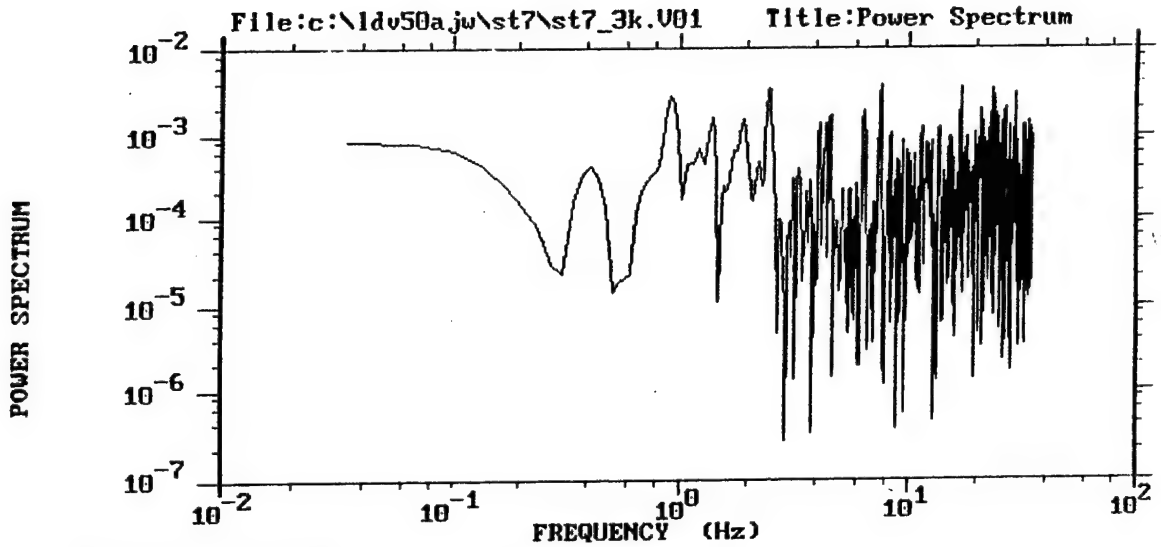

Graph Component: U
% of Bins Containing Data = 100
Scaling Factors (X,Y) = 1.0 , 1.0

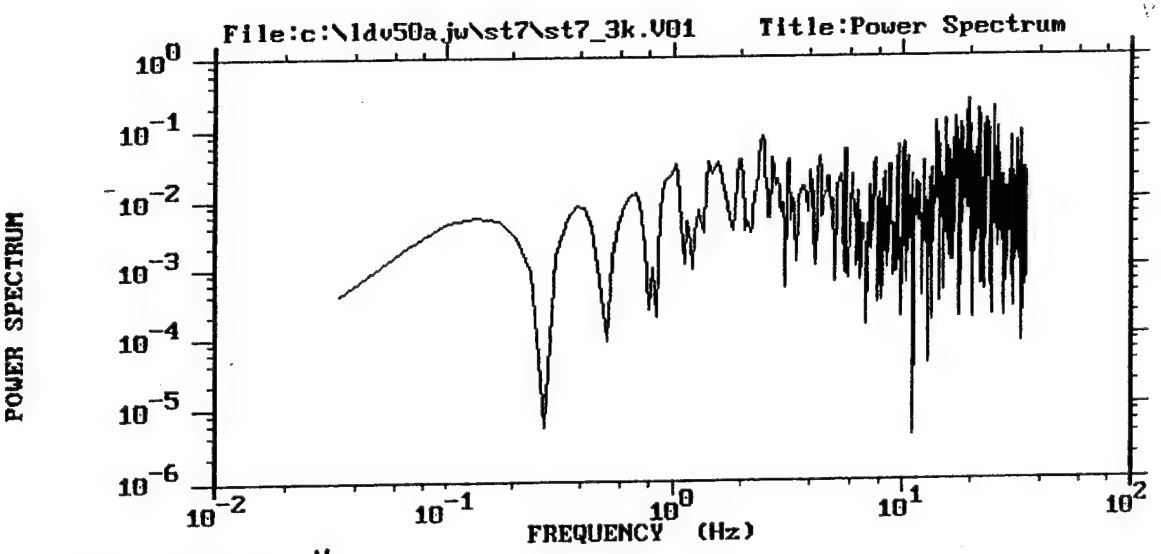

Graph Component: V
% of Bins Containing Data = 100
Scaling Factors (X,Y) = 1.0 , 1.0

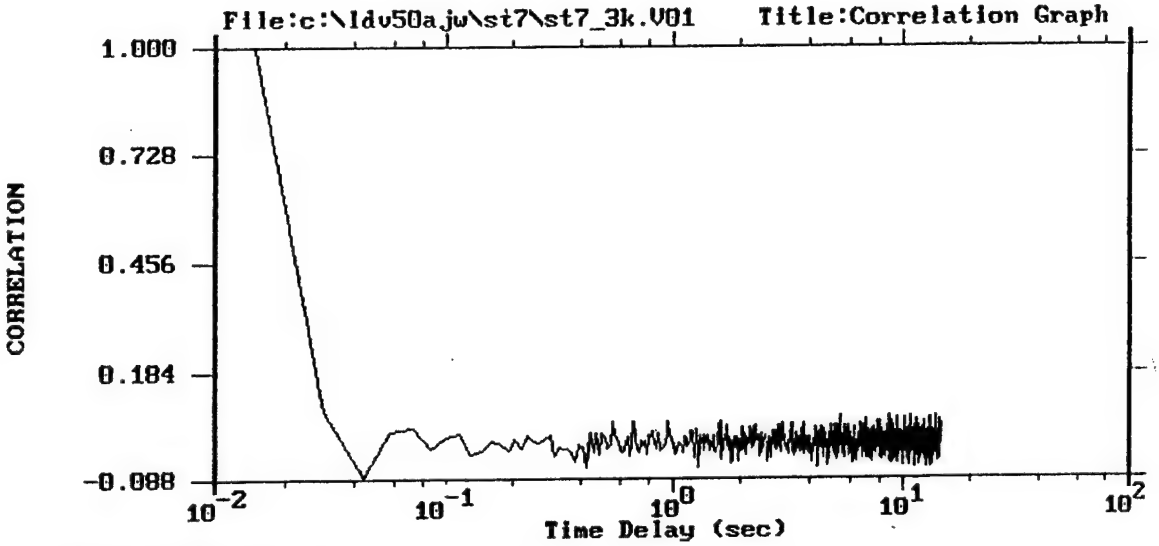

Graph Component: U
% of Bins Containing Data = 100
Scaling Factors (X,Y) = 1.0 , 1.0

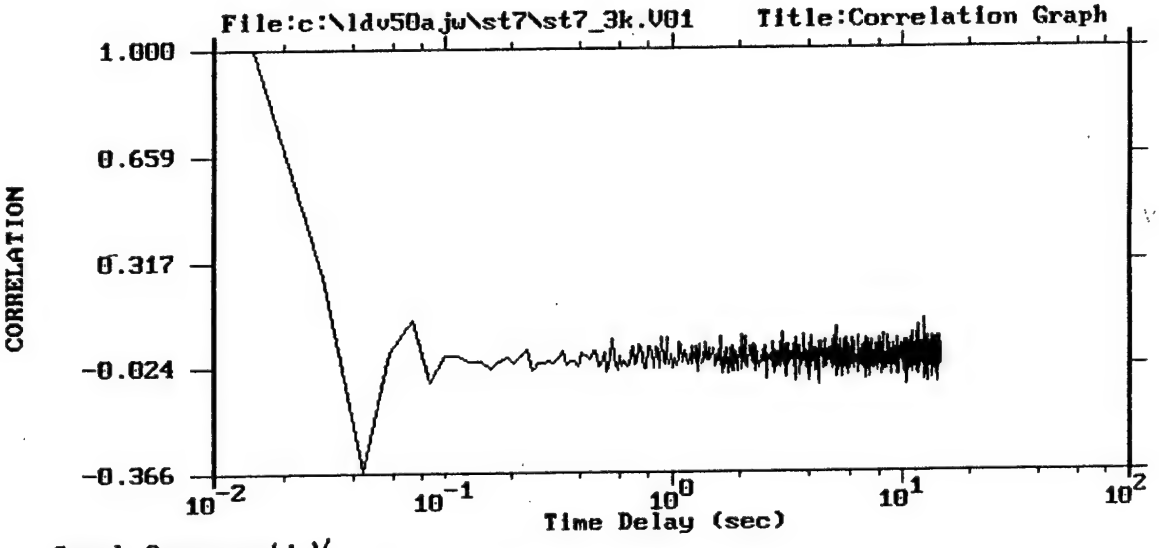

Graph Component: V
% of Bins Containing Data = 100
Scaling Factors (X,Y) = 1.0 , 1.0

b. 30K Data Points

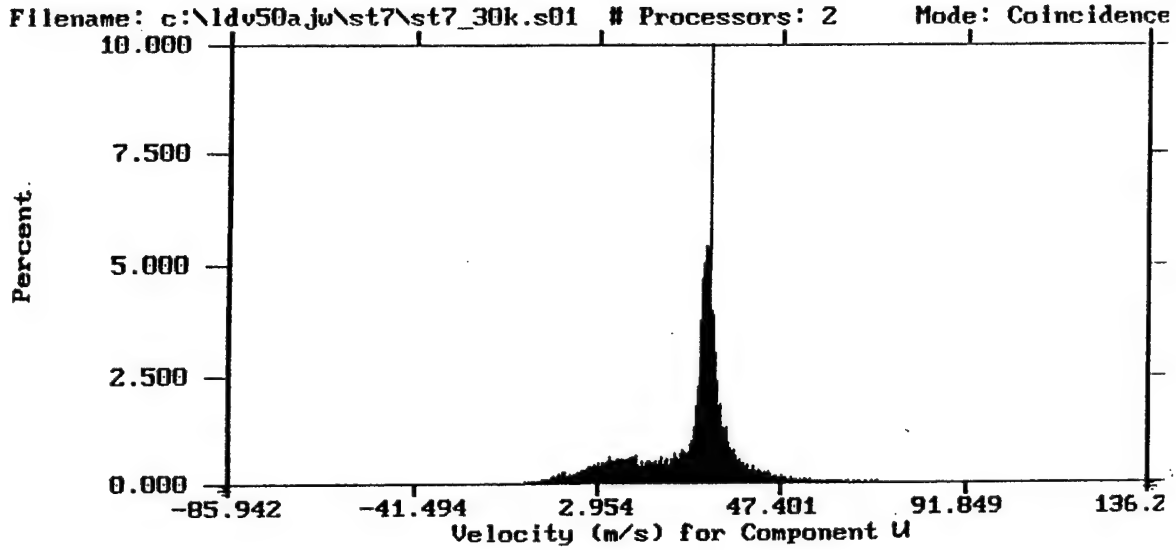

Position (rec/in) (0.3653, -0.0001, -3.2920) Velocity at cursor = 30.0
Velocity mean = 25.181 Percent at cursor = 6.04

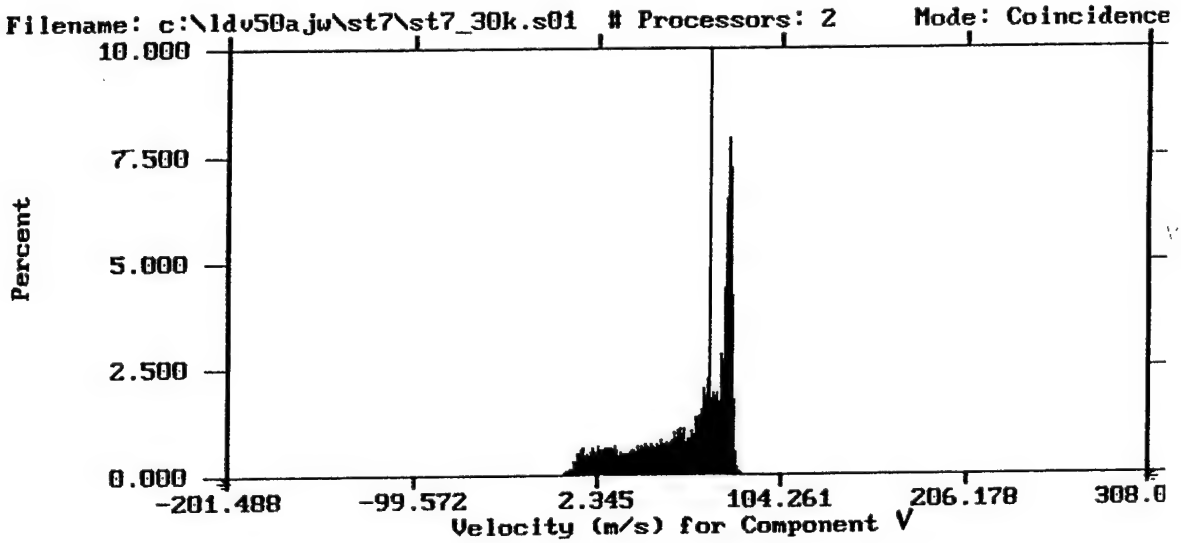

Position (rec/in) (0.3653, -0.0001, -3.2920) Velocity at cursor = 64.5
Velocity mean = 53.312 Percent at cursor = 1.83

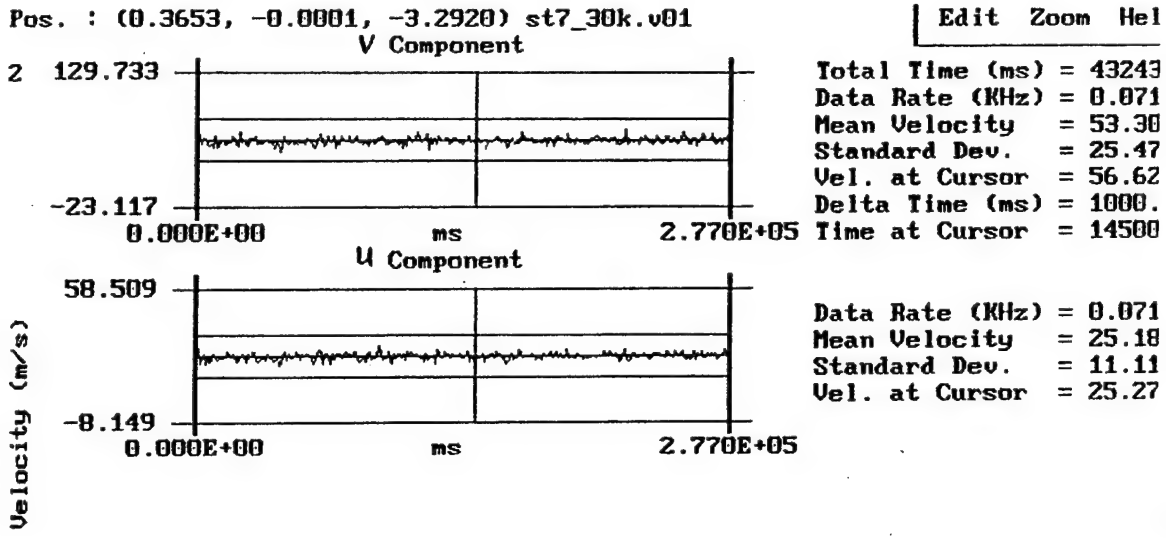
Pos. : (0.3653, -0.0001, -3.2920) st7_30k.v01
Edit Zoom Hel
V Component
2 129.733
-23.117
0.000E+00
ms
2.770E+05
Total Time (ms) = 43243
Data Rate (KHz) = 0.071
Mean Velocity = 53.30
Standard Dev. = 25.47
Vel. at Cursor = 56.62
Delta Time (ms) = 1000.
Time at Cursor = 14500
U Component
58.509
-8.149
0.000E+00
ms
2.770E+05
Velocity (m/s)
Data Rate (KHz) = 0.071
Mean Velocity = 25.18
Standard Dev. = 11.11
Vel. at Cursor = 25.27

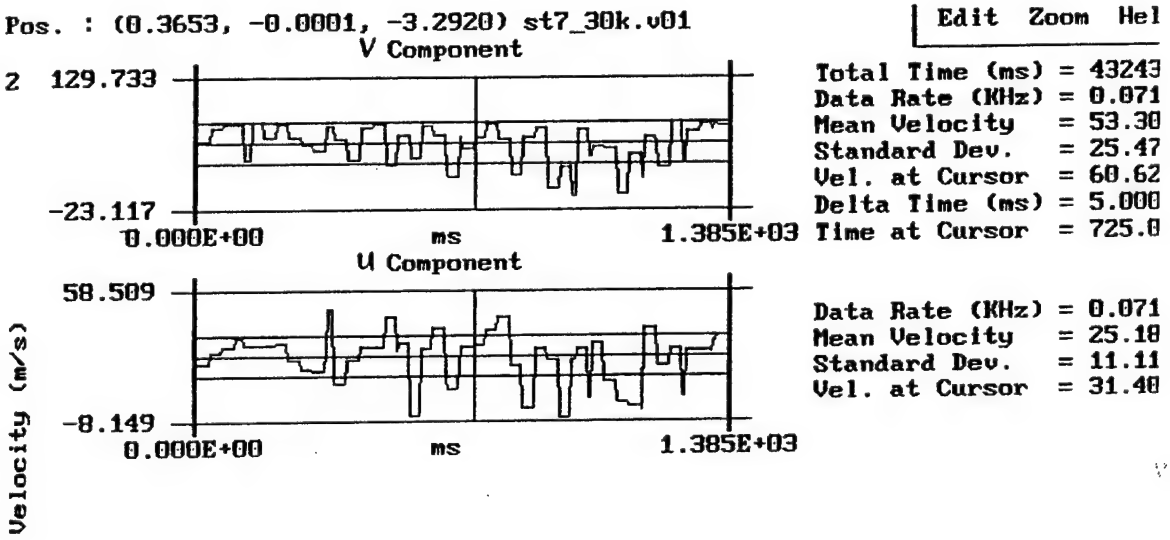
Pos. : (0.3653, -0.0001, -3.2920) st7_30k.v01
Edit Zoom Hel
V Component
2 129.733
-23.117
0.000E+00
ms
1.385E+03
Total Time (ms) = 43243
Data Rate (KHz) = 0.071
Mean Velocity = 53.30
Standard Dev. = 25.47
Vel. at Cursor = 60.62
Delta Time (ms) = 5.000
Time at Cursor = 725.0
U Component
58.509
-8.149
0.000E+00
ms
1.385E+03
Velocity (m/s)
Data Rate (KHz) = 0.071
Mean Velocity = 25.18
Standard Dev. = 11.11
Vel. at Cursor = 31.40

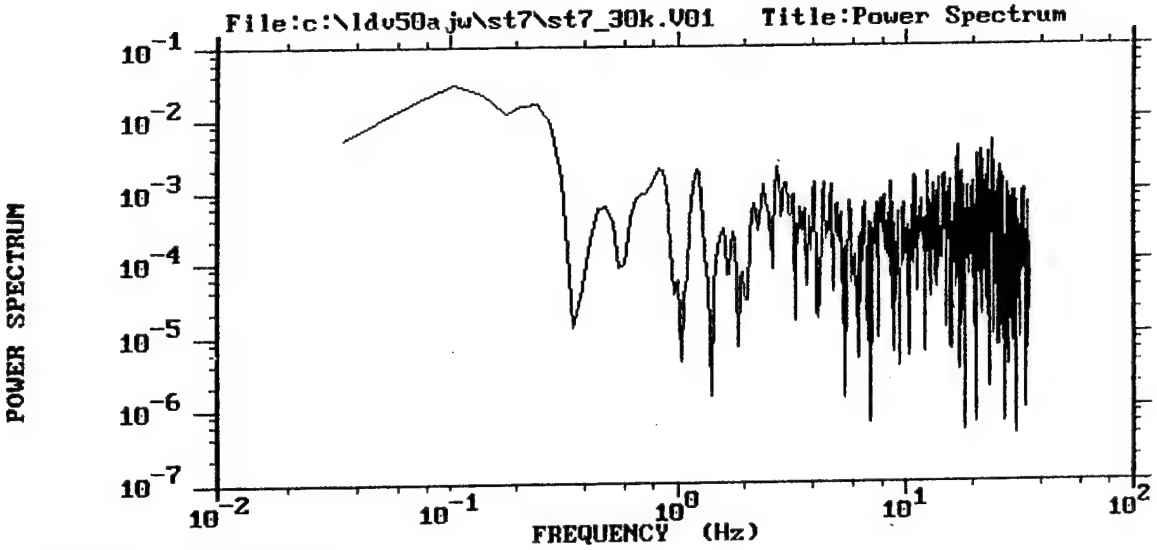

Graph Component: U
% of Bins Containing Data = 100
Scaling Factors (X,Y) = 1.0 , 1.0

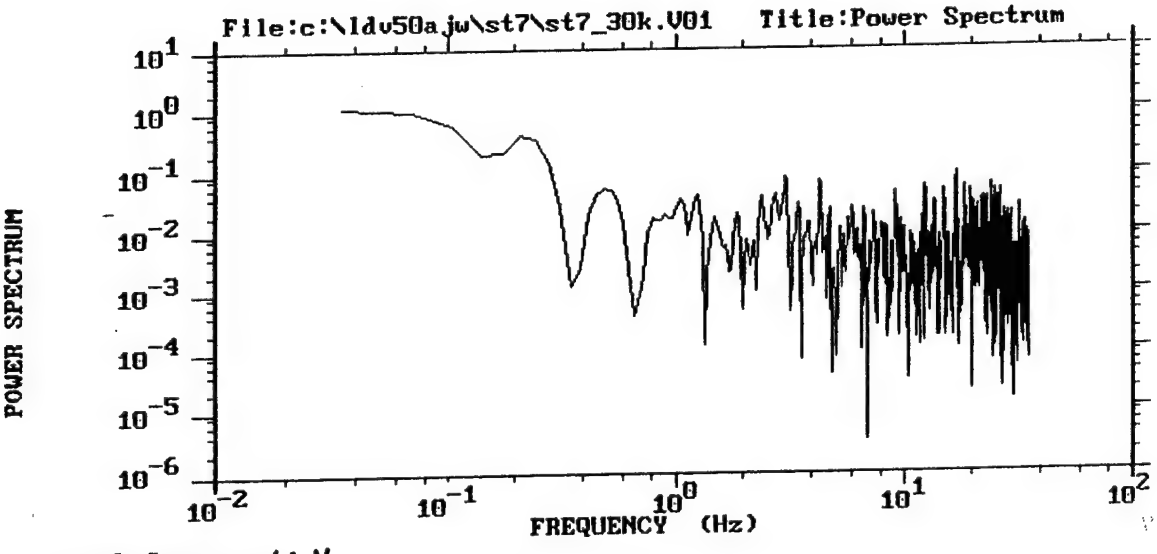

Graph Component: V
% of Bins Containing Data = 100
Scaling Factors (X,Y) = 1.0 , 1.0

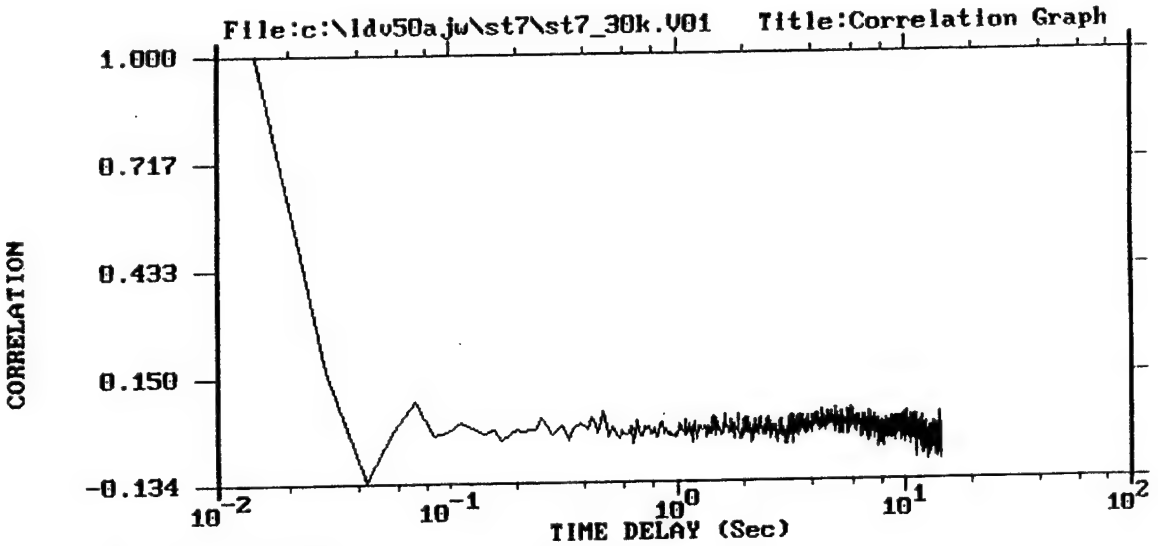

Graph Component: U
% of Bins Containing Data = 100
Scaling Factors (X,Y) = 1.0 , 1.0

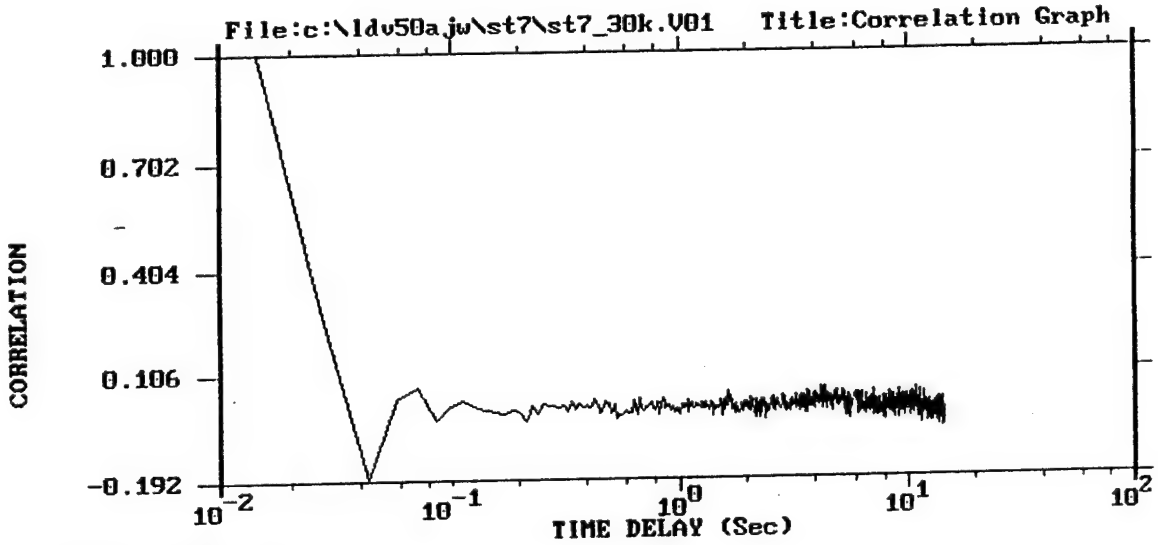

Graph Component: V
% of Bins Containing Data = 100
Scaling Factors (X,Y) = 1.0 , 1.0

c. Ganaim 3K Data Points

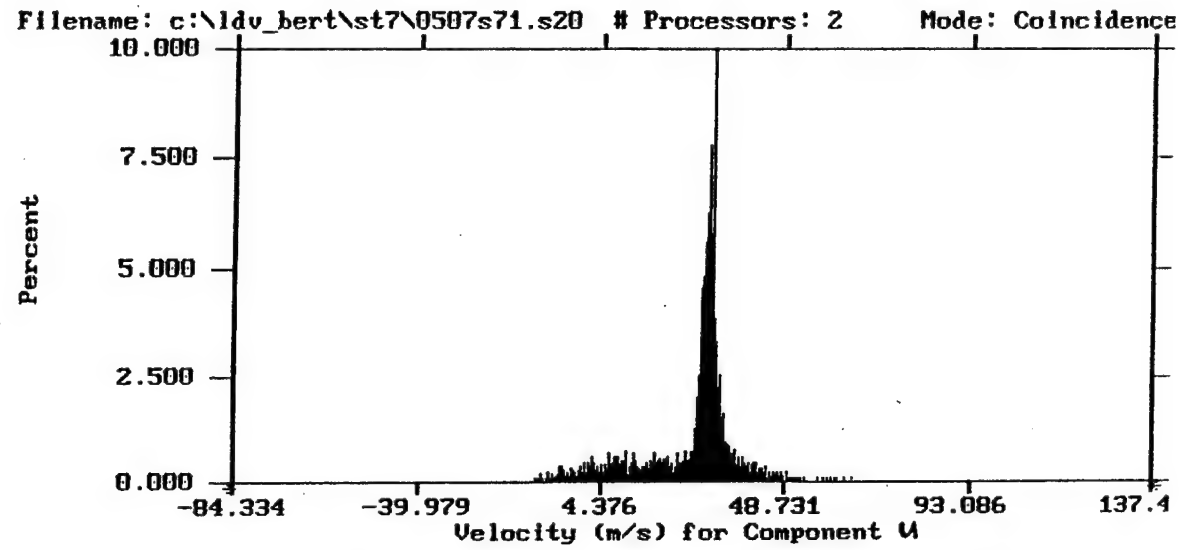

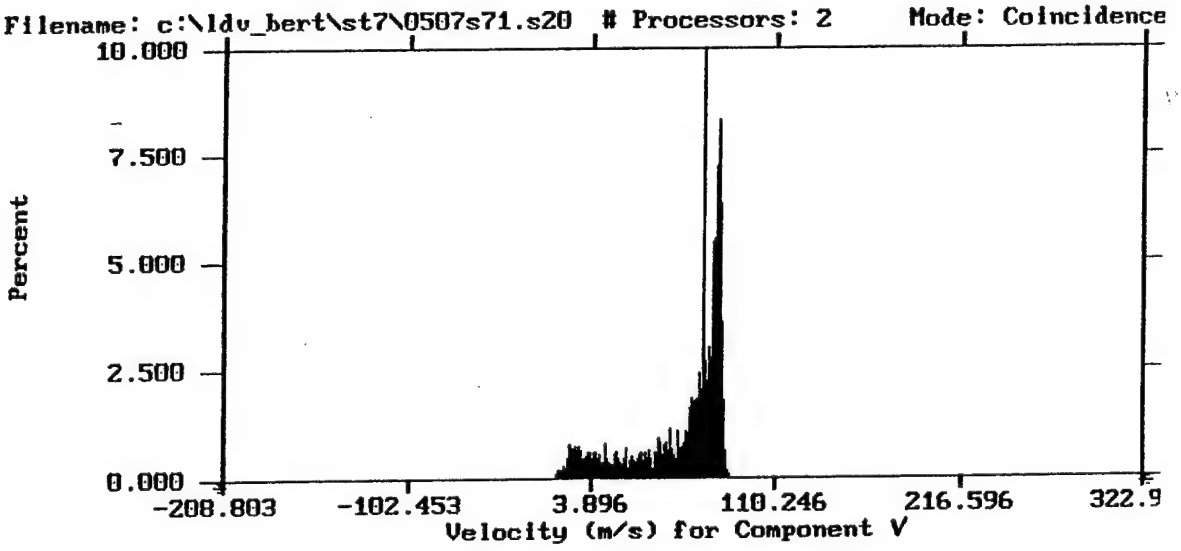

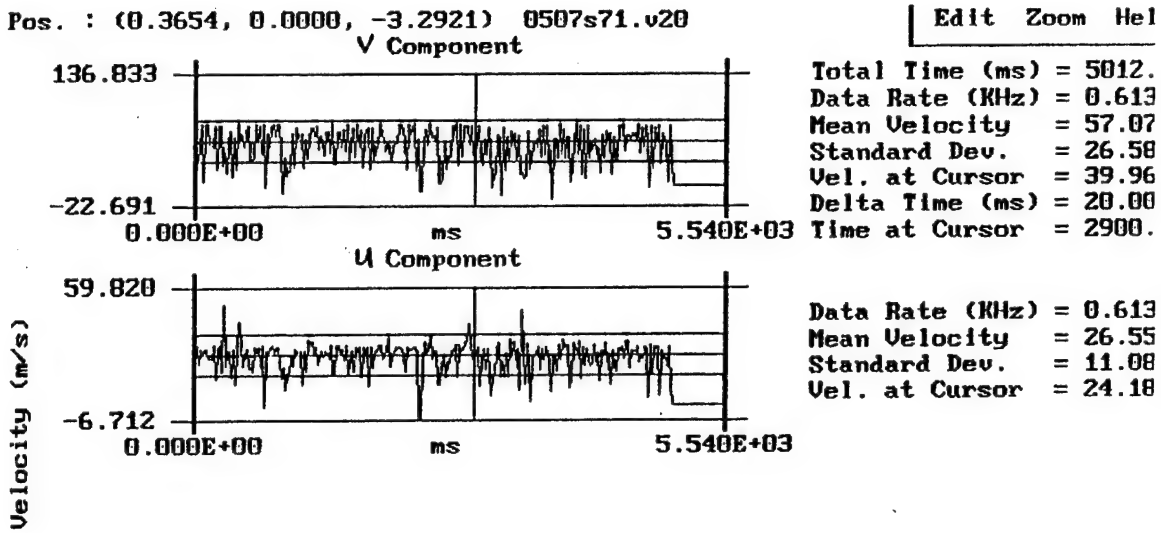
Pos. : (0.3654, 0.0000, -3.2921) 0507s71.v20
Edit Zoom Hel
V Component
136.833
-22.691
0.000E+00
ms
5.540E+03
Total Time (ms) = 5012.
Data Rate (KHz) = 0.613
Mean Velocity = 57.07
Standard Dev. = 26.58
Vel. at Cursor = 39.96
Delta Time (ms) = 20.00
Time at Cursor = 2900.
U Component
59.820
-6.712
0.000E+00
ms
5.540E+03
Velocity (m/s)
Data Rate (KHz) = 0.613
Mean Velocity = 26.55
Standard Dev. = 11.08
Vel. at Cursor = 24.18

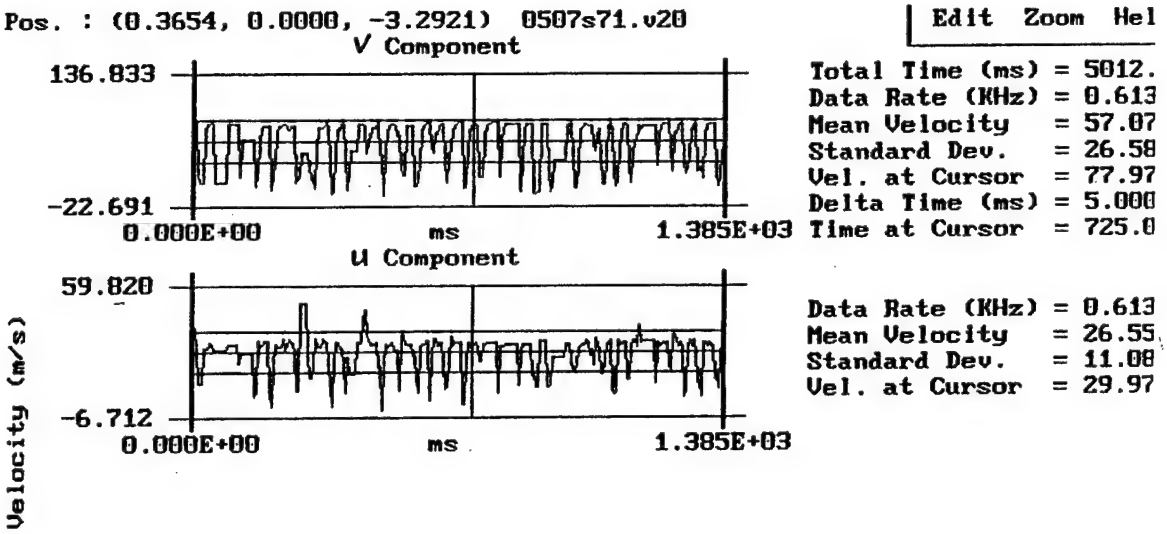
Pos. : (0.3654, 0.0000, -3.2921) 0507s71.v20
Edit Zoom Hel
V Component
136.833
-22.691
0.000E+00
ms
1.385E+03
Total Time (ms) = 5012.
Data Rate (KHz) = 0.613
Mean Velocity = 57.07
Standard Dev. = 26.58
Vel. at Cursor = 77.97
Delta Time (ms) = 5.000
Time at Cursor = 725.0
U Component
59.820
-6.712
0.000E+00
ms
1.385E+03
Velocity (m/s)
Data Rate (KHz) = 0.613
Mean Velocity = 26.55
Standard Dev. = 11.08
Vel. at Cursor = 29.97

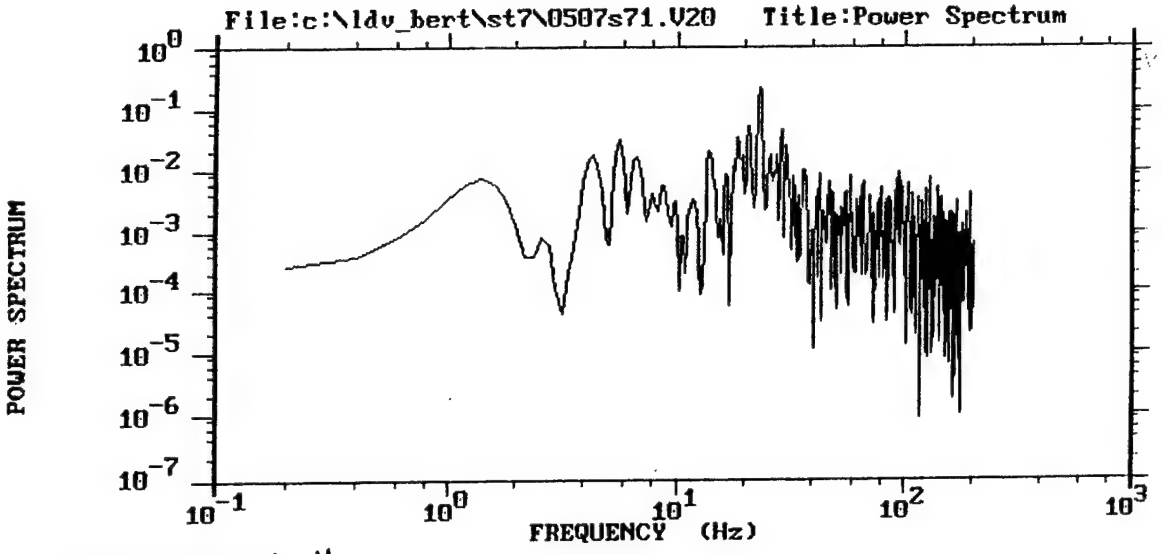

Graph Component: U
% of Bins Containing Data = 100
Scaling Factors (X,Y) = 1.0 , 1.0

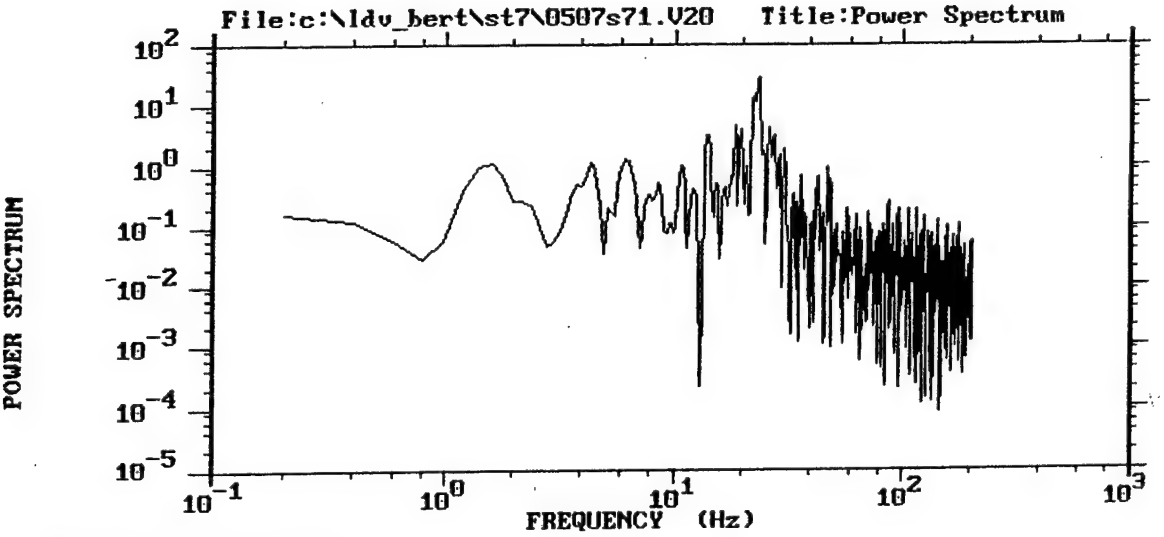

Graph Component: V
% of Bins Containing Data = 100
Scaling Factors (X,Y) = 1.0 , 1.0

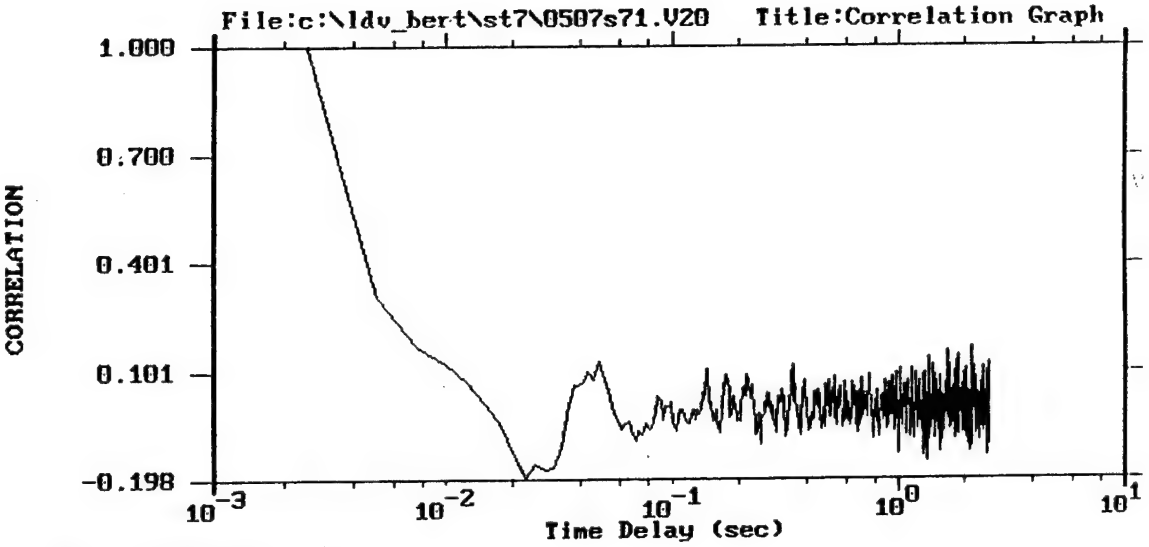

Graph Component: U
% of Bins Containing Data = 100
Scaling Factors (X,Y) = 1.0 , 1.0

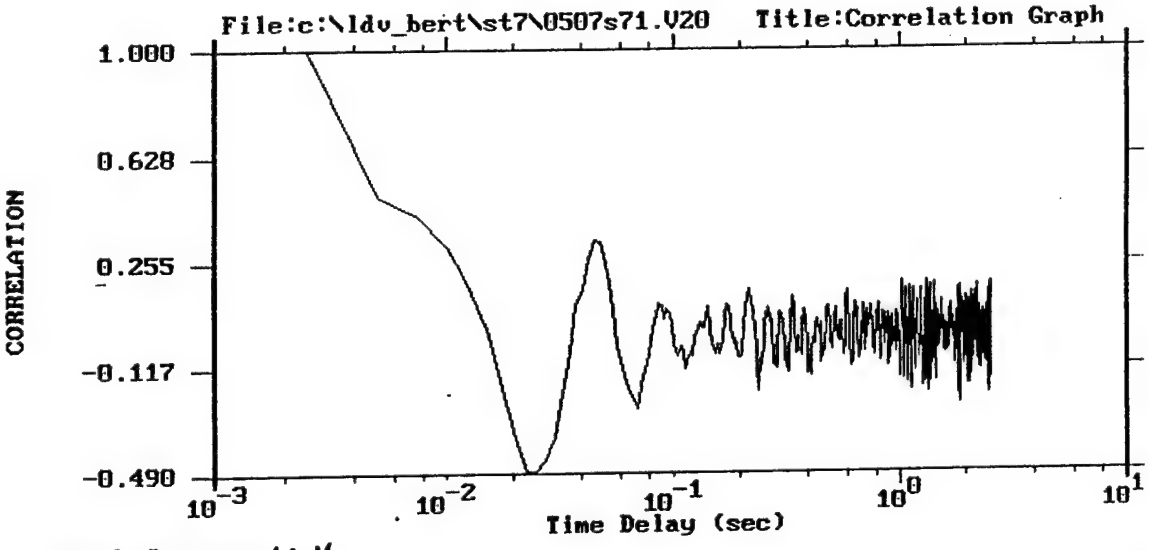

Graph Component: V
% of Bins Containing Data = 100
Scaling Factors (X,Y) = 1.0 , 1.0

APPENDIX D: REDUCED DATA FROM STATIONS 1, 3, 7, 19

Pitchwise Survey at Station 1

X (in)	Y (in)	U / Vref	V / Vref	UV Mag / Vref	U - Turbulence	V - Turbulence	Reynolds Stress	Correlation Coefficient
1.00	-6.29	0.7560	0.6273	0.9824	4.5167	4.2288	-0.5645	-0.0459
0.75	-6.29	0.7527	0.6348	0.9847	4.2846	4.1545	-0.1621	-0.0141
0.50	-6.29	0.7549	0.6361	0.9872	4.1377	4.1513	-0.8599	-0.0778
0.25	-6.29	0.7532	0.6393	0.9879	3.9633	4.2387	-0.0287	-0.0027
0.00	-6.29	0.7551	0.6417	0.9910	4.2522	4.0219	-0.0638	-0.0058
-0.25	-6.29	0.7573	0.6399	0.9914	4.1720	4.0454	-0.0756	-0.0070
-0.50	-6.29	0.7646	0.6367	0.9950	4.3993	3.9576	0.4649	0.0415
-0.75	-6.29	0.7671	0.6362	0.9966	4.3408	3.9461	0.1865	0.0169
-1.00	-6.29	0.7655	0.6322	0.9929	4.5415	3.8821	0.4439	0.0391
-1.25	-6.29	0.7685	0.6303	0.9940	4.0621	3.6989	0.3160	0.0327
-1.50	-6.29	0.7622	0.6312	0.9896	4.9631	3.7591	0.0913	0.0076
-1.75	-6.29	0.7527	0.6333	0.9837	5.6056	3.5044	0.2665	0.0211
-2.00	-6.29	0.7505	0.6371	0.9844	4.0228	3.4712	-0.0511	-0.0057
-2.25	-6.29	0.7509	0.6368	0.9846	3.6099	3.5205	-0.0113	-0.0014
-2.50	-6.29	0.7519	0.6417	0.9885	3.5904	3.3798	0.1693	0.0217
-2.75	-6.29	0.7512	0.6462	0.9909	3.5229	3.4416	-0.1665	-0.0213
-3.00	-6.29	0.7553	0.6495	0.9961	3.5721	3.2735	0.1392	0.0185
-3.25	-6.29	0.7576	0.6500	0.9982	3.9669	3.3235	-0.2241	-0.0264
-3.50	-6.29	0.7767	0.6438	1.0088	3.5708	3.4123	-0.3948	-0.0503
-3.75	-6.29	0.7787	0.6344	1.0044	3.5851	3.5118	-0.3790	-0.0468
-4.00	-6.29	0.7753	0.6322	1.0004	3.4988	3.3147	-0.1981	-0.0265
-4.25	-6.29	0.7714	0.6303	0.9962	3.4435	3.3032	-0.1314	-0.0179
-4.50	-6.29	0.7634	0.6295	0.9894	3.7142	3.1308	0.0422	0.0056
-4.75	-6.29	0.7596	0.6341	0.9895	3.4552	2.9855	0.2140	0.0322
-5.00	-6.29	0.7592	0.6383	0.9918	3.3208	2.9673	-0.2577	-0.0406
-5.25	-6.29	0.7596	0.6459	0.9971	2.9610	2.8494	-0.2546	-0.0469
-5.50	-6.29	0.7652	0.6516	1.0050	3.2893	2.7745	0.0387	0.0066
-5.75	-6.29	0.7714	0.6537	1.0111	2.9942	3.0307	-0.3735	-0.0639
-6.00	-6.29	0.7748	0.6563	1.0154	3.2675	2.9769	-0.1074	-0.0171
-6.25	-6.29	0.7782	0.6528	1.0157	2.9052	2.6739	-0.1011	-0.0202
-6.50	-6.29	0.7787	0.6490	1.0137	3.4300	2.7946	-0.0564	-0.0091
-6.75	-6.29	0.7773	0.6426	1.0085	2.7609	2.5602	-0.0539	-0.0119
-7.00	-6.29	0.7767	0.6388	1.0057	3.0063	2.5740	0.4140	0.0831
-7.25	-6.29	0.7741	0.6370	1.0024	3.1116	2.4751	0.2009	0.0405
-7.50	-6.29	0.7727	0.6406	1.0038	2.7515	2.3997	0.2478	0.0583
-7.75	-6.29	0.7686	0.6405	1.0005	2.5751	2.2243	0.1246	0.0338
-8.00	-6.29	0.7665	0.6444	1.0014	2.8413	2.2209	0.1098	0.0270
-8.25	-6.29	0.7686	0.6469	1.0046	3.1292	2.2872	0.0908	0.0197
-8.50	-6.29	0.7694	0.6525	1.0089	3.0650	2.0272	0.0634	0.0158
-8.75	-6.29	0.7739	0.6534	1.0129	2.9483	2.1966	0.0291	0.0070
-9.00	-6.29	0.7783	0.6542	1.0167	2.4833	2.1338	0.0240	0.0070

Pitchwise Survey at Station 3

		Total Flow Average					Negative Average		Positive Average	
X (in)	Y (in)	U / Vref	V / Vref	Utot / Vref	U - Turb	V - Turb	U / Vref	V / Vref	U / Vref	V / Vref
-0.9160	-4.5421	-0.0508	-0.0820	0.0964	-6.8660	-7.5121	-0.0745	-0.1005	0.0976	0.1242
-0.9061	-4.5420	-0.0566	-0.0813	0.0991	-7.0072	-9.0429	-0.0780	-0.1061	0.0952	0.1348
-0.8951	-4.5420	-0.0566	-0.0807	0.0986	-7.3448	-10.6218	-0.0814	-0.1091	0.1169	0.2125
-0.8831	-4.5420	-0.0524	-0.0713	0.0885	-10.4817	-13.7893	-0.0855	-0.1150	0.1897	0.2506
-0.8699	-4.5420	-0.0105	-0.0184	0.0212	-18.3077	-24.1420	-0.0848	-0.1154	0.3524	0.4773
-0.8553	-4.5420	0.0692	0.0767	0.1033	26.3741	33.9905	-0.0825	-0.1146	0.4479	0.5715
-0.8393	-4.5420	0.2345	0.2896	0.3726	33.1398	43.3500	-0.0812	-0.1178	0.5142	0.6610
-0.8217	-4.5420	0.3414	0.4153	0.5377	33.9309	43.6112	-0.0799	-0.1182	0.5525	0.6905
-0.8023	-4.5420	0.4373	0.5191	0.6787	33.0556	41.3025	-0.0764	-0.1118	0.5858	0.7099
-0.7811	-4.5420	0.5376	0.6040	0.8086	29.6847	36.5104	-0.0753	-0.1088	0.6291	0.7162
-0.7575	-4.5420	0.5532	0.5886	0.8078	28.0982	34.1066	-0.0704	-0.1176	0.6245	0.6757
-0.7317	-4.5420	0.6236	0.6658	0.9122	23.7893	30.3195	-0.0718	-0.0978	0.6634	0.7168
-0.7035	-4.5420	0.6598	0.6660	0.9375	20.8838	26.3703	-0.0571	-0.0992	0.6841	0.6953
-0.6723	-4.5420	0.6963	0.6885	0.9792	17.4786	23.8027	-0.0673	-0.1251	0.7080	0.7041
-0.6377	-4.5420	0.7192	0.7057	1.0076	14.4658	22.1652	-0.0455	-0.1565	0.7255	0.7169
-0.6001	-4.5420	0.7387	0.7207	1.0320	12.5289	20.1208	0.0000	0.0000	0.7422	0.7275
-0.5585	-4.5420	0.7553	0.7316	1.0515	10.5465	18.8519	0.0000	0.0000	0.7565	0.7352
-0.5127	-4.5420	0.7781	0.6664	1.0245	10.0197	15.9950	0.0000	0.0000	0.7794	0.6687
-0.4626	-4.5420	0.7642	0.7640	1.0806	8.0755	15.7110	0.0000	0.0000	0.7642	0.7643
-0.4073	-4.5420	0.7645	0.7642	1.0809	8.4760	15.8142	0.0000	0.0000	0.7645	0.7647
-0.3465	-4.5420	0.7524	0.7933	1.0933	8.0195	15.1845	0.0000	0.0000	0.7524	0.7933
-0.2796	-4.5420	0.7442	0.7777	1.0764	8.2561	14.5299	0.0000	0.0000	0.7442	0.7777
-0.2060	-4.5420	0.7460	0.7736	1.0746	8.6669	13.4328	0.0000	0.0000	0.7460	0.7736
-0.1251	-4.5420	0.7330	0.7705	1.0635	9.0455	13.2214	0.0000	0.0000	0.7330	0.7705
-0.0361	-4.5420	0.7322	0.7560	1.0525	9.3525	12.0596	0.0000	0.0000	0.7322	0.7560
0.0619	-4.5420	0.7208	0.7548	1.0437	9.5275	11.5091	0.0000	0.0000	0.7208	0.7548
0.1696	-4.5420	0.7186	0.7403	1.0317	9.6073	10.9092	0.0000	0.0000	0.7186	0.7406
0.2882	-4.5420	0.6990	0.7356	1.0148	9.5020	10.1140	0.0000	0.0000	0.6990	0.7356
0.4185	-4.5420	0.6903	0.7245	1.0007	9.2803	9.0998	0.0000	0.0000	0.6903	0.7245
0.5620	-4.5420	0.6706	0.7162	0.9811	9.0082	8.4316	0.0000	0.0000	0.6706	0.7162
0.7196	-4.5420	0.6449	0.6946	0.9479	8.7474	8.0618	0.0000	0.0000	0.6449	0.6946
0.8932	-4.5420	0.6282	0.6704	0.9187	7.8477	7.6788	0.0000	0.0000	0.6282	0.6704

Pitchwise Survey at Station 7

		Total Flow Average					Average of Negative		Average of Positive	
X (in)	Y (in)	U / Vref	V / Vref	Utot / Vref	U - Turb	V - Turb	U / Vref	V / Vref	U / Vref	V / Vref
-0.1435	-3.2920	0.1749	0.4748	0.5060	12.2241	26.7540	-0.0643	-0.1126	0.2064	0.5479
-0.1335	-3.2920	0.1809	0.4820	0.5148	12.9712	26.9304	-0.0657	-0.1081	0.2146	0.5524
-0.1225	-3.2920	0.1780	0.4843	0.5159	13.8963	28.4924	-0.0656	-0.1100	0.2211	0.5748
-0.1105	-3.2920	0.1861	0.4919	0.5259	14.7300	30.1213	-0.0748	-0.1079	0.2333	0.5898
-0.0973	-3.2920	0.1889	0.4992	0.5338	15.0800	30.5573	-0.0691	-0.1077	0.2385	0.6005
-0.0827	-3.2920	0.1857	0.4874	0.5216	15.8231	31.1735	-0.0719	-0.1014	0.2387	0.5935
-0.0667	-3.2920	0.1938	0.5026	0.5387	15.9031	32.6549	-0.0739	-0.1024	0.2487	0.6161
-0.0481	-3.2920	0.2026	0.5130	0.5515	16.1680	33.0578	-0.0707	-0.1090	0.2588	0.6283
-0.0297	-3.2920	0.2116	0.5290	0.5698	16.4695	33.2063	-0.0736	-0.0988	0.2664	0.6396
-0.0084	-3.2920	0.2166	0.5227	0.5658	16.8288	35.1634	-0.0681	-0.0991	0.2776	0.6503
0.0151	-3.2920	0.2136	0.5201	0.5622	16.7788	36.0857	-0.0675	-0.0983	0.2728	0.6490
0.0409	-3.2920	0.2162	0.5202	0.5634	16.9932	36.5286	-0.0664	-0.0981	0.2778	0.6529
0.0692	-3.2920	0.2401	0.5600	0.6093	17.0275	37.3337	-0.0654	-0.0937	0.3014	0.6985
0.1004	-3.2920	0.2453	0.5712	0.6216	16.7892	37.0429	-0.0686	-0.0993	0.2974	0.6905
0.1348	-3.2920	0.2533	0.5765	0.6297	16.9775	38.0062	-0.0604	-0.0986	0.3091	0.7065
0.1725	-3.2920	0.2580	0.5909	0.6448	16.8549	37.0968	-0.0574	-0.0974	0.3106	0.7097
0.2141	-3.2920	0.2733	0.6101	0.6685	16.1963	36.6200	-0.0642	-0.0975	0.3161	0.7126
0.2599	-3.2920	0.2849	0.6250	0.6869	15.8988	36.1124	-0.0660	-0.0930	0.3271	0.7290
0.3100	-3.2920	0.2988	0.6631	0.7273	15.0613	33.7251	-0.0568	-0.0940	0.3324	0.7409
0.3654	-3.2920	0.3156	0.7053	0.7726	14.0393	31.8136	-0.0652	-0.0853	0.3420	0.7700
0.4259	-3.2920	0.3282	0.7261	0.7969	12.8077	29.6575	-0.0678	-0.0934	0.3481	0.7733
0.4930	-3.2920	0.3323	0.7293	0.8014	12.6994	27.7864	-0.0715	-0.1135	0.3496	0.7683
0.5666	-3.2920	0.3469	0.7369	0.8145	11.3452	25.8805	-0.0583	-0.0838	0.3550	0.7616
0.6474	-3.2920	0.3549	0.7283	0.8102	11.2177	24.6712	-0.0594	-0.0810	0.3644	0.7534
0.7365	-3.2920	0.3667	0.7457	0.8310	10.4527	22.1508	-0.0553	-0.0619	0.3716	0.7615
0.8345	-3.2920	0.3819	0.7624	0.8527	9.8618	18.9547	0.0000	0.0000	0.3835	0.7707
0.9422	-3.2920	0.3868	0.7551	0.8484	10.0925	17.5833	0.0000	-0.0553	0.3885	0.7614
1.0608	-3.2920	0.3912	0.7689	0.8627	9.6454	15.1138	0.0000	0.0000	0.3914	0.7730
1.1911	-3.2920	0.3919	0.7749	0.8683	9.1682	12.5425	0.0000	0.0000	0.3921	0.7761
1.3345	-3.2920	0.3849	0.7814	0.8710	8.8570	10.8529	0.0000	0.0000	0.3849	0.7814
1.4922	-3.2920	0.3739	0.7863	0.8706	7.9523	8.9572	0.0000	0.0000	0.3739	0.7863
1.6657	-3.2920	0.3500	0.7726	0.8482	6.8941	7.5859	0.0000	0.0000	0.3500	0.7729

Pitchwise Survey at Station 19

		Total Flow Average					Average of Negative		Average of Positive	
X (inches)	Y (inches)	U / Vref	V / Vref	UVtot / Vref	U-Turb	V-Turb	U / Vref	V / Vref	U / Vref	V / Vref
3.9999	1.0620	0.0253	0.6604	0.6609	7.7800	24.6470	-0.0637	-0.0788	0.0565	0.7056
3.8750	1.0620	0.0237	0.6190	0.6194	8.1843	25.8908	-0.0709	-0.0775	0.0604	0.6619
3.7499	1.0620	0.0195	0.5861	0.5864	8.5960	25.6453	-0.0669	-0.0846	0.0684	0.6254
3.6250	1.0620	0.0197	0.5217	0.5220	9.1367	24.5519	-0.0690	-0.0831	0.0751	0.5499
3.5001	1.0620	0.0198	0.4731	0.4735	9.5804	22.3559	-0.0723	-0.0780	0.0751	0.4960
3.3751	1.0620	0.0168	0.4034	0.4038	10.0333	19.5244	-0.0739	-0.0786	0.0777	0.4141
3.2499	1.0620	0.0312	0.3255	0.3270	12.0674	17.0258	-0.0693	-0.0608	0.1015	0.3312
3.1251	1.0620	0.0546	0.3268	0.3313	13.4243	15.0200	-0.0629	-0.0498	0.1278	0.3488
3.0000	1.0620	0.0888	0.5394	0.5466	10.7297	15.4455	0.0000	0.0000	0.1275	0.5590
2.8750	1.0620	0.0594	0.7741	0.7764	6.3753	11.0721	0.0000	0.0000	0.0748	0.7823
2.7498	1.0620	0.0458	0.8239	0.8251	5.0207	5.1598	0.0000	0.0000	0.0567	0.8254
2.6249	1.0620	0.0428	0.8278	0.8289	4.3926	3.6575	0.0000	0.0000	0.0521	0.8267
2.5000	1.0620	0.0412	0.8272	0.8282	3.9808	3.3833	0.0000	0.0000	0.0488	0.8268
2.3751	1.0620	0.0394	0.8275	0.8284	3.5717	3.0630	0.0000	0.0000	0.0459	0.8272
2.2500	1.0620	0.0383	0.8259	0.8268	3.7252	3.5124	0.0000	0.0000	0.0455	0.8261
2.1251	1.0620	0.0403	0.8262	0.8272	4.5719	5.5106	0.0000	0.0000	0.0498	0.8268
2.0001	1.0620	0.0399	0.8256	0.8266	4.3079	5.3561	-0.0098	-0.1220	0.0484	0.8273
1.8750	1.0620	0.0387	0.8217	0.8227	4.5239	6.3894	0.0000	0.0000	0.0485	0.8232
1.7500	1.0620	0.0378	0.8125	0.8134	5.1930	8.7774	0.0000	0.0000	0.0486	0.8173
1.6250	1.0619	0.0368	0.8066	0.8075	5.1928	10.1244	0.0000	0.0000	0.0474	0.8132
1.5000	1.0620	0.0500	0.7315	0.7332	8.6155	19.3049	-0.0967	-0.0481	0.0707	0.7458
1.3750	1.0620	0.0507	0.7019	0.7038	8.7904	22.0152	-0.0643	-0.0590	0.0711	0.7229
1.2500	1.0620	0.0410	0.7076	0.7087	8.1040	22.2274	-0.0594	-0.0786	0.0626	0.7366
1.1250	1.0621	0.0373	0.6794	0.6804	7.8614	24.8061	-0.0612	-0.0784	0.0596	0.7198
1.0000	1.0620	0.0393	0.6499	0.6511	8.0620	26.0936	-0.0509	-0.0969	0.0640	0.6913
0.8750	1.0620	0.0328	0.6525	0.6533	7.8186	24.9827	-0.0613	-0.0801	0.0620	0.6917
0.7499	1.0620	0.0304	0.5986	0.5994	8.5539	25.4173	-0.0544	-0.0882	0.0691	0.6326
0.6250	1.0620	0.0305	0.5419	0.5428	8.3361	23.6395	-0.0700	-0.0797	0.0724	0.5647
0.5000	1.0620	0.0267	0.4712	0.4720	8.5616	22.6358	-0.0644	-0.0942	0.0747	0.4977
0.3750	1.0620	0.0321	0.3932	0.3945	10.3141	19.8753	-0.0570	-0.0763	0.0825	0.4085
0.2500	1.0620	0.0439	0.3235	0.3265	12.6135	16.9451	-0.0607	-0.0652	0.1039	0.3344
0.1250	1.0620	0.0717	0.3254	0.3332	13.0058	14.8209	-0.0643	-0.0313	0.1275	0.3390
-0.0001	1.0620	0.0900	0.5310	0.5386	10.3600	16.2890	0.0000	0.0000	0.1242	0.5487
-0.1250	1.0620	0.0575	0.7944	0.7965	6.4601	10.7090	0.0000	0.0000	0.0731	0.8025
-0.2501	1.0620	0.0476	0.8425	0.8438	5.0608	4.6542	0.0000	0.0000	0.0582	0.8430
-0.3751	1.0620	0.0417	0.8439	0.8449	4.5586	3.8154	0.0000	0.0000	0.0520	0.8431
-0.4999	1.0620	0.0388	0.8446	0.8454	4.2244	3.5776	0.0000	0.0000	0.0488	0.8437
-0.6250	1.0620	0.0384	0.8438	0.8447	3.8185	3.2821	0.0000	0.0000	0.0467	0.8436
-0.7500	1.0620	0.0365	0.8424	0.8432	3.7316	3.2875	0.0000	0.0000	0.0449	0.8419
-0.8750	1.0620	0.0362	0.8393	0.8400	3.6055	3.7414	0.0000	0.0000	0.0437	0.8395
-1.0000	1.0620	0.0340	0.8357	0.8364	3.5738	4.0021	0.0000	0.0000	0.0418	0.8367
-1.1251	1.0620	0.0325	0.8338	0.8345	3.6817	4.7620	0.0000	0.0000	0.0417	0.8361
-1.2500	1.0620	0.0343	0.8329	0.8336	3.7131	5.2161	0.0000	0.0000	0.0412	0.8347
-1.3750	1.0620	0.0323	0.8272	0.8279	3.9602	6.7284	0.0000	0.0000	0.0398	0.8296
-1.5000	1.0620	0.0305	0.8207	0.8213	4.4862	8.7431	-0.1331	-0.0914	0.0401	0.8274
-1.6250	1.0621	0.0331	0.8017	0.8024	5.1570	13.3611	-0.0295	-0.1048	0.0441	0.8119
-1.7500	1.0620	0.0429	0.7382	0.7394	7.8387	20.1948	-0.0238	-0.0818	0.0646	0.7614
-1.8750	1.0620	0.0379	0.7059	0.7069	7.8834	22.3243	-0.0529	-0.0771	0.0637	0.7381
-2.0000	1.0620	0.0318	0.6920	0.6927	7.6868	23.7145	-0.0669	-0.0788	0.0598	0.7296

APPENDIX E: CFD GRID GENERATION

The FORTRAN grid generation program employed was the modified version of GRAPE (GRids About Aerofoils using Poisson's Equation) by R. V. Chima, [Ref. 11]. Prior to this study, the grid's leading edge was blunt or flat-faced, which led to inaccuracies in the computed solutions. It was determined that GRAPE properly smoothed the points around the leading edge, and that it required definition of the leading edge with more user-supplied coordinates. Careful attention was given to properly blending the top and bottom grid surfaces into the 0.045 inch radius circular arc that defines the leading edge. This was done by ensuring that first derivative continuity was within a few percent difference. The final coordinates for the CD blade definition are contained below in namelist &GRID3.

```
&GRID1
JMAX=240,KMAX=49,NTETYP=3,NAIRF=5,JAIRF=163,NIBDST=7,
DSI=0.0002,JTEBOT=60,JTETOP=181,XLE=0.0,NOBSHP=7,XTE=1.0,
ALAMF=0.0,ALAMR=0.0,XLEFT=-.3,XRIGHT=3.,
RCORN=.10,NOUT=4,NORDA=5,3,MAXITA=100,100,
&END
&GRID2
AAAI=.3,BBBI=.3,DSOBI=0.01,ROTANG=-14.4,
XTFRAC=1.5,PITCH=.5988,DSRA=.4920,DSLE=.0008,DSTE=.001,
NLE=28,NTE=18,WAKEP=1.,OMEGR=1.0,OMEGS=1.0,OMEGP=1.0,OMEGQ=1.0,
&END
&GRID3 AIRFX=
0.9996, 0.9971, 0.9929, 0.9876, 0.9830, 0.9803, 0.9776, 0.9749,
0.9601, 0.9453, 0.9305, 0.9157, 0.9010, 0.8862, 0.8714, 0.8567,
0.8419, 0.8271, 0.8124, 0.7976, 0.7828, 0.7681, 0.7533, 0.7385,
0.7238, 0.7090, 0.6942, 0.6795, 0.6647, 0.6499, 0.6352, 0.6204,
0.6056, 0.5908, 0.5760, 0.5612, 0.5465, 0.5317, 0.5169, 0.5022,
0.4874, 0.4726, 0.4579, 0.4431, 0.4283, 0.4136, 0.3988, 0.3840,
0.3693, 0.3545, 0.3397, 0.3250, 0.3102, 0.2954, 0.2807, 0.2659,
0.2511, 0.2364, 0.2216, 0.2068, 0.1920, 0.1772, 0.1624, 0.1477,
0.1329, 0.1181, 0.1034, 0.0886, 0.0738, 0.0591, 0.0443, 0.0343,
0.0244, 0.0114, 0.0097, 0.0080, 0.0063, 0.0047,
0.0033, 0.0021, 0.0011, 0.0005, 0.0001, 0.0001, 0.0004,
0.0010, 0.0019, 0.0030, 0.0044, 0.0045, 0.0177, 0.0310, 0.0443,
0.0591, 0.0738, 0.0886, 0.1034, 0.1181, 0.1329, 0.1477, 0.1624,
0.1772, 0.1920, 0.2068, 0.2216, 0.2364, 0.2511, 0.2659, 0.2807,
0.2954, 0.3102, 0.3250, 0.3397, 0.3545, 0.3693, 0.3840, 0.3988,
0.4136, 0.4283, 0.4431, 0.4579, 0.4726, 0.4874, 0.5022, 0.5169,
0.5317, 0.5465, 0.5612, 0.5760, 0.5908, 0.6056, 0.6204, 0.6352,
```

```
0.6499, 0.6647, 0.6795, 0.6942, 0.7090, 0.7238, 0.7385, 0.7533,
0.7681, 0.7828, 0.7976, 0.8124, 0.8271, 0.8419, 0.8567, 0.8714,
0.8862, 0.9010, 0.9157, 0.9305, 0.9453, 0.9601, 0.9749, 0.9802,
0.9855, 0.9908, 0.9956, 0.9988, 1.0000, 0.9996,
AIRFY=
0.0093, 0.0044, 0.0012, 0.0000, 0.0008, 0.0018, 0.0028, 0.0038,
0.0089, 0.0135, 0.0178, 0.0218, 0.0256, 0.0291, 0.0323, 0.0353,
0.0381, 0.0407, 0.0431, 0.0453, 0.0474, 0.0494, 0.0513, 0.0530,
0.0546, 0.0561, 0.0575, 0.0589, 0.0601, 0.0612, 0.0623, 0.0633,
0.0643, 0.0652, 0.0661, 0.0669, 0.0676, 0.0683, 0.0690, 0.0697,
0.0703, 0.0709, 0.0714, 0.0717, 0.0719, 0.0719, 0.0717, 0.0713,
0.0707, 0.0699, 0.0688, 0.0675, 0.0659, 0.0641, 0.0621, 0.0597,
0.0570, 0.0540, 0.0509, 0.0478, 0.0446, 0.0413, 0.0379, 0.0344,
0.0309, 0.0274, 0.0238, 0.0202, 0.0165, 0.0127, 0.0088, 0.0061,
0.0033, 0.0004, 0.0001, 0.0001, 0.0005, 0.0011,
0.0021, 0.0033, 0.0047, 0.0063, 0.0080, 0.0097, 0.0114,
0.0130, 0.0144, 0.0157, 0.0167, 0.0168, 0.0244, 0.0319, 0.0391,
0.0468, 0.0543, 0.0613, 0.0680, 0.0743, 0.0804, 0.0863, 0.0920,
0.0974, 0.1025, 0.1074, 0.1120, 0.1163, 0.1204, 0.1240, 0.1272,
0.1299, 0.1323, 0.1345, 0.1363, 0.1379, 0.1391, 0.1401, 0.1407,
0.1411, 0.1413, 0.1413, 0.1411, 0.1406, 0.1399, 0.1389, 0.1375,
0.1359, 0.1340, 0.1320, 0.1297, 0.1272, 0.1246, 0.1218, 0.1188,
0.1157, 0.1124, 0.1090, 0.1054, 0.1018, 0.0981, 0.0943, 0.0904,
0.0864, 0.0824, 0.0784, 0.0744, 0.0704, 0.0663, 0.0622, 0.0580,
0.0539, 0.0498, 0.0456, 0.0415, 0.0373, 0.0331, 0.0289, 0.0274,
0.0259, 0.0244, 0.0219, 0.0176, 0.0124, 0.0093,
&END
```

APPENDIX F: RVCQ3D CODE INPUT

A sample namelist input file for RVCQ3D is shown below. Namelist 6 contains the definition for a linear 6% streamtube contraction which accounts for AVDR and the "Quasi-3D" effect in the code. All solutions were run to 6,000 iterations and consumed, on the average, only 55 minutes on the NPS CRAY ("Sirius") and 4 minutes on the NAS CRAY ("Von Neumann").

```
'SANGER CONTROLLED DIFFUSION BLADE'
 &NL1 M=240,N=49,MTL=60,MIL=108 &end

 &NL2 NSTG=4,IVDT=1,IRS=1,EPI=.30,EPJ=.40,CFL=4.0 AV2=0.,
    AV4=1. &END

 &NL3 IBCIN=1,IBCEX=1,ITMAX=6000,IRESTI=0,IRESTO=1,IRES=1,ICRNT=10000,
    IXRM=0 &END

 &NL4 AMLE=0.24,ALLE=43.0,BETE=0,PRAT=0.9750,P0IN=1.0,T0IN=1.0,G=1.40,
    &END

 &NL5 ILT=2,JEDGE=30,RENR=1.0e6,PRNR=.70,PRTR=0.9,TW=0.0,VISPWR=.666666,
    CMUTM=14.0 &END

 &NL6 OMEGA=0.0,NBLADE=1,NMN=2 &end
-.3000 3.000
1.0000 1.000
1.0000 .9434
```

APPENDIX G: DENSITY RESIDUALS FOR CFD SOLUTIONS

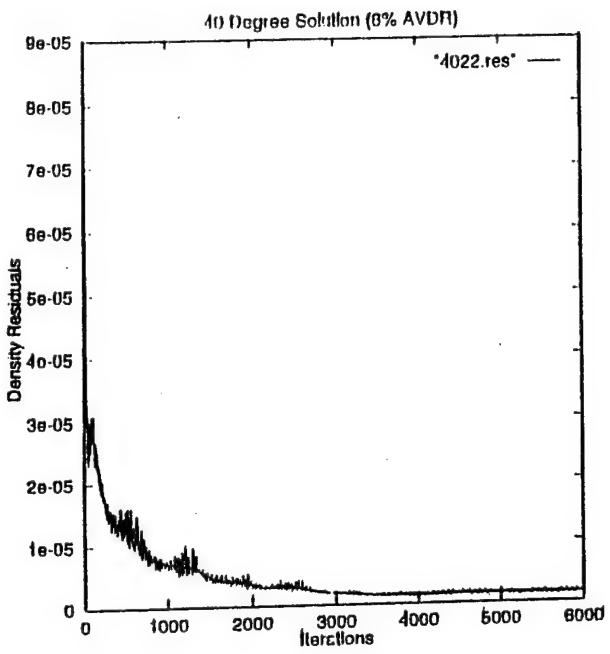

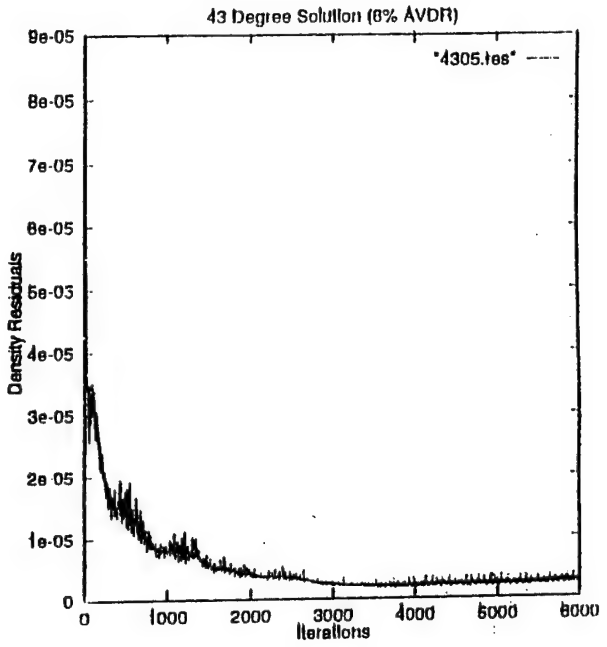

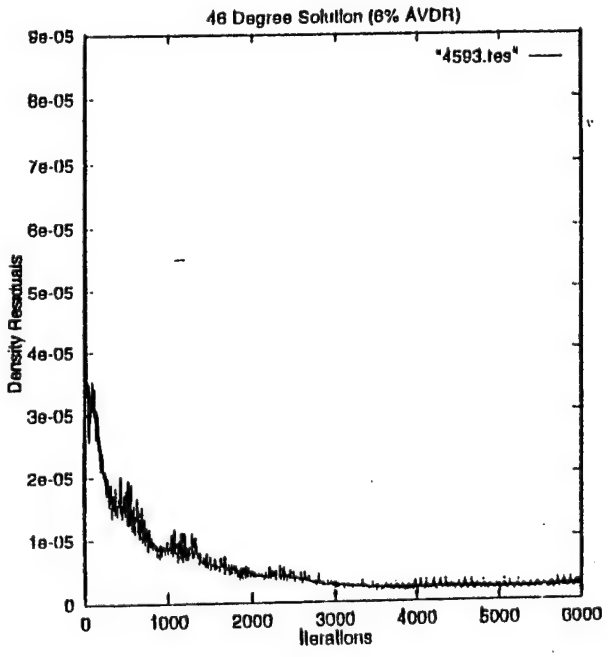

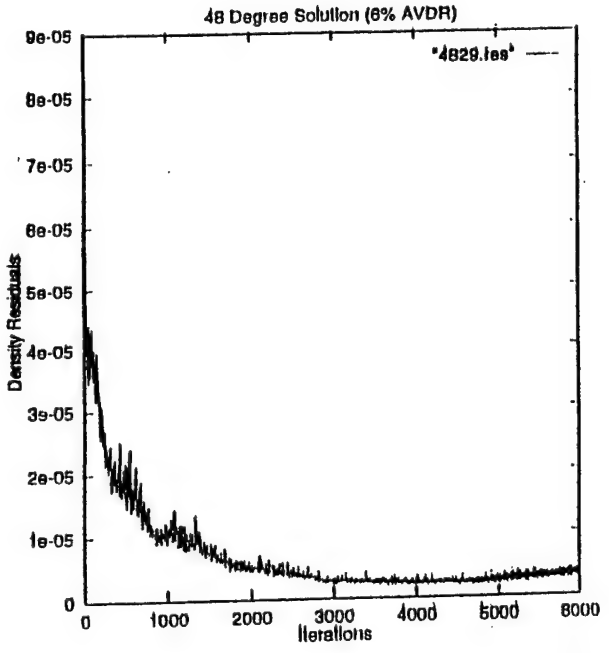

APPENDIX H: Cp VERSUS X/C FORTRAN PLOTTING PROGRAM

```
CCCCCCCCCCCCCCCCCCCCCCCCCCCCCCCCCCCCCCCCCCCCCCCCCCCCC
C    Program To Read The Output From Rvcq3d.F And Grape.F          C
C    And Generate A Data File For A P/P0 Vs Chord Plot             C
C    Around The Airfoil.                    Aug.22, 1991           C
CCCCCCCCCCCCCCCCCCCCCCCCCCCCCCCCCCCCCCCCCCCCCCCCCCCCC

C    IMPLICIT REAL*8(A-H,O-Z)
     DIMENSION Q(300,300,4),X(300,300),Y(300,300)
     DIMENSION U(300,300),V(300,300),P(300,300)
C
C    CALCULATE THE CRITICAL VELOCITY
     cepe=1.00
     rgas=1.0
     pi=1.0
     ti=1.0
     PRAT=0.685
     rhoi=pi/(rgas*ti)
     ceve=cepe-rgas
     g=1.40
     gp=g+1
     cstar=sqrt(2*g*pi/(gp*rhoi))
C
     ISTART=60
     IFINIT=181
C
     READ(7,*)NI,NJ
     print *,ni,nj
     READ(7,*)((X(I,J),I=1,NI),J=1,NJ),
    &         ((Y(I,J),I=1,NI),J=1,NJ)
     READ(7,*)MTL,MIL
C
     READ(3,*)NI,NJ
     READ(3,*)FSMACH,ALF,RE,TIME
     READ(3,*)((((Q(I,J,K),I=1,NI),J=1,NJ),K=1,4)
     GAMMA=1.4
     DO 1234 I=1,NI
     DO 4321 J=1,NJ
     U(I,J)=Q(I,J,2)/Q(I,J,1)
     V(I,J)=Q(I,J,3)/Q(I,J,1)
     P(I,J)=(GAMMA-1)*(Q(I,J,4)-.5*Q(I,J,1)*(U(I,J)**2+V(I,J)**2))
    &       *RHOI*CSTAR**2
 4321  CONTINUE
 1234  CONTINUE
C
C    DETERMINE THE XMIN AND XMAX GRID POINT POSITION
     XMIN=0.0
     XMAX=0.0
     DO 2 I=ISTART,IFINIT
      IF(X(I,1).LE.XMIN)THEN
      IMIN=I
       PRINT *,IMIN
```

```
      XMIN=X(I,1)
      END IF
      IF(X(I,1).GE.XMAX)THEN
      IMAX=I
c      PRINT *,IMAX
      XMAX=X(I,1)
      END IF
    2 CONTINUE
C
C     FREE STREAM STATIC PRESSURE USES THE XMIN GRID POINT
      P0=P(IMIN,NJ)+.5*Q(IMIN,NJ,1)*(U(IMIN,NJ)**2+V(IMIN,NJ)**2)
     &            *RHOI*CSTAR**2
C
      i=imin
      j=nj
      t0=1/rgas*((g-1)*q(i,j,4)/q(i,j,1)-(g-1)**2/(2*g)*
     &    (q(i,j,2)**2+q(i,j,3)**2)/q(i,j,1)**2)
      t0=t0*cstar**2
c     print *,p0,t0,p(imin,nj),q(imin,nj,1),u(imin,nj),v(imin,nj)
C
C     CALCULATE THE MASS FLOW RATE FROM THE INPUT DATA
C     NORMALIZED WITH THE INLET AREA
      dmass=pi/(rgas*ti)*(1/prat)**(-1/g)*sqrt(g*(g-1)*rgas*ti/2*
     &     (1-1/(1/prat)**((g-1)/g)))
c     print *,'cal. inlet mass flow rate =',dmass,'* area'
C
      dmasse=q(imin,nj,1)*RHOI*u(imin,nj)
c     print *,'comp. inlet mass flow rate / area =',dmasse
C
C     PRINT OUT DOWN STREAM CONDITIONS
      p1=p(1,1)+.5*q(1,1,1)*(u(1,1)**2+v(1,1)**2)*RHOI*CSTAR**2
      t1=1/rgas*((g-1)*q(1,1,4)/q(1,1,1)-(g-1)**2/(2*g)*
     &    (q(1,1,2)**2+q(1,1,3)**2)/q(1,1,1)**2)
      t1=t1*CSTAR**2
c     print *,'downstream condition'
c     print *,p1,t1,p(1,1),q(1,1,1),u(1,1),v(1,1)
C
C     CALCULATE THE MASS FLOW RATE AT EXIT
      smass=0.0
      ra=0.0
      ba=0.0
      do 21 j=1,nj-1
      smass=smass+(q(1,j,1)+q(1,j+1,1))*(u(1,j)+u(1,J+1))*
     &      RHOI*CSTAR*(abs(y(1,j+1)-y(1,j)))*0.25
      ra=ra+(q(1,j,1)+q(1,j+1,1))*(abs(y(1,j+1)-y(1,j)))*0.5*
     &      RHOI
      ba=ba+abs(y(1,j+1)-y(1,j))
   21 continue
      do 22 j=1,nj-1
      smass=smass+(q(ni,j,1)+q(ni,j+1,1))*(u(ni,j)+u(ni,J+1))*
     &      RHOI*CSTAR*(abs(y(ni,j+1)-y(ni,j)))*0.25
      ra=ra+(q(n1,j,1)+q(ni,j+1,1))*(abs(y(ni,j+1)-y(ni,j)))*0.5
     &      *RHOI
      ba=ba+abs(y(ni,j+1)-y(ni,j))
```

```
  22  continue
C
C     AVERAGE VELOCITY
      va=smass/ra
      dr=ra/ba
c     print *,'vel. downsteam,vd =',va
c     print *,'ave. density,dr =',dr
C
C     CALCULATE THE INPUT INLET VELOCITY
C     NORMALIZED BY CSTAR
      c0=sqrt(g*rgas*ti)
      vin=sqrt(g*(g-1)*rgas*ti/2*(1-(1/prat)**((1-g)/g)))/c0
c     print *,'input inlet velocity / c0 =',vin
C
C     CALCULATE THE CORRECTED DOWNSTREAM VELOCITY
      do 23 j=nj,1,-1
      vac=u(ni,j)*vin/va
      alpha=atan(abs(v(ni,j)/u(ni,j)))
      vtc=vac*tan(alpha)
      vc=sqrt(vac**2+vtc**2)
      yy=abs(y(ni,nj)-y(1,nj))
c      write(24,*)abs(y(ni,j)-y(ni,nj))/yy,vc
  23  continue
C
      do 25 j=2,nj
      vac=u(1,j)*vin/va
      alpha=atan(abs(v(1,j)/u(1,j)))
      vtc=vac*tan(alpha)
      vc=sqrt(vac**2+vtc**2)
c     write(24,*)abs(y(1,j)-y(ni,nj))/yy,vc
  25  continue
C
C
      CHORD=ABS(X(IMAX,1)-X(IMIN,1))
C
      DO 1 I=ISTART,IFINIT
       DIST=ABS(X(I,1)-X(IMIN,1))
       XS=DIST/CHORD
       CP=1.0+(-P0+P(I,1))/(.5*Q(IMIN,NJ,1)*(U(IMIN,NJ)**2
     &                  +V(IMIN,NJ)**2)*RHOI*CSTAR**2)
       vvcr=sqrt(u(i,1)**2+v(i,1)**2)
C      THE SURFACE POINT P(I,1) ALWAYS EQUAL 0 ?
       PT=P(I,1)/P0
c      WRITE(63,*)XS,VVCR
c      WRITE(64,*)XS,PT
       WRITE(65,*)XS,CP
   1  CONTINUE
C
      STOP
      END
```

APPENDIX I: UPSTREAM FLOW ANGLE FORTRAN PROGRAM "angle.f"

```
ccccccccccccccccccccccccccccccccccccccccccccccccccccccccccccccccccccccccccccccccccccccccccccccccc
c  'angle.f' READS FILES 'fort.7' & 'fort.3' WRITES OUTPUT TO FILE 'fort.10'
c  PROGRAM READS THE OUTPUT FROM RVCQ3D.f AND GRAPE.f AND GENERATES A
c DATA FILE CONTAINING THE Y-POSITION AND INLET FLOW ANGLE AT A DESIRED
c LOCATION UPSTREAM OF THE BLADE IN TERMS OF PERCENT CHORD.  DATA IS
c CALCULATED USING SIMPLE LINEAR INTERPOLATION.
c                SEPTEMBER 29, 1994     WRITTEN BY LT. DREW WILLIAMS
ccccccccccccccccccccccccccccccccccccccccccccccccccccccccccccccccccccccccccccccccccccccccccccccccc

      real beta(300)
      dimension x(300,300),y(300,300),q(300,300,4)
      dimension xx(300),yy(300),u(300,300),v(300,300)
      dimension uu(300),vv(300)

          open(10)
          rewind(10)
          pi=3.1415926

c  Read in the C-grid created by GRAPE
          read (7,*) ni,nj
          read (7,*) ((x(i,j),i=1,ni),j=1,nj),
     &          ((y(i,j),i=1,ni),j=1,nj)
          read (7,*) mtl,mil
c       write(10,*) x(mtl,1)

c  Read in the Solution file created by RVCQ3D
          read (3,*) ni,nj
          read (3,*) fsmach,alpha,reyn,iters
          read (3,*) (((q(i,j,k),i=1,ni),j=1,nj),k=1,4)

c  Calculate the velocities u and v at every grid point
          do 100 i = 1,ni
          do 200 j = 1,nj
           u(i,j)=q(i,j,2)/q(i,j,1)
           v(i,j)=q(i,j,3)/q(i,j,1)
  200     continue
  100     continue

c  Define the Chord length and then prompt for an upstream location
          chord=x(mtl,1)
          write(*,*) 'Input Upstream Chord Location in Percent (i.e., -10, -20,...)'
c  (NOTE: You must be aware of the maximum upstream position available from your
c       GRAPE output.  Beyond the maximum upstream location, the values calculated
c       are all the same as that at the maximum.)
          read(*,*) ax
          axperc=ax/100
          vertx=axperc*chord
```

```
c       write(10,*) chord
c       write(10,*) vertx

c  Bracket the vertical x-position
c  (Note:  Depending on your grid size, the 'i' index may have to be adjusted to
c       ensure the entire inlet flow region is covered.)
        do 300 i = 1,240
        do 400 j = 1,nj
        flag=0
         if (x(i,j).gt.vertx) jsx1=j
         if (x(i,j).lt.vertx) then
          jsx2=j
          flag=2
          goto 500
         endif
400   continue
500   continue
        if (flag.gt.1) then

c  Calculate the u and v velocities and compute the inlet angle
c  Linear Interpolation in the form of:  ynew = yold + (dy/dx)*dx
        yy(i)=y(i,jsx1)+(vertx-x(i,jsx1))*(y(i,jsx1)-y(i,jsx2))/
     &                    (x(i,jsx1)-x(i,jsx2))
      uu(i)=q(i,jsx1,2)+(vertx-x(i,jsx1))*(q(i,jsx1,2)-q(i,jsx2,2))/
     &                     (x(i,jsx1)-x(i,jsx2))
      vv(i)=q(i,jsx1,3)+(vertx-x(i,jsx1))*(q(i,jsx1,3)-q(i,jsx2,3))/
     &                     (x(i,jsx1)-x(i,jsx2))
        beta(i)=atan(vv(i)/uu(i))*180/pi
        write(10,*) yy(i),beta(i)
        endif
300     continue
        stop
        end
```

REFERENCES

1. Elazar, Y., *A Mapping of the Viscous Flow Behavior in a Controlled Diffusion Compressor Cascade Using Laser Doppler Velocimetry and Preliminary Evaluation of Codes for the Prediction of Stall*, Doctoral Dissertation, Naval Postgraduate School, Monterey, California, March 1988.

2. Murray, K. D., *Automation and Extension of LDV Measurements of Off-Design Flow in a Subsonic Cascade Wind Tunnel*, Master's Thesis, Naval Postgraduate School, Monterey, California, June 1989.

3. Hobson, G. V., and Shreeve, R. P., *Inlet Turbulence Distortion and Viscous Flow Development in a Controlled-Diffusion Compressor Cascade at Very High Incidence*, AIAA paper 91-2004 presented at the 27th Joint Propulsion Conference, Sacramento, California, June 24-26 1991.

4. Ganaim, J. G. R., *Laser-Doppler Velocimeter Measurements in a Cascade of Controlled Diffusion Compressor Blades at Stall*, Master's Thesis, Naval Postgraduate School, Monterey, California, June 1994.

5. Ho, Y. K., Walker, G. J., and Stow, P., *Boundary Layer and Navier-Stokes Analysis of a NASA Controlled-Diffusion Compressor Blade*, ASME 90-GT-236.

6. Hobson, G. V., *A Navier-Stokes Analysis of a Controlled-Diffusion Compressor Cascade at Increasing Inlet Flow Angles*, accepted for publication by the International Journal of Turbo and Jet Engines, May 1995.

7. Kang, S. H., Lee, J. S., Choi, M. R., and Kim, K. Y., *Numerical Calculations of the Turbulent Flow Through a Controlled-Diffusion Compressor Cascade*, Journal of Turbomachinery, April 1995.

8. Chima, R. V., *Explicit Multigrid Algorithm for Quasi-Three-Dimensional Viscous Flows in Turbomachinery*, Journal of Propulsion and Power, Vol. 3, No. 5, Sept.-Oct. 1987, pp. 397-405.

9. Chima, R. V., Turkel, E., Schaffer, S., *Comparison of Three Explicit Multigrid Methods for the Euler and Navier-Stokes Equations*, NASA TM-88878, Jan. 1987.

10. Classick, M. A., *Off-Design Loss Measurements in a Compressor Cascade*, Master's Thesis, Naval Postgraduate School, Monterey, California, September 1989.

11. Chima, R. V., *Revised GRAPE Code Input for Cascades*, NASA Lewis Research Center, June 1990.

12. Baldwin, B. S., and Lomax, H., *Thin-Layer Approximation and Algebraic Model for Separated Turbulent Flows*, AIAA Paper 78-257, January 1978.

13. Numerical Aerodynamic Simulation (NAS) Division, *Flow Analysis Software Toolkit (FAST)*, Version 1.1a, June 1993.

14. Dreon, J. W., Report on *Controlled Diffusion Compressor Blade Wake Measurements*, Master's Thesis, Naval Postgraduate School, Monterey, California, September 1986.

15. Hobson, G. V., *Unpublished Experimental Results for a Controlled-Diffusion Compressor Cascade at an Inlet Flow Angle of 46 Degrees*, Naval Postgraduate School, Monterey, California, August 1994.

16. Koyuncu, Y., *Report of Tests of a Compressor Configuration of CD Blading*, Master's Thesis, Naval Postgraduate School, Monterey, California, 1984.

17. Armstrong, J. H., Report on *Near-Stall Loss Measurements in a CD Compressor Cascade With Exploratory Leading Edge Flow Control*, Master's Thesis, Naval Postgraduate School, Monterey, California, June 1990.

18. Shreeve, R. P., Elazar, Y., Dreon, J. W., and Baydar, A., *Wake Measurements and Loss Evaluation in a Controlled-Diffusion Compressor Cascade*, Journal of Turbomachinery, October 1991.

19. Sanger, N. L., and Shreeve, R. P., *Comparison of Calculated and Experimental Cascade Performance for Controlled-Diffusion Compressor Stator Blading*, Journal of Turbomachinery, Vol. 108, July 1986.

INITIAL DISTRIBUTION LIST

1. Defense Technical Information Center — 2
   Cameron Station
   Alexandria, Virginia 22304-6145

2. Library, Code 52 — 2
   Naval Postgraduate School
   Monterey, California 93943-5101

3. Department Chairman, AA — 1
   Department of Aeronautics and Astronautics
   Naval Postgraduate School
   699 Dyer Road - Room 137
   Monterey, California 93943-5106

4. Garth V. Hobson, Turbopropulsion Laboratory, Code AA/Hg — 7
   Department of Aeronautics and Astronautics
   Naval Postgraduate School
   699 Dyer Road - Room 137
   Monterey, California 93943-5106

5. Raymond P. Shreeve, Turbopropulsion Laboratory, Code AA/Sf — 1
   Department of Aeronautics and Astronautics
   Naval Postgraduate School
   699 Dyer Road - Room 137
   Monterey, California 93943-5106

6. Naval Air Systems Command — 1
   AIR-4.4.T (Attn: Charles Gordon)
   Washington, District of Columbia 20361-5360

7. Naval Air Warfare Center — 1
   AIR-4.4.3.1 (Attn: Stoney McAdams)
   Propulsion and Power Engineering
   Bldg. 106, Sears Road
   Patuxent River, Maryland 20670-5304

8. Lt. Drew Williams — 2
   4493 Mt. Henry
   San Diego, California 92117